ROLLING CONTACT FATIGUE BEHAVIOR OF THREE EUTECTOID RAIL STEELS

Xiaonong Qiu
Beijing University of Iron
and Steel Technology, 1982

A thesis submitted to the faculty
of the Oregon Graduate Center
in partial fulfillment of the
requirements for the degree
Master of Science
in
Materials Science and Engineering

November, 1987

The thesis "Rolling Contact Fatigue Behavior of Three Eutectoid Rail steels" by Xiaonong Qiu has been examined and approved by the following Examination Committee:

Paul Clayton
Professor
Thesis Research Advisor

Jack H. Devletian
Professor

S. Shankar
Assistant Professor

Anthony E. Bell
Associate Research Profeesor

ACKNOWLEDGEMENTS

I would like to thank Dr. Paul Clayton for introducing me to an interesting topic and for the support and guidance from beginning the research to completing the thesis. I appreciate the close contact I had with all the members of the thesis committee: Dr. Jack Devletian, Dr. S. Shankar and Dr. Anthony E. Bell.

Also, I would like to thank Mr. Dale Christensen, Mr. Dan Danks, Dr. Milton Scholl, Mr. Vivek Dikshit and Mr. Ramaswamy Devanathan as well as those who helped me during this work. This work was supported by the Burlington Northern Railroad.

TABLE OF CONTENTS

LIST OF TABLES

LIST OF FIGURES

ABSTRACT

Rolling Contact Fatigue Behavior of Three
Eutectoid Rail Steels

Xiaonong Qiu
Oregon Graduate Center, 1987

Supervising Professor: Dr. Paul. Clayton

In recent years a Japanese head hardened (HH) premium rail steel in North America has experienced rolling contact fatigue (RCF) problems. Field observations suggest that this material exhibits premature surface spalling, however no controlled field experiments have been carried out to support this view.

The current work was undertaken on behalf of a major railroad which uses the HH rail steel. The rolling contact fatigue behavior of this and two other rail steels used by the company, namely a standard carbon (STD) rail steel and a second premium rail steel alloyed with chromium and molybodenum (CrMo), was evaluated in laboratory tests.

The experiments were conducted using an Amsler wear testing machine under water lubricated, rolling-sliding conditions over a range of contact pressures. It was found that the HH rail steel possesses the best RCF resistance of the three steels. Further, an attempt was made to characterize the fatigue crack appearance and to correlate it to RCF resistance.

The results suggest that HH rail steel and CrMo rail steels are superior to STD rail steel in terms of both crack initiation and propagation.

Supporting microstructural and mechanical test evaluations show that HH rail steel has the smallest pearlite interlamellar spacing, lowest inclusion content, and the highest tensile strength, ductility, impact resistance and wear resistance.

It is therefore concluded that the investigation has revealed no metallurgical deficiency that could explain why HH rail should experience a RCF problem in practice with respect to other rail steels.

While it is not possible, from the small number of mechanical tests on only three materials, to draw any firm conclusions about the correlation between RCF resistance, microstructure, and mechanical properties, the data does suggest that RCF resistance correlates directly with tensile strength, and wear resistance.

INTRODUCTION

In recent years, a new high-strength head hardened rail (HH) has been developed by Nippon Steel Corporation in order to enhance the capability of railway transportation. However, HH rail steel has in some cases exhibited a poor resistance to rolling contact fatigue (RCF) in practice as shown in Fig. 1, as compared to other premium rail steels.

The main aim of this program is therefore to determine possible causes which could account for HH rail steel suffering premature rolling contact fatigue failure in service. To achieve this goal, the evaluation of the RCF resistance of HH rail steel was carried out with respect to two different rail steels, namely Colorado Fuel and Iron (CF&I) standard carbon (STD) rail steel and CF&I CrMo rail steel. Supporting mechanical tests and microstructrural examinations were also conducted for the three rail steels.

A number of studies [1-6] have been carried out to investigate the cause of failure in rails. It has been shown that surface initiated RCF of rail is one of the causes of rail failure. Crack initiation and propagation in RCF have not been extensively investigated. It has been shown by several investigators, [2,5,7] on a laboratory scale, that cracks in RCF initiate at the surface of rollers. One study made [2], using roller specimens, showed that RCF cracks initiated at 25 to 50% of the total RCF life. However, no attempt has been made to characterize crack appearance and to establish a relationship between crack appearance for different steels and their RCF behavior.

Limited work has been done to explore the role of microstructure and mechanical properties on RCF life. It has been demonstrated [1,4,6] that a fine pearlitic steel with higher tensile strength is superior to a coarse pearlitic steel, with lower tensile strength, and other rail steels. It has been demonstrated [5,6] that the wear resistance of rail steel with a fine pearlite spacing is superior to that of rail steel with a coarse pearlite spacing. But no attempt has been made to correlate wear resistance under rolling-sliding contact conditions to RCF resistance.

In the current work, the RCF tests were conducted on the Amsler testing machine under water lubricated, rolling -sliding conditions over a range of contact pressures to compare the RCF resistance of three steels and evaluate their RCF behavior. This work studies the appearances of RCF cracks and attempted to correlate the crack appearance to the RCF resistance of three rail steels.

Supporting laboratory tests such as the microstructural characterization of the three rail steels together with tensile and Charpy V-notch Impact tests were carried out. Wear resistance was also assessed.

An hypothesis of the possible causes to explain premature RCF failure in HH rail steel in practice is made on the basis of the experimental results obtained in this work.

2. REVIEW OF LITERATURE

2.1. Rolling Contact Fatigue

Failures caused by rolling contact fatigue (RCF) are the result of cyclic contact stresses developed at or near contact surfaces during rolling motion. RCF has a profound effect on the endurance of engineering rolling bodies such as wheel on rail, ball-and roller-bearings and gear teeth [8]. Hence, theoretical and experimental studies have attempted to establish the relationship between RCF resistance and system variables such as load, creepage, microstructure and mechanical properties of material. RCF is a very complex process [9] involving complicated stress distributions and other influencing factors such as microstructure, mechanical properties of material, surface topography, lubrication, residual stresses and the environment under which the rolling motion takes place.

2.1.1. Stress Distribution and Its Effect on RCF

2.1.1.1. Hertz Theory

The stress distribution at the cylinders contact surface and throughout the depth of the surface layers was first established by Hertz [10]. In the case of the contact between two identical cylinders under a load, a plane contact zone, where the stress is not evenly distributed along the contact zone as shown in Fig. 2,

stress can also be calculated [8,10]. Even though Hertz theory is based on some assumptions such as perfectly elastic materials, topographically smooth surfaces and no tangential force being transmitted, the results of the hertz theory have been successfully applied to many situations [8,10,11].

2.1.1.2. RCF Failure and Maximum Hertzian Stress

Attempts have been made to establish a relationship between RCF life of rail steels and a critical stress in laboratory tests with cylindrical specimens. The hypothesis that the maximum Hertzian stress, Po, is the critical stress under cylindrical contact conditions has been suggested by McKelvey and Moyer [6]. The tests were conducted on a twin cylinders machine under oil lubrication condition. The maximum contact pressure (two contacting cylinders with parallel axes) is given by [12]:

$$Po=0.418\{ [NE(R+R')]/(2aRR') \}^{1/2}$$

where N is normal force, E is Young's Modulus, R and R' are top and bottom roller radii respectively, and 2a is the contact length.

Some work [2,13,14] has been done using cylindrical specimens to investigate the correlation between RCF failure of steels and maximum hertzian contact pressure. RCF tests [2] have been conducted using BS11 carbon (standard carbon) rail steel under water lubrication condition. The results, Fig. 3, shows that the RCF life of rail steel increases with decreasing maximum Hertzian contact pressure. The

same trends [13,14] have been obtained using the rollers made from standard carbon rail and 0.45% C steel under oil lubricated and rolling-sliding conditions.

2.1.2. Crack Initiation and Propagation in RCF

RCF tests carried out [2,5] using rail steel have shown that a crack initiates on the surface and propagates along plastic flow lines (inclined with respect to a surface) in the subsurface as shown in Fig. 4.

RCF tests have been conducted using rollers to investigate a correlation between crack initiation and propagation and residual stress produced during rolling-sliding contact. It has been demonstrated [7,15,16] that a maximum tensile residual stress exists just below the contacting surface under rolling-sliding conditions. Thus it was suggested that this maximum tensile residual stress causes crack initiation at the surface. The direction of crack propagation has been explained [17] by the fact that the residual tensile stress acts perpendicularly to the direction of crack propagation. This leads to the inclination of a crack at the subsurface.

Dawson [18] conducted tests to investigate the pitting behavior in rolling contact. The experimental work was done in a twin disc machine using 0.3C steel discs under oil lubricated conditions. Sections through some of the cracks were examined. The depths of these cracks were less than 0.025mm, but no crack was found to be completely subsurface. Hence, they suggested that the cracks start

at the surface or within 0.025mm depth of surface.

Recently, Clayton and Hill [2] carried out experiments using rollers lubricated with water in a twin disc machine to determine the RCF behavior of a 0.5%C steel. It was found that crack initiation occurred at between 25 and 50% of total RCF life.

2.1.3. Effect of Creepage on RCF

Creepage is defined as the difference in velocities of the contacting surfaces with respect to their mean velocity, which means that the higher the creepage, the greater the degree of sliding. Experiments to assess the influence of creepage on RCF have been conducted by several investigators [2,5,19,20,21] using cylindrical specimens. It has been shown [5] that the increase of creepage leads to a reduction in the RCF life at 10%, 25% and 45% creepage. Most recently, Clayton and Hill [2] demonstrated that RCF life falls considerably with just a small increase in creepage from 0 to 0.3% and as creepage is increased further to 1%, RCF life increases and then this is followed by a further drop as creepage goes from 1 to 5%, beyond which the effect of creepage can be ignored as shown in Fig. 5. They suggested that the complicated effect of creepage on RCF could involve the interaction of creepage on traction, surface roughness, lubrication and wear.

2.1.4. Effect of Mechanical Properties and Microstructure on RCF

Only a few attempts have been made to correlate RCF resistance

and mechanical properties and microstructure of rail steels. One study has been conducted by Sugino and Kageyama [4] using rollers with crowned contact surfaces in a twin disk machine under rolling-sliding and oil lubricated contact. They demonstrated that the RCF resistance of Nippon head hardened rail steel (NHH) with the highest tensile strength, which is attributed to its having the finest pearlitic structure, was superior to tempered martensitic steel and steels with coarse pearlite spacing. The same result has been obtained by a different investigator [6,14] under approximately the same test conditions.

RCF tests [5] were conducted using rail and tire disk roller specimens under oil lubricated and rolling-sliding conditions. It was found that cracks propagate to a certain depth coinciding with the work-hardened depth. It was therefore suggested that deformation plays an important role in the mechanism of crack propagation. It has been also demonstrated [22] in the RCF test that a material with high tensile strength can withstand a high critical contact pressure before plastic deformatoin, which is associated with RCF failure, takes place.

Experiments [1,23,24] have been performed to investigate the influence of strength of rail steel on fatigue resistance in conventional fatigue tests. This may be considered to correlate RCF resistance to some degree.

The experiments has been carried out by Barsom et al [23] on a rotating beam fatigue testing machine and materials testing system machine which was used to measure fatigue crack propagation rate. It has been showed that the fatigue crack initiation and propagation

resistance increases with increasing the tensile strength of the rail steel.

Marich and Imhof [24] carried out tests to investigate the effect of working hardening of rail steel on the depth of deformation below surface in laboratory tests. Specimens from various rail steels were subjected to certain amounts of prestrain (up to 80 percent reduction) by means of cold rolling. It was found that high strength rail steel gives rise to less depth of deformation. They then proposed that high-strength steels exhibited a higher resistance to deformation which, in turn, decreases depth of deformation of subsurface.

Masumoto and Sugino [1] have carried out tests to investigate the effects of microstructure on crack initiation in RCF using crowned rollers in a twin disk machine. It has been shown that in the RCF test, a fine pearlite microstructure is most suitable for the prevention of crack initiation and tempered martensite has a favorable effect on fatigue crack propagation rates. They concluded that fine pearlitic rail steel is preferable for their practical purpose because initiation always precedes propagation.

While the effect of microstructure on RCF resistance of pearlitic steel has not been studied extensively, much more has been done to investigate the relationship between microstructural parameters and mechanical properties, which may be considered to have an influence on RCF resistance.

It is commonly accepted [4,6,25,26,27] that tensile strength mainly depends on pearlite spacing. A smaller pearlite spacing gives rise to a higher tensile strength. The pearlite interlamellar

spacing decreases with decreasing transformation temperature [4].

Hyzak and Bernstein [26] carried out experiments to study the structure-property relationships in fully-pearlitic steels. Based on a statistical analysis, it was shown that the tensile strength was controlled primarily by the interlamellar pearlite spacing, and that prior austenite grain size and pearlite colony size have only a minor influence.

Some work [28] has shown that fatigue crack propagation rate is associated with the spacing of the pearlite lamellar. In other words, a fine pearlite spacing gives rise to a lower fatigue crack propagation rate.

Some attempt has been made to establish the correlation between the grain size and mechanical properties of pearlitic steel. Grain size in pearlitic steel has been considered as a main contribution to toughness [26,29,30] at temperatures below the ductile to brittle transition temperature (DBTT) which is approximately 160^{o}C for pearlitic steels. It has been demonstrated [26,29] that the prior austenite grain size controls the cleavage fracture facet size which leads to a change of direction of the crack during propagation. Therefore, absorbed energy for a propagating crack can be enhanced.

2.1.5. Effect of Lubrication on RCF

All RCF tests [1,2,4,5,6,13,14,31] so far were conducted under lubricated condition due to a lubricant reducing wear in order for RCF to occur. RCF tests of rail steel [2,13] were conducted

under water lubricated condition. This is because water is more likely to be found on rails than oil and a water lubricated test seems to give similar results to oil lubricated test (qualitatively at least).

The role of lubrication in rolling and rolling-sliding contact has been studied by many workers [2,32,33,34,35,36]. The effect of lubrication on crack propagation in RCF has been explained first by Way [34]. It was postulated that when the crack on the surface of rolling bodies passes through the contact area, water is entrapped and forced deeper into the crack, finally pressurizing the crack tip and extending the crack network. Later, Dawson [36] has conducted RCF tests (oil lubricated) in which a roller was run to produce a crack and then the direction of rotation of roller was changed so that the oil would be squeezed out of the crack, and it was found that the crack did not show obvious growth. It was therefore said that this supports Way's suggested mechanism of crack propagation. Recently, Clayton and Hill [2] carried out lubrication tests using different lubricants to investigate the role of lubrication in RCF. It was found that glycerol gives a longer RCF life than a more fluid liquid lubricant because glycerol does not easily penetrate to the crack tip. This may be evidence in support of Way's ideas.

2.2. Laboratory Wear Test Under Rolling-Sliding Condition

The wear behavior of rail steels under rolling-sliding conditions have been investigated by several workers [37,38,39,40]. Bolton

and Clayton [39] investigated wear behavior of rail steels at 1%-35% creepage over a wide range of contact pressure under rolling-sliding conditions. It was found that the wear rate of rail steel increases linearly with increasing contact pressure as shown Fig. 6. They proposed three wear regimes, termed Types I, II and III wear. Type I wear consists of a combination of an oxidative mode and a metallic flake formation mode. In the former material is removed by the progressive growth and mechanical breakdown of a continuous oxide film. The latter involves flake formation over a large number of contact cycles which is related to the emergence of highly deformed manganese sulphide inclusions at the roller surface.

The characteristic of type II wear is associated with completely metallic debris, and involves a plastic deformation and fracture process. However, a wider range of particle sizes and less prominent flake formation make it difficult to determine the detailed mode of material removal in this case.

The wear transition between I and II wear [39] can occur as contact pressure and creepage reach a certain value. This transition was also found [37] under approximately the same test condition.

Type III wear was characterized by the fact that materials have been considerably gouged out of the surface. As a result, the rate of material removal was so high that the uniform depth of deformation observed in type I and type II wear was not developed. Type II and III correlate well to those found to occur in side-worn rails in the UK.

Wear tests have been carried out by Danks and Clayton [37]

to correlate the laboratory wear test to the wear process occurring in the field in the U.S.A. The tests under rolling-sliding conditions were conducted in the range of 1%-35% creepage and 500-1280 N/mm^2 contact pressure using standard carbon rail steel in an Amsler twin disk machine. It was shown that the wear rate of rail steel increases linearly with increasing contact pressure, Fig. 7. It was found that the Amsler wear tester is capable of generating similar surface damage processes to those produced in the field. In addition, it was observed that the three wear regimes were all represented in the tests.

Wear tests [5] were carried out using disk rollers of rail steels with different microstructures under rolling-sliding conditions in a twin disk machine. The results suggested that for pearlitic steels, wear resistance is improved as the average pearlite interlamellar spacing decreases. Also it was shown that wear resistance increases with increasing hardness. Rail steels with different microstructures but the same hardness do not necessarily have the same wear resistance such that wear resistance is arranged in order of microstructure as follows: pearlite > tempered martensite > bainite.

Under approximately the same test conditions mentioned above, it has been demonstrated [4,6] that the wear resistance of a head hardened rail steel with a fine pearlite spacing is superior to that of tempered martensite rail steel and bainitic rail steel.

3. EXPERIMENTAL METHODS

3.1 General

3.1.1. The Test Rig

The RCF tests and the wear tests were carried out on an Amsler twin disk test machine (Fig. 8) in which the bottom shaft (400rmp) rotates 1.104 times faster than the top shaft and two rollers mounted on shafts can be run together in rolling-sliding contact. The top shaft is mounted in a swinging bracket, to which load is applied by means of a compressed spring giving a range of 0-2000 N at the specimen.

A chart recorder attached to a torque dynamometer gives a continuous record of the torque. This can be used to calculate the friction coefficient. A mechanical counter records the number of revolutions of the bottom shaft. An integrating counter on the Amsler machine can record the work done by the rolling contact during a test.

An accelerometer is attached to the Amsler machine to record the vibration caused by the contact of the roller surfaces. When the vibration exceeds a certain pre-set value, a cut out switch is triggered and the machine is switched off automatically.

3.1.2. Calculation of Contact Pressure and Creepage

The normal maximum contact pressure in the contact area of two cylindrical rollers can be calculated, assuming hertzian contact, according to the following equation:

$$Po = 0,418 \frac{\left[NE(R_T+R_B) \right]^{1/2}}{2aR_TR_B}$$

where P_o is the maximum herzian contact pressure, N is normal load, E is Young's modulus, R_T and R_B are top and bottom roller radii respectively, and 2a is the contact length.

Creepage is defined as the difference in velocities of the contacting surfaces with respect to their mean velocity, and for the Amsler machine is given by:

$$\gamma = \frac{2(1.104D_2-D_1)}{D_1+1.104D_2}$$

where D_1 and D_2 are the diameters of the top and bottom rollers respectively.

3.2. Rolling Contact Fatigue (RCF) Tests

3.2.1. Specimens

The materials used for the top roller specimens were Colorado Fuel and Iron (CF&I) standard carbon (STD) unused and used rail steels (O.G.C. rail x35 and x60), CF&I CrMo unused rail steel (O.G.C. rail x34) and Japanese Nippon head-hardened (HH) unused rail steel (O.G.C. rail x33). For all the RCF tests the bottom roller was made of STD rail steel. Chemical compositions are given in Table (1).

Most rollers were taken from the heads of unused rails such that

the axis of the roller was parallel to the longitudinal axis of the rail (vertical) as shown in Fig. 9.

The hardness profile of a transverse section of HH rail is different from that of CrMo and STD rails, Fig. 10. To ensure that the hardness of the rollers was constant around the circumference, the rollers were taken with a different orientation such that the axis of the roller was normal to the longitudinal axis of the rail (horizontal), Fig. 11.

Because the rail is manufactured by a hot rolling process, it was anticipated that the test specimen orientation might affect RCF behavior. To investigate this possibility, some specimens were taken from the head of the STD used rail with both the vertical and horizontal orientation and the head of the CrMo unused rail with the horizontal orientation.

To investigate reproducibility of RCF life data, two RCF tests for vertical roller were carried out at contact pressure 1354 and 1254 N/mm^2 respectively, and four tests for horizontal roller were conducted at a contact pressure 1354 N/mm^2.

The specimen geometries of the RCF tests are shown in Fig. 12(a). The top roller was always 35mm in diameter with the diameter of the bottom roller chosen to give the desired creepage. The widths of the top roller (contact width) and the bottom roller are 4mm and 10mm respectively.

3.2.2. Test Conditions

Some preliminary tests were carried out to determine the effect

of creepage on RCF life, and 0.3%, 2% and 10% creepages were used over a range of contact pressure 800-1500 N/mm^2. All subsequent tests were conducted at 10% creepage over a contact pressure range of 900-1500N/mm^2. Each test was run under water lubricated conditions at room temperature. All tests were conducted with the bottom shaft rotating at 400rpm.

3.2.3. Test Procedure

The water supply was set up to provide 1 drop every 4 secs before the test was started. An accelerometer was set to the value corresponding to the normal vibration caused by rolling motion at the beginning of each test. When rolling contact fatigue occurred, the surface of the rollers became rough due to the collapsed or pitted surface. This caused excessive vibration of the machine. When the vibration exceeded the pre-set maximum value of the accelerometer, the machine was turned off automatically. The water supply was also halted automatically at the same time and methanol released onto the surfaces of the rollers to prevent rusting. The number of revolutions between the start of the test and the end of the test were recorded to obtain RCF life.

3.2.4. Examination of Failed Rollers

The subsurface appearance of the fatigue cracks in the failed rollers was studied by examining longitudinal sections of rollers, taken as shown in (Fig. 13) in the optical microscope.

3.3. Wear Tests

3.3.1. Specimens

Top rollers of CrMo and STD rail steels were taken from the heads of rails, in the same manner as for the RCF rollers (Fig. 9). For HH rail steel, the top rollers were taken in the same position as the rollers of HH rail steel for the RCF tests (Fig. 11). The bottom rollers were taken from O.G.C.wheel #2 (composition Table 1) as shown in Fig. 14. The geometry of the rollers is shown in Fig. 12(b).

3.3.2 Test Condition

Wear tests for three different rails were conducted on the Amsler machine using the test condition of 35% creepage, a contact pressure range of 500-1220 N/mm^2 and a speed of 200 rpm. All wear tests were run without a blast of dry compressed air at room temperature.

3.3.3. Test Procedure

Wear was measured by taking off both rollers periodically and weighing them. The wear rates were calculated as micrograms / meter rolled from weight loss and corresponding number of revolutions.

3.4. Characterization of Materials

All three rail steels tested have a fully pearlitic microstructure which can be characterized by three parameters: pearlite interlamellar spacing, pearlite colony size and prior austenite grain size. These

are illustrated schematically in Fig. 15. Inclusion levels were also determined. Based on the hardness profile of three rail steels Fig. 10, the samples for microstructural examination were cut out of the head of the rails as shown in Fig. 16 and polished and etched in the normal metallographic manner.

3.4.1. Pearlite Interlamellar Spacing and Colony Size

Interlamellar pearlite spacing and pearlite colony size were determined by using the scanning electron microscope (SEM) on longitudinal sections etched with 2% nital. The circular intercept method [41] was used to measure 20 fields to obtain the mean true pearlite interlamellar spacing over a range of magnification 10,000x-20,000x.

The number (n) of intersections of carbides with a circular of diameter (d) 100mm was counted for each field, and the mean random spacing (Sr) calculated from

$$Sr=(d/M)/n$$

where M is magnification.

The mean true spacing St for each field can be obtained from

$$St=0.5Sr$$

The mean and 95% confidence interval for the mean true spacing were calculated for the 20 fields.

The circular intercept method of Hilliard ASTM Method (E112-82)

was used on 26 fields for each rail to obtain the average pearlite colony size at a range of magnification 1500x-4500x. The total number of colony boundary intersections with the test circle of circumference 250mm was counted. The colony size was directly determined from the chart by using the average value of the intercepts count per 500mm test length. 95% confidence interval in ASTM size number can be determined from the chart (Fig 8 E112-82) using the coefficient of variation of counts C.V. which can be calculated from

$$C.V. = So/N$$

where So is the standard deviation of observations and N is the mean count.

3.4.2. Prior Austenite Grain Size

The measurement of prior austenite grain size of STD rail and CrMo rail steels was facilitated by the presence of proeutectoid ferrite formed from decarburization of the surface of the rail during manufacture. Since the proeutectoid ferrite forms preferentially at the prior austenite grain boundaries in decarburized layers near the rail surface, the ferrite network is an outline of the prior austenite grain size. It was, therefore, possible to reveal prior austenite grain size for STD rail and CrMo rail by simply etching the polished surface of the two rail steels in 2% nital. However, decarburization was not observed in the HH rail and the above method

could not be applied. It was thus necessary to follow a different procedure to reveal the prior austenite grain size.

A heat treatment method was used in which the pearlite microstructure is changed to one of martensite outlined by fine pearlite to reveal the original austenite grain boundaries (E112-82. A3.3.1.4). A "gradient quench" was employed such that the heated piece is for a portion of its length immersed in water and therefore fully hardened, the remainder of the piece above the quenching bath is, therefore, not hardened. Consequently, there was a small zone which was almost but not quite fully hardened, and in this zone, the prior austenite grains consist of martensite grains surrounded by small amounts of fine pearlite, thus revealing the grain size. The heat treatment to reveal grain size was conducted at $1575\pm25^{0}F$ ($857\pm14^{0}C$) for 30 min and the specimens were etched in 2% nital.

The prior austenite grain size for all three rail steels was measured using a three-circle procedure following the ASTM Standard Method for Determining Average Grain Size (E112-82), using the optical microscope. 15 fields were measured for each rail. The test pattern consists of three concentric and equally spaced circles having a total circumference of 500mm. This pattern was successively apply to randomly selected and widely spaced fields, and the total number of grain boundary intersections with the test circles was counted. The average value of the intercept count per 500-mm test pattern was calculated. The subsequent procedure is the same as that described in the measurement of pearlite colony size above.

3.4.3. Volume Fraction of Inclusions

Inclusion contents of the different rails were measured from unetched samples by using the ASTM Standard Method for Determining Volume Fraction by Systematic Manual Point Count (E562-83) using the optical microscope. 120 fields were used to make the measurement in each rail. The test grid consists of equally spaced points formed by the intersection of fine lines on a transparent sheet. This is superimposed upon the viewing screen of the optical microscope for the measurements. The number of points (inclusions) falling on the points of the test grid was counted for each field. The volume fraction (Vv) was calculated using

$$Vv=Pp + CI$$

where Pp is arithmetic average of points falling in the points of th test grid and CI is the 95% confidence interval.

3.5. Mechanical Tests

Tensile specimens and the Charpy V-notch (CVN) impact specimens were cut from the head of the rails in the longitudinal orientation. Fig. 17 and 18 shows the specimens position for HH rail steel and other two rail steels respectively.

3.5.1. Tensile Tests

The tensile specimens were machined to round specimens with ASTM

standard diameters and parallel lengths (ASTM E8-82) as shown in Fig. 19. The tests were conducted at room temperature in a Tinius Olsen testing machine. Three specimens were used for each rail steel. An extensometer was attached to the specimen for measuring the strain. The yield strength was determined by the "offset method" (0.2%) from the stress-stain curve recorded during tests.

3.5.2. Charpy V-notch Impact Tests

The instrumented impact tests were carried out using a standard CVN Impact specimen having a U-type tup in accordance with ASTM Standard E-23 as shown in Fig. 20. Tests were conducted with specimens at the pendulum impact machine at $22^{o}C$ and $-20^{o}C$. The load-time curves for the test were recorded on an Applescope disk in the computer. Analysis was done using Astir (computer program) which directly provides the load, displacement, time and energy absorbed at various points during the fracture event.

4. RESULTS

4.1. Microstructure

Typical scanning electron microscope micrographs of pearlite and optical microscope micrographs of the prior austenite grains are shown in Figs. 21 and 22 respectively for all three rail steels. The quantitative microstructural analysis reveals (Table2) that the HH rail has the finest pearlite interlamellar spacing, the smallest pearlite colony size and prior austenite grain size and the lowest volume fraction of inclusions. By comparison with STD rail steel, CrMo rail exhibits a smaller pearlite interlamellar spacing and colony size and lower volume fraction of inclusion but similar prior austenite grain size.

4.2. Mechanical Properties

The load-time curves of the instrumented Impact tests for the three rail steels at two temperatures are presented in Fig. 23 to 28. The total energy absorbed during the Impact test and the energy required to initiate fracture (premaximum load energy) of the three rail steels are shown in Table 3.

It is seen that at room temperature, HH rail is tougher than both CrMo and STD rails which are similar. In contrast, the impact behavior of all three rails are similar at $-20C^{O}$. It seems therefore that HH rail is more sensitive to change in temperature in the CVN

impact test than the other two rail steels.

Figs. 29, 30 and 31 show the load-strain curves of tensile tests for the three rail steels. Table 4 shows the yield strength and ultimate tensile strengths which were obtained from the load-strain curves. The reduction in area and elongation as well as the hardness (rollers) of the three rail steels are also included. Both HH and CrMo rail steels show higher tensile strengths and hardness and better ductility than STD rail steel. It is seen that HH rail steel is slightly better in these respects than the CrMo rail steel.

4.3. RCF Tests

4.3.1. Effect of Creepage

The RCF life for STD rail steel at 0.3%, 2% and 10% creepage is plotted against contact pressure in Fig. 32. It is seen that the general pattern of behavior is the same for all three creepage levels with the suggestion of a fatigue limit at lower stress levels.

As has been observed previously [15] the lower creepage generates lower RCF life over a wide range of contact pressures. At high contact pressure, the three creepages show a complex RCF behavior. In view of the data obtained in these tests and previous observations of complex behavior at the lower creepage levels [2], all remaining tests were conducted at 10% creepage.

4.3.2. Effect of the Specimen Orientation on RCF and Reproducibility of RCF Tests

Figs. 33 and 34 show the results obtained with CrMo rail steel and STD used rail steel using specimens taken in two different orientations. It is noted that the RCF life in these two different orientations is almost identical. Fig. 34 also shows the reproducibility of the RCF tests at contact pressure 1254 and 1354 N/mm^2. For the vertical and horizontal rollers, the fluctuation of RCF life in terms of mean and standard deviation is shown in Table 6.

4.3.3. RCF Tests for Three Rail Steels

The results obtained in the 10% creepage RCF tests for the three rail steels are presented in Fig. 35. It is seen that all three rail steels exhibit the same pattern of behavior. The RCF life decreases linearly with decreasing contact pressure. In addition, the RCF resistance of the HH rail steel is seen to be marginally better than that of the CrMo steel and they both have significantly higher RCF resistance than the STD steel.

4.3.4. Friction Coefficient Between Top and Bottom Rollers

The torque recorded for all the RCF tests showed two types of behavior Fig. 36. The first type (for the most tests) involved an increasing torque during the initial stage before achieving a steady state. The second type (only for 2% creepage) showed a maximum torque in the initial stage followed by steady state. The friction coefficient corresponding to the steady stage of torque for all the RCF tests was

calculated and the results (Fig. 37) show that all the data are within a range 0.2-0.4 irrespective of load, creepage and type of rail steel.

4.3.5. Surface Appearance of the Failed Rollers

The surface appearances of some failed top rollers used in the experiments were examined in the SEM. It was observed that almost all of the rollers have identical surfaces containing large flakes evenly distributed around the circumference of the failed roller as shown in Fig. 38.

4.3.6. Crack Examination of Failed Rollers

Fig. 39 shows the appearance of cracks below the surface in longitudinal vertical section of rollers of different rail steels tested at a contact pressure of 1354N/mm^2. The cracks can be characterized in terms of 'network cracks', 'long cracks' (which are nearly perpendicular to the surface of the roller), and 'surface cracks' (which are linked to the surface of roller with an acute angle between them) as shown in Fig. 40.

The density of surface cracks, the depth of long cracks and the depths of network cracks were measured. The acute angle between the surface crack and the surface were also determined. The results are shown in Table 5.

The surface crack density per cycle (density of surface cracks divided by total number of cycles corresponding to each contact pressure, number of cracks/mmcycle) of the three rail steels are plotted against the contact pressure in Fig. 41. It is seen that

the three rail steels show similar trends such that the surface crack density per cycle increases with increasing contact pressure. It is also noted that STD rail steel has a higher surface crack density per cycle value than the other two rail steels over a wide range of contact pressures. Basically, HH rail steel shows a similar behavior to CrMo rail steel in this respect.

Fig. 42 shows the depths of the long cracks per cycle (in the same manner as the density of surface crack) plotted against contact pressure for the three rail steels. It is noted that the depths of the long cracks per cycle for all three rail steels increase with increasing contact pressure. In addition, the depth of long cracks per cycle of STD rail steel has a higher value than that of the other two rail steels especially at higher contact pressure. HH rail steel is slightly superior than CrMo rail steel in this respect at higher contact pressure.

The depths of network cracks for all three rail steels were plotted against the contact pressure as shown in Fig. 43. It is seen that the three rail steels exhibit similar patterns such that the depth of network cracks increases with increasing contact pressure. On the other hand, the depth of network cracks for STD rail steel is substantially greater than the other two rail steels. Furthermore, HH rail steel is marginally better than CrMo rail steel at higher contact pressures.

Fig. 44 shows the results of the measurements of the surface cracks angles for three rail steels in a range of contact pressure 1145-1450N/mm^2. It is seen that all data fall into a band of 18-28^o

degrees regardless of the contact pressure, revolutions and materials.

4.4. Wear Test

In the tests conducted at 35% creepage and contact pressures of 500-1220N/mm^2 to evaluate relative wear resistance, it was found that HH rail exhibited the lowest wear rate at all contact pressures followed by CrMo and STD rail steels as shown in Fig. 45. Also, it is noted that over a wide range of contact pressures, the wear rate for HH rail steel is very low and independent of contact pressure. Under these conditions the surfaces of HH rollers were covered by a black film. As contact pressures reached a critical level (approximately 1100 N/mm^2), the wear rate for HH rail steel increased significantly. In contrast, the wear rate of the CrMo and STD rail steels increase linearly with increasing contact pressure.

Fig. 46 shows the wear surfaces for HH rail steel. It is seen (Fig. 46 a & b) that the wear surfaces of HH rail steel (with the black film) are smoother at contact pressure 900 N/mm^2 than that of HH rail steel (without black film) at contact pressure 1220N/mm^2. Fig. 47 shows schematicaly how the torque was reduced with the formation of a black film. The torque increases to a maximum and decreases to a steady state corresponding to the formation of a black film. In the absence of a black film, torque rises and reaches a stable stage.

5. Discussion

5.1. RCF Tests for Three Rail steels

Fig. 35 shows the RCF behavior for the three rail steels. It is seen that the patterns of behavior i.e. decreasing RCF life with increasing contact pressure are the same for all three rail steels. Fig. 3 shows some previous results of RCF test which shows the same trend as the current result. Similar patterns also have been shown by many investigators [2,5, 13,31] even though those RCF tests were carried out using different materials and test rigs and various lubricants.

The RCF results show that at contact pressure in a range of 1000-1500 N/mm^2, the RCF life of HH rail steel is 2.0-2.6 (100%-160% better) and 1.1-1.5 (10%-50% better) times longer than that of STD and CrMo respectively. The RCF life of CrMo rail steel is 1.7-1.8 times longer (70%-80% better) than that of STD rail steel. This indicates that RCF resistance of HH rail steel is much higher than that of STD rail steel, and slightly better than CrMo rail steel.

Figs. 33 and 34 show the effect of the specimen orientation on RCF for CrMo rail steel and STD used rail steel. It is demonstrated that the effect of the specimen orientation on RCF is negligible. This implies that the RCF life data of HH rail steel obtained with different specimen orientation can be used to compare with that of the other two rail steels.

Table 6 shows variations of the RCF tests data for STD used rail

steels. It is seen that RCF life varies approximately ±13% (average for three tests) with respect to mean value. This implies that the RCF tests conducted on an Amsler machine exhibits an acceptable reproducibility. This provides some evidence to ensure the reliability of the RCF data obtained for the three rail steels. Even though a small amount of data were obtained at the several contact pressures, it is still reasonable to assume that the results may be applied to the other RCF tests in this experiment.

Based on regression analysis, Table 7, the relationship between the RCF life (L) and maximum contact pressure (Po) for the three rail steels can be expressed by a linear relationship (this fits the data better according to the coefficient of correlation). However, previous laboratory investigations have led to the exponential relation between RCF life and contact pressure.

Clayton and Hill [2] conducted RCF test on an Amsler machine under water lubrication condition using BS11 O rail steel (0.54wt.% C) and D tyre steel (0.64wt.% C). It was found that the power index in the exponential L-Po relation for 10% creepage is -4.2. Ollerton and Morey [13] used a specially constructed rig using rail steel under free rolling conditions and water lubrication. An approximate relationship was found in which the power index is -1.

In considering an exponential relation in this RCF test only for comparison with previous work, the power indices in the exponential L-Po relations for three rail steel at 10% creepage are -5.9 for STD, -4.5 for CrMo and -4.3 for HH rail steels respectively. Those are basically consistent with the previous result [2]. However, the

previous results [2] in terms of the RCF life at 10% creepage at contact pressure 800-1500N/mm^2 are two to four times shorter than the RCF lifes in this test. This is due to the differences in the rail steel used in the two investigations.

5.2. Appearance of Cracks in Failed Rollers

5.2.1. Correlation Between Crack Appearance and RCF Resistance for Three Rail Steels

It has been found [2] that RCF cracks were present at between 25% and 50% of the RCF life of the roller made from rail steel under water lubricated condition, which means that the RCF test involves both fatigue crack initiation and propagation. Thus both higher crack initiation resistance and lower crack propagation rate should give rise to a higher RCF life.

It may be considered that cracks initiate at a surface of a roller because no single crack could be found to be contained in the subsurface in this work. Previous work also support this point of view. It has been shown [2,5] that the cracks initiate at the surface of the roller and propagate into it as shown in Fig. 4. Moreover, it has been found [7,15] that tensile residual stress is produced very near the surface, which is a maximum, at a certain depth below a surface in the presence of a tangential force under rolling-sliding contact. As a result, cracks initiate at a surface and propagate into the subsurface.

Hence, the surface crack density per cycle, which is the number

of cracks generated in 1 mm of the surface per cycle, may be considered as an indication of surface crack initiation resistance. The surface crack density per cycle for all three rail steels (Fig. 41) shows that HH and CrMo rail steels have a higher crack initiation resistance than STD rail steel. HH and CrMo rail steels show a similar value of the surface crack density per cycle.

For the same rail steel, it is noted, Fig. 41, that the surface crack density per cycle increases with increasing contact pressure for all three rail steels. In other words, higher contact pressure causes the initiation of more cracks on the surface of a roller. Therefore, it can be said that a lower value of surface crack density per cycle gives rise to a higher surface crack initiation resistance. As a result, RCF resistance is enhanced.

Based on the trend of surface crack density per cycle data changing with different rail steel and contact pressure, this variable seems to correlate with the RCF results for the three rail steels obtained in this investigation.

In this test, it is impossible to measure a crack length to obtain a crack propagation rate because the cracks are so complicated (all cracks are connected) that a single crack could not be identified. Alternatively, the depths of the long cracks per cycle can be considered to represent a crack propagation rate.

Fig. 42. shows that the depths of the long cracks per cycle were plotted against contact pressure. It is seen that HH and CrMo rail steels have a lower crack propagation rate than STD rail steel. In addition, crack propagation resistance of HH rail steel is slightly

superior to that of CrMo rail steel except at lower contact pressure.

Furthermore, on examining the crack propagation rate in the same rail (Fig 42), it is found that the crack propagation rate increases with an increase in contact pressure for all the three rail steels. This implies that a higher contact pressure gives rise to a higher crack propagation rate which leads to a lower RCF resistance. Therefore, this could explain why the RCF resistance decreases with increasing contact pressure, Fig. 35. It is apparent that a higher crack propagation rate (a higher value of a depth of long crack per cycle) gives rise to lower RCF resistance. From this point of view, the overall pattern of the depth of the long cracks per cycle for all three rail steels appears to be consistent with the RCF results obtained.

The depths of network cracks of the three rail steels were plotted against contact pressure as shown in Fig. 43. It is obvious that the shallower depth of network crack is associated with higher RCF resistance. It is seen that HH rail steel exhibits a slightly better performance than CrMo rail steel at higher contact pressure, and STD rail steel shows the greatest depths. Also, it can be noted that for all three rail steels, the depths of network cracks increase with increasing contact pressure, which means that RCF resistance of the three rail steels decrease as contact pressure increases. Again, these trends are basically similar to the RCF results of the three rail steels.

In summary, the results of fatigue crack characterization indicate that these crack variables seem to correlate with the RCF results obtained for the three rail steels. As a result, this

supports the pattern of RCF resistance of the three rail steels such that HH rail steel is slightly superior to CrMo rail steel and much better than STD rail steel.

It should be pointed out that no attempt has been made to study quantitatively crack initiation resistance and propagation resistance in the laboratory RCF test. The current approach is an attempt to establish some possible way to describe crack initiation and propagation resistance in RCF. Certainly, more work needs to be done to throw more light on this topic.

5.2.2. Crack Appearance and the Subsurface Deformation

Fig. 39 shows the crack appearances in the failed roller for three rail steels. It is seen that surface cracks, which are the cracks near surfaces, have a certain orientation with respect to the direction of a surface traction. In addition, it is noted that the direction of the plastic flow is similar to the direction of surface cracks Fig. 39 c & d. Fig. 44 shows that all surface crack angle data fall into a band in a range of 18-28 degrees, which is consistent with previous results [2], regardless of the contact pressure, revolutions and materials.

The above relationship between the inclination of cracks, direction of plastic flow and surface traction has been observed by several investigators [2,5,17] previously. It has been demonstrated [5] that the plastic flow is easily reversed by means of changing the direction of surface traction, and as a result, the cracks change their propagation direction in accordance with the change of plastic

flow.

It has been demonstrated [17,15,16] under a similar test condition that a crack propagates at an acute angle with respect to a surface traction. The tensile residual stress is perpendicular to the direction of crack propagation. This indicates that the tensile residual stress causes the crack to propagate at an acute angle with respect to the surface. In the case of this test, the inclination of the surface cracks could be attributed to a tensile residual stresses.

However, it is seen, Fig. 39, that the orientations of some cracks in network and long cracks, which are at some depth below the surface, do not agree with the direction of the surface cracks. In other words, below a certain depth, cracks seem to propagate in different directions. This might be due to a change of stress distribution after the formation of surface cracks.

Figs. 48, 49 and 50 show the hardness distribution below the surfaces of the rollers for three rail steel. The profile of hardness distribution for all three is similar such that the hardness tends to decrease as the distance from a surface increases till reaching a stable stage. This demonstrates that there is a gradient in a subsurface deformed layer which consists of a visible plastic flow region, Fig. 39 d, and a work-hardened region which is below a visible plastic flow region.

Table 8 shows the depth of the visible plastic flow, the depth of work-hardened region (which is the depth of the total subsurface deformed layer as measured by microhardness) and the depth of the

network cracks and long cracks for the three rail steels. It is seen that the depths of the network cracks do not coincide with the depths of the visible plastic flow and work hardened region such that it is deeper than that of the visible plastic flow and shallower than that of work-hardened region. In contrast, the depths of the long cracks are basically consistent with the depth of the work hardened region.

Marich [24] conducted tests to investigate the effect of working hardening of rail steel on depth of deformation below the surface using cold rolling and found that higher strength rail steels give rise to lower depths of deformation. They then proposed that high-strength steels have a higher resistance to deformation and thus decrease the depths of subsurface deformation.

Based on the observations in this investigation and the above work, variation in the depth of network cracks and long cracks with the strength of rail steels could be reasoned to be as follows: high strength rail gives rise to high resistance to deformation which, in turn, decreases the depth of subsurface deformation. Consequently, crack initiation and propagation are restricted to this deformed layer. Thus network cracks and long cracks are formed only in this deformed layer and their depths are shallower than that of rail steel with lower strength. This can also be used to explain why increasing the higher contact pressure increases the depth of network cracks in the same rail i.e. a higher contact pressure causes a deeper deformed subsurface layer which in turn leads to the formation of deeper network cracks.

Furthermore, the depth of network and long cracks in the different

rails is relatively independent of the subsurface stress distribution in the roller. This is due to the fact that under the same contact pressure conditions, the stress distribution should be identical for the different rail steels, but the depth of network and long cracks appears to be only related to the subsurface deformation layer.

In view of the above analysis, a resistance of rail steel to deformation seems to play an important role in RCF resistance. This implies that the strength of rail steel may have a dominant effect on RCF resistance due to its connection with deformation such that the higher strength, the higher resistance to deformation.

5.2.3. Correlation Between Crack Appearance in Failed Rollers and the Crack Appearance in Rails

The crack appearances in the failed rollers show some similarity to those in rails used in service. Fig. 1 shows the crack appearances in a longitudinal section of a HH rail subjected to axle heavy loads in North America. Figs. 51, 52 and 53 show the crack appearances in a longitudinal section of German rail [24], British [3] and Japanese rails [1], which were subject to high speed traffic. It is seen that these cracks all have an acute angle to the surface, which is similar to that of the failed roller, Fig. 39. In addition, a network crack pattern can be observed in HH rail and German rails similar to that found in the RCF tests.

However, British and Japanese rails do not exhibit a network crack pattern. In addition, the long cracks connecting with the network crack observed in the failed rollers, Fig. 39, have not been

found in the above rails. Furthermore, the depths of the cracks of the rails are all greater (approximately 1.5-2 times) than that of the network crack and the long crack in the failed rollers. In spite of this, the crack appearance of the failed roller in the RCF test indicates that the laboratory RCF test basically simulates the real situation encountered by rail and wheel contact.

5.3. Effect of Mechanical Properties on RCF

On relating the RCF test results of the three rails (Fig. 35) to their mechanical properties (Table 4), it was found that the tensile strength of rails appears to play an important role in RCF resistance. It is seen that the RCF life of these rail steels increases with an increase in the tensile strength of rails.

HH rail steel has the highest tensile strength, thus it shows the longest RCF life. CrMo rail steel has slightly lower RCF life due to its marginally lower tensile strength. STD rail steel exhibits a much lower RCF life than HH and CrMo, due to its relatively lower tensile strength. these results are consistent with results from the previous work [4,6] which show that the resistance to RCF increases with increasing tensile strength.

It is interesting to note that HH rail steel which has sightly higher tensile strengths than CrMo rail steel is marginally superior to CrMo rail steel in terms of depth of network crack and crack propagation rate, Figs. 42.and 43. In contrast, STD rail steel with a much lower tensile strength exhibits a substantially greater depth of

network crack and higher crack initiation and propagation rate.

It is apparent that the shallower the network crack is, the less material loss due to RCF because it is most likely that a depth of spalling would correspond to a depth of network crack. This has an important practical significance in grinding rail surface in practice so as to eleminate defects on the surface of the rail.

RCF life for three rail steels at contact pressure 1500 N/mm^2 was plotted against their yield strength as shown in Fig. 54. Though there are only three data points, it is still seen that the RCF life increases sharply with increasing yield strength. This indicates that tensile strength may be considered as an important means to enhance RCF resistance of rail steel.

To summarize, it was found that the RCF life may be dependent upon the strength of rail steel such that the high strength of rail steel enhances RCF resistance. High strength rail steel may also gives rise to high resistance to surface crack initiation and crack propagation in RCF and decrease depth of network cracks. This may provide further evidence to support the RCF results obtained in this test for the three rail steels. Furthermore, all mechanical tests carried out to assess mechanical properties of HH rail steel show no deficiencies to explain why the HH rail steel would show poor performce in service.

It should be pointed out that a firm conclusion about a relationship between RCF resistance and tensile strength of rail steel can not be drawn because only three rail steels were tested. It is suggested that further rail steels with different tensile strengths should be

taken to further verify and quantify this relation in the future.

5.4. Effect of Microstructure on RCF

A metallurgical analysis [28] has been previously made of 33 standard carbon rail steels (data for HH and CrMo rail steels has not been found). The results are consistent with the metallurgical analysis obtained for STD rail steel in this test. It is presented as follows:

Rail	Pearlite Interlamellar Spacing (A)	Pearlite Colony Size (um)	Prior Austenite Grain Size (um)	Volume Fraction of Inclusions (%)
Pre*	2030±178**	9.8±2.1	70±5	0.30±0.07
STD	2200±200	15±2.0	60±5	0.27±0.12

*: Previous data for 33 standard carbon rail steels.

**: Mean of 33 rail steels + standard deviation.

This indicates that the methods used in the test to measure metallurgical data are reliable.

5.4.1. Pearlite Interlamellar Spacing

In the case of the pearlitic rail steels, it has been demonstrated that the strength of rail steel increases with decreasing pearlite spacing [4,6,25,26,27]. The high strength of HH rail steel can be thus attributed to the finest interlamellar spacing as found by the microstructural examination of the three rails (Table 2). The pearlite spacing of CrMo rail steel is slightly finer than that of STD rail steel. Nevertheless, CrMo rail has much higher strength than STD rail. This may be due to alloying addition in CrMo rail resulting in solid solution strengthening. It has been shown that the Cr and Mo addition to pearlitic steel can enhance the strength of a steel [24,42] by reducing pearlite spacing and solid solution strengthening. Hence it may be considered that both pearlite spacing and alloying addition contribute to the high strength of CrMo rail steel.

Based on the above, it is expected that the pearlite interlamellar spacing has a dominant effect on the RCF resistance and the factor of alloying addition should also be taken into account, due to their contribution to strength.

Fig. 55 shows that the RCF life at contact pressure 1500 N/mm^2 increases with decreasing pearlite spacing. As mentioned above, a fine pearlite spacing gives rise to high tensile strength. Thus Fig. 55 is consistent with Fig. 54. In other words, RCF resistance increases with increasing tensile strength of pearlitic steel which can be achieved by reducing pearlite spacing and/or alloying addition. It is therefore suggested that reducing pearlite spacing by heat treatment and alloying addition have very important practical significance

in improving the RCF resistance of rail steel.

5.4.2. Prior Austenite Grain Size

It is noticed from (Table 2) that CrMo and STD rail steels have similar grain sizes, but the RCF resistance of the former is much higher than that of the latter. This indicates that there is no significant influence of prior austenite grain size on RCF. Previous experimental results [26] statistically show that the strength of pearlitic steel is mainly attributed to the fine pearlite spacing rather than the prior austenite grain size. The result of tensile tests (Table 4) indicates that CrMo and STD rail steels of similar grain sizes have different tensile strengths-the former having a much higher strength than the latter. This shows that the grain size has a negligible effect on the tensile strength as compared to the pearlite interlamellar spacing and alloying addition. Thus, its effect on RCF resistance is negligible.

Table 3 shows that HH rail has a higher toughness at the room temperature than the other two rails. This is because the grain size of HH rail is smaller. It is not surprising that CrMo and STD rails have similar CVN impact values since they have similar grain size (Table 2).

Thus, it is suggested that Charpy V-notch Impact property is affected mainly by the prior austenite grain size of the rail steel. This is consistent with previous studies [26,29,30] which showed that a finer prior austenite grain size in pearlitic steel gives rise to a higher dynamic fracture toughness.

Furthermore, the values of CVN Impact data of all three rails are very close at $-22^{o}C$ (Table3). It seems that the head hardened rail is more sensitive to a change of temperature in CVN impact test than the other two rails.

5.4.3. Pearlite Colony Size

Due to the number of variables involved , the effect of pearlite colony size could not be clearly understood. However, it has been statistically shown [26] that the pearlite colony size has only a minor influence on the strength of pealitic steel. Hence its effect on the RCF may be relatively small.

Table 3 shows that even though CrMo steel has smaller colony size than STD rail steel (Table 2), their CVN impact values are similar. This shows that the pearlite colony size has a minor influence on the toughness of the rail steel as compared to the effect of prior austenite grain size.

This result is consistent with previous works [26,30] which shows that pearlite colony size of pearlitic steel has an insignificant effect on CVN Impact behavior comparing with prior austenite grain size.

5.4.4. Inclusion Contents

Inclusions are generally considered as potential crack initiation sites in the RCF process [7,43]. The lower inclusion contents in HH and CrMo rail steel as shown in (Table 2) could provide fewer crack initiation sites in these rail steels during the RCF tests.

This could contribute to the higher RCF resistance to some degree. Nonetheless, the inclusion contents of the three rail steels indicate that HH rail steel is slightly better or as good as CrMo rail steel and much better than STD rail steel in this respect.

In summary, it could be said that the pearlite interlamellar spacing has the most dominant effect on the RCF due to its contribution to the strength of the rail steel. Again, the pearlite interlamellar spacing of the three rail steels revealed here gives the evidence to support the RCF results obtained for the three rail steels. Moreover, the microstructural examination of the three rail steels does not reveal any deficiencies to account for HH rail steel premature failure in service.

However, it should be noted that no firm conclusions between microstructural parameters of rail steels and RCF resistance can be drawn due to the small amount data and the numerous variables involved.

5.5. Wear Under Rolling-Sliding Condition

Fig. 45 shows that the wear rate for CrMo and STD rail steels increases linearly with increasing contact pressure. Similar linear relationships between wear rate of rail steel and contact pressure have been obtained in previous investigations [37,39], Figs. 6 and 7. Comparing with the wear rate (Fig. 7) obtained from approximately the same test conditions (35% creepage and over a range of contact pressure 500-1100N/mm^2) and almost the same rail steel, the wear rate

of this test is 1.1-1.6 (9%-60%) times higher than that of the previous test. This large scatter is not understood.

It is seen that STD rail steel has the highest wear rate and HH rail steel has the lowest. This indicates that the wear resistance of rail steel may be directly related to its strength (Table4) such that the higher strength of the rail steel, the better its wear resistance. This is consistent with previous results [5,6] obtained under similar test conditions, which demonstrated that wear resistance is improved as the tensile strength increases.

The results of the wear tests (Fig. 45) show that HH rail steel exhibits a dramatically different wear behavior from CrMo and STD rail steels under the same test conditions. It is seen that the wear rate of HH rail steel changes suddenly at a contact pressure of approximately 1100N/mm^2. This suggests that HH rail steel apparently goes through a totally different wear mechanism.

The wear of HH rail steel seems to be similar to Type I wear [41], which is of very low wear rate and relative smooth wear surface, below a certain contact pressure Fig. 46 a. Beyond a certain contact pressure, it seems that HH rail steel encountered Type III wear, which involves material being considerably gouged out of the surface, Fig. 46b.

It can be also noted that there is a critical contact pressure (1100 N/mm^2) below which the wear is Type I wear, and above which Type III wear controls wear behavior. Below a critical contact pressure, the wear involves the formation of a black film which prevents HH rail steel from severe wear and gives rise to excellent wear resistance.

It has been shown [39,44,45,46,47] that wear in steel involves the formation of an oxide film on the wear surface which protects further wear. It is thus reasonable to assume that the black film may be oxide film.

In addition, It has been proposed [48] that the strain hardened layer provides adequate strength to support the oxide film. Beyond a critical load, the supporting layer breaks down and the material starts to undergo severe wear. It has been also suggested [44] that oxide films can inhibit the deformation of asperities and reduce the surface's adhesivity, which reduces the coefficient of friction.

Based on the above, the reason for the high wear resistance of HH rail steel can be suggested as follows: head hardened rail steel has a higher strength which provides higher resistance to deformation. This provides adequate strength to support the formation of an oxide film. After an oxide film is formed, the wear surface becomes smoother (Fig. 46 (a)) and a high friction reduces (Fig. 47). As a result, this diminishes the tangential force, which is mainly responsible for subsurface deformation and material loss. Consequently, wear resistance is enhanced.

As contact pressure increases, the film mechanically breaks down [39,49] and also, the working hardening layer can not support a formation of the oxide film any more. As a result, Type III wear takes place. This is why the wear rate of the head hardened rail steel dramatically increases at higher contact pressure.

It is interesting to note that under identical test conditions, there was no formation of black film on CrMo and STD rail steels

during tests. Therefore, it is suggested that there is a critical strength of rail steel, below which the protective film can not form. In other words, the formation of protective film needs a support of adequate strength and the strength of CrMo and STD rail steels is not enough to support its formation.

It seems that there is a connection between wear resistance and RCF resistance. This is because that the wear resistance of three rail steels is consistent with their RCF resistance. In other word, a higher wear resistance may give rise to a higher RCF resistance vice verse. Also, wear resistance depends mainly on tensile strength, and so does RCF resistance, based on the above discussion. This indirectly relates the wear resistance to the RCF resistance.

5.6. Summary and Possible Explanations for HH rail failure in Service

The main objective of this work was to evaluate the RCF resistance of HH rail steel with respect to CrMo and STD rail steels. The overall experimental results indicate that HH rail steel is superior to the other two rail steels from this point of view. According to the experimental results, no metallurgical and mechanical deficiencies have been found for HH rail steel in comparison with the other two rail steels in the scope of this test.

Hence, it could be that other factors involved account for HH rail steel failure in practice. First, HH rail steel has a higher strength than CrMo rail steel. therefore, it is more difficult for HH

rail steel to deform during wheel/rail contact than for CrMo rail steel. On the other hand, the original rail surface profile is the same for the both rail steels. However, during service, CrMo rail steel could be subjected to more deformation than HH rail steel. This may lead to larger contact area between wheel/rail contact for CrMo rail steel. Consequently, contact pressure encountered by CrMo rail steel would be reduced. As compared to CrMo rail steel, HH rail steel would be subjected to a higher contact pressure due to a relative smaller change of contact area. As a result, HH rail steel showed lower RCF life than CrMo rail steel in service.

Second, HH rail steel could be subjected to less surface wear than CrMo rail steel because of its higher wear resistance. Based on previous observations [1,2] and the present experimental results, cracks initiate at a surface and lead to RCF failure. Thus more cracks in a CrMo rail surface would be eliminated by the wear process as compared to HH rail steel. This could enhance RCF resistance of CrMo rail steel in practice.

The combination of these two factors could possibly explain the reported poor performance of HH rail steel in service. It is obvious that further field work needs to be done to explore the causes for HH rail steel failure.

CONCLUSIONS

The evaluation of the RCF resistance of three different eutectoid rail steels (HH, CrMo and STD) in a laboratory test was carried out. The characterization of the crack appearance of the failed rollers and the correlation with RCF resistance of the three rail steels have been made. Supporting mechanical property and microstructural parameter evaluation were conducted. The wear resistance of the three rail steels was also investigated. According to the experimental results and analyses, the conclusions can be drawn as follows:

1. The head hardened (HH) rail steel has the highest RCF resistance followed by CrMo rail steel and STD rail steel.
2. A higher RCF resistance gives rise to a shallower depth of network crack in failed roller.
3. Resistance to crack initiation and propagation decreases with increasing contact pressure. The depth of the network cracks increases with increasing contact pressure.
4. The surface crack angles for all three rail steels fall into a band in a range of 18-28 degree regardless of contact pressure, revolutions and materials.
5. HH rail steel does not exhibit microstructural and mechanical deficiencies by comparison with the other two rail steels in the test carried out.
6. HH rail steel has the highest wear resistance as compared with the other two rail steels followed by CrMo rail steel and STD rail steel.

7. Wear resistance is related to RCF resistance such that the higher wear resistance, the higher RCF resistance and vice versa.
8. For HH rail steel, there is a critical contact pressure below which Type I wear is dominant and above which Type III wear takes place.
9. Network cracks and long cracks can only develop within work-hardened region below a surface of a roller.

REFERENCES

1. H. Masumoto, D. Sugino, S. Nisida, et al., Some features and metallurgical considerations of surface defects in rail due to contact fatigue, Rail Steels-Developments, Processing, and Use, ASTM Special Technical Publication 644, Pa., 1976, p.233-256.

2. P. Clayton and D. N. Hill., Rolling Contact Fatigue of a Rail Steel, Wear. 117 (1987)-334.

3. P. Clayton and M. B. P. Allery, Metallurgical aspects of surface damage problems in rails, Can. Metall. Q., 21(1) (1982) 31-46

4. K. Sugino, H. Kageyama and H. Masumoto., Development of weldable high-strength steel rails, Paper, Wear Conference.

5. H. Ichinose, J. Takehara, N. IWasaki and M. Ueda., An investigation contact fatigue and wear resistance behavior in rail steels, Perth Australia 18-22nd, September 1978.

6. H. Masumoto, et al., Development of Wear Resistant and Anti-Shelling High Strength Rails in Japan, Session 212 ,Paper H.1, 1978.

7. H. Muro, T. Tsushima and M. Nagafuchi, Initiation and propagation of surface cracks in rolling fatigue of high hardness steel.

8. J. Halling, Principles of Tribology, The Macmillan Press Ltd, London, 1979, p.174.

9. Horst Czichos, Tribology, Elsevier Scientific Publishing Company, Netherlands, 1979, p.105.

10. K. L. Johnson., One hundred years of Hertz contact, Proc Instn Mech Engrs Vol 196. 1982.

11. Hans Krause and Gerhard Poll., The influence of tangential tractions at the aurface on the atresses in contacting bodies during rolling-sliding contact et al., Wear, 88, 1983, p.221-232.

12. S. Timoshenko and J. N. Goodier, Theory of elasticity, McGraw-Hill, New York, 1951.

13. H. Ollerton and J. W.W. Morey, Fatigue strength of rail steel in rolling contact,Proc. Symp. on Fatigue in Rolling Contact, March 28, 1963, Institution of Mechanical Engineers, London, 1963.

14. K. Fujita and A. Yoshida., Effect of hardness difference on the surface durability and surface failure of steel rollers, Wear, 67, 1981, p.187-200.

15. A. V. Olver and H. A. Spikes, The residual stress distribution in a plasticlly deformed model asperity, Wear, 107 (1986) 151-174.

16. A. V. Olver, Micropitting and asperity deformation, Developments in Numerical and Experimental Methods Applied to Tribology Proc. 10th Leeds-Lyon Symp. on Tribology, Lyon, september 1983, Butterworths London, 1984.

17. K. Maeda, N. Tsushima and H. Mure, The inclination of cracking in the peeling failure of a ball bearing steel and its relation to the inclination of the principal residual stress, Wear, 65(1980), 175-191.

18. P. H. Dawson., Effect of metallic contact on the pitting of lubricated rolling surfaces, J. Mech Eng Sci, Vol. 4, No.1, 1962, p.16-21.

19. J. O. Smith, Chang Deng Liu and Urbana,Ill., Stresses due to tangential and normal loads on an elastic solid with application to some contact stress problems Appl. Mech., 20, 1953, p.157-166.

20. H. Masumoto, K. Sugino, S. Nisida, R. Kurihara and S. Matsuyama. ASTM Committee A-i Proc Symp on Rail Steels-Developments, Processing and Use. 17-18th November 1976.

21. J. Akaoka and K. Hirasawa., Fatigue phenomena under rolling contact accompanied with sliding, Bulletin of JSMe, Vol. 2, No. 5, 1959.

22. K. L. Johnson., Correlation of theory and experiment in research on fatigue in rolling contact, Instn Mech Engrs, p.155-159.

23. J. M. Barsom and E. H. Imhof, Jr., Fatigue and fracture behavior of carbon-steel rails Rail Steels-Developments, Processing, and Use, ASTM Special Technical Publication 644, Pa., 1976, p.387-410.

24. S. Marich and P. Curcio., Development of high-strength alloyed rail steels suitable for heavy duty applications, Rail Steels-Developments, Processing, and Use, ASTM Special Technical Publication 644, Pa., 1976, p.167-198.

25. H. Sunwoo, M. E.Fine, M. Meshii, and D. H. Stone, Met. Trans., 13A (1982) p.2035-2047.

26. J. M. Hyzak and I. M. Bernstein., The role of microstructure on the strength and toughness of fully pearlitic steels, Met. Trans., Vol 7A, 1976, p.1217.

27. D. H. Stone and R. K. Steele., the effect of Mechanical Properties upon the performance of railroad rails, Rail Steels-Developments, Processing, and Use, ASTM Special Technical Publication 644, Pa., 1976, p.21-48.

28. D. E. Sonon, J. V. Pellegrino, and J. M. Wandrisco., a Metallurgical examination of control-cooled, carbon-steel rails with service-developed defects Rail Steels-Developments, Processing, and Use, ASTM Special Technical Publication 644, Pa., 1976, p.99-118.

29. Yong-Jin Park and I. M. Bernstein., Mechanism of cleavage fracture in fully pearlitic 1080 rail steel Rail Steels-Developments, Processing, and Use, ASTM Special Technical Publication 644, Pa., 1976, P287-303.

30. G. K. Bouse, I. M. Bernstein, and D. H. Stone., Role of alloying and microstrcture on the strength and toughness of expeimental rail steels, Rail Steels-Developments, Processing, and Use, ASTM Special Technical Publication 644, Pa., 1976,p.145-162.

31. R. E. McKelvey and C. A. Moyer, the Relation between critical maximum compressive stress and fatigue life under rolling contact, Proc. Symp. on Fatigue in Rolling Contact, London, 1963.

32. A. W. Bush, P. H. Skinner and R.D. Gibson., Surface roughness effects in point contact elastohydrodynamic lubrication, Wear, 83, 1982, p.285-303.

33. C. J. Hooke., The elastohydrodynamic lubrication of a cylinder on an elastomeric layer, Wear, 111, 1986, p.83-99.

34. S. Way, Pitting due to rolling cntact, Trans A.S.M.E.J. App Mch 57, 1935, p.49.

35. K. L. Johnson and J. A. Greenwood, Private Communication.

36. P. H. Dawson, The pitting of lubricated gear teeth and rollers, J. Mech Eng Sci, Vol. 4, No. 1, 1962, p.1-11.

37. D. Danks and P. Clayton., Comparison of wear processes for eutectoid rail steels in field and laboratory tests, Wear, 120 (2), 1987.

38. T. M. Beagley., Severe wear of rolling/sliding contacts, Wear, 36, 1976, p.317-335.

39. P. J. Bolton, P. Clayton., Rolling-sliding wear damage in rail and tyre steels, Wear, 93, 1984, p.145-165.

40. H. A. Spikes, Wear in rolling contacts, Wear, 112, 1986, p.121-144.

41. G.F. Vander Voort and A. Roosz, Measurement of the Interlamellar Spacing of Pearlite, Metallography 17:1-17 (1984).

42. Y. E. Smith and F. B. Flectcher., Alloy steels for high-strength, as-rolled rails, Rail Steels-Developments, Processing, and Use, ASTM Special Technical Publication 644, Pa., 1976, p.212-233.

43. Metals Handbook, Ninth Edition, Vol. 11, American Society for Metals, OHIO, 1986, p.483-514.

44. A. W. Batchelor, The relationship between oxide films and the wear of steels, Wear, 113, 1986, p.203-223.

45. J. Molgaard, A discussion of oxidation, oxide thickness and oxide transfer in wear, Wear, 40(1976) 277-291. 1983.

46. V. Aranov, Kinetic characteristics of the transformation and failure of the surface layers under dry friction, Wear,41 (1977) 205-212.

47. F. H. Stott, J. Glascott and G. C. Wood, Factors affecting the progressive development of wear-protective oxides on iron-base alloys during sliding at elevated temperatures, Wear, 97 (1984), 93-107.

48. N. C. Welsh., The Dry Wear of Steels, Roy Soc London Phil Trans, Vol. 257. A.1077, Jan,1965. P 51-70

49. T. F. J. Quinn, J. L. Sullivan and D. M. Rowson, Origins and development of oxidational wear at low ambient temperatures, ASLE Trans., 10, 1967, p.158-168.

50. A. V. Olver, Micropitting and asperity deformation. In D. Dowson and M. Godet (eds.), Developments in numerical and experimental methods applied to tribology, Proc. 10th Leeds-Lyon Symp. on Tribology, Lyon, September 1983, Butterworths London, 1984.

51. D. J. Alexander and I. M. Bernstein., Microstructural control of flow and fracture in pearlitic steels., Met. A. 8504-72-0174, P 243-257, 1984.

Table 1 Chemical compositions of Rail and Wheel Steels

	C	Al	Cr	Cu	Mn	Mo	Ni	P	Si	S	V
HH	0.75	0.007	0.01	0.01	0.82	0.01	0.01	0.009	0.20	0.019	0.009
CrMo	0.71	0.008	0.57	0.26	0.59	0.21	0.10	0.005	0.41	0.017	0.002
STD	0.63	0.014	0.14	0.29	0.88	0.05	0.13	0.005	0.17	0.010	0.002
STD'*	0.79	0.011	0.02	0.12	0.71	0.005	0.07	0.01	0.11	0.05	0.009
Wheel	0.69	0.038	0.028	0.066	0.678	0.008	0.01	0.019	0.049	0.024	0.011

*: O.G.C. rail x60 (STD, O.G.C. rail x35)

Table (2) Metallographic Data

Rail	Pearlite Interlamellar Spacing (A)	Pearlite Colony Size (um)	Prior Austenite Grain Size (um)	Volume Fraction of Inclusions (%)
HH	1200±100*	6.7±0.4	34±4	0.11±0.07
CrMo	1900±200	9.4±0.9	62±3	0.13±0.07
STD	2200±200	15.0±1.0	60±5	0.27±0.12

*: Mean ± 95% confidence interval

Table (3) Charpy V-notch Impact Properties

Rail	(22°C)* (ft-lbs)	(-20°C) (ft-lbs)	PmE** (22°C) (ft-lbs)	PmE(-20°C) (ft-lbs)
HH	7.2±0.5***	3.2±0.4	6.0±0.4	2.4±0.3
CrMo	4.0±0.9	4.0±0.4	3.4±0.8	3.0±0.1
STD	4.7±0.1	3.0±0.7	3.1±0.1	2.1±0.9

*: Total Energy
**: Premaximum Load Energy
***: Standard Deviaton

Table (4) Mechanical Properties

Rail	Hardness RC	2% Yield Strength (ksi)	Ultimate Strength (ksi)	Reduction in area %	Elongation %
HH	39.3±0.5*	123.2±5.9	180.5±4.1	36.2±4.2	13.3±1.0
CrMo	35.3±0.5	112.6±9.1	170.9±3.2	28.3±3.2	12.4±1.1
STD	28.0±1.0	89.7±3.6	141.3±0.3	18.9±2.8	11.5±0.6

*: Standard Deviation

Table (5) Measurement of Cracks in Failed Rollers

Rail	Contact Pressure (N/mm2)	Network Crack Depth Mean (um)	Long Crack Depth Mean (um)	Surface Crack Density (cracks/mm)	Surface Crack Angle (degree)	Revolutions
HH	1448	153±25*	234±53	7.1	23±3	493,140
HH	1354	146±23	488±70	11.5	22±4	680,820
HH	1254	105±38	493±55	12.1	24±6	1,214,180
HH	1145	69±14	172±56	17.1	20±4	1,529,940
CrMo	1448	301±41	613±43	7.2	18±2	339,650
CrMo	1354	165±64	464±85	8.1	19±5	507,360
CrMo	1254	133±35	280±52	8.0	20±4	912,490
CrMo	1145	72±15	169±31	6.5	22±4	1,406,580
STD	1448	439±66	781±135	3.0	24±5	128,140
STD	1354	408±55	814±88	11.4	28±4	306,710
STD	1254	320±59	689±82	14.0	20±5	517,730
STD	1145	265±57	574±127	6.2	19±4	564,340

*: Standard Deviation

Table 6. Reproducibility of RCF Tests

roller	Contact Pressure (N/mm^2)	Mean	Standard Deviation
Vertical	1354	157565	27635
Vertical	1254	298205	11815
Horizontal	1354	201310	26569

Table 7. Regression Analysis

Specimen	r^{2*} (linear)	r^2 (exponential)
HH	0.98	0.90
CrMo	0.89	0.84
STD	0.95	0.91

*: Coefficient of Correlation

Table 8. Measurement of Cracks and Deformation in Failed Rollers

Rail	Network Crack Depth Mean (um)	Long Crack Depth Mean (um)	Work-Hardened Region Depth (um)	Visible Plastic Flow Depth (um)
HH	146±23*	488±70	480	50±6
CrMo	165±64	464±85	470	121±13
STD	408±55	814±88	800	229±15

*: Standard Deviation

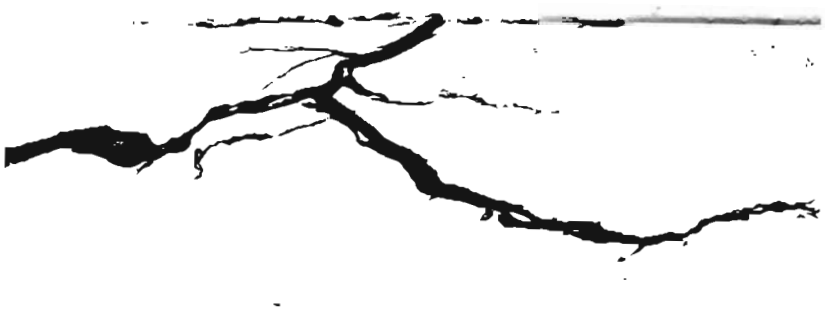

FIGURE 1. CRACK APPEARANCE IN A LONGITUDINAL SECTION OF HH RAIL USED IN SERVICE

OREGON GRADUATE INSTITUTE

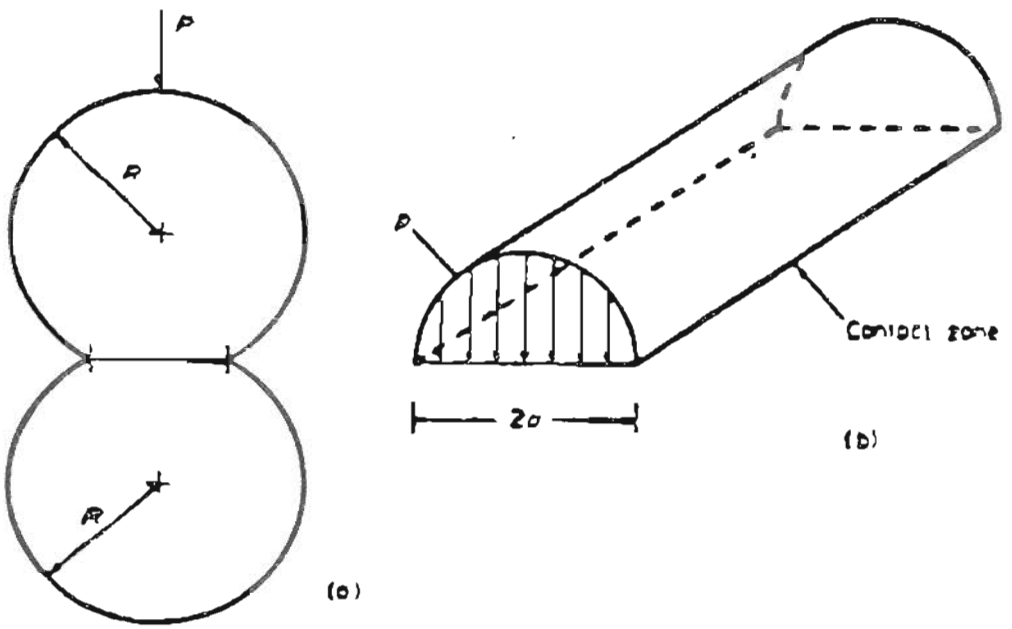

FIGURE 2. CONTACT PRESSURE DISTRIBUTION (p) FOR THE CONTACT OF TWO CYLINDERS, P: NORMAL LOAD 2a: CONTACT WIDTH

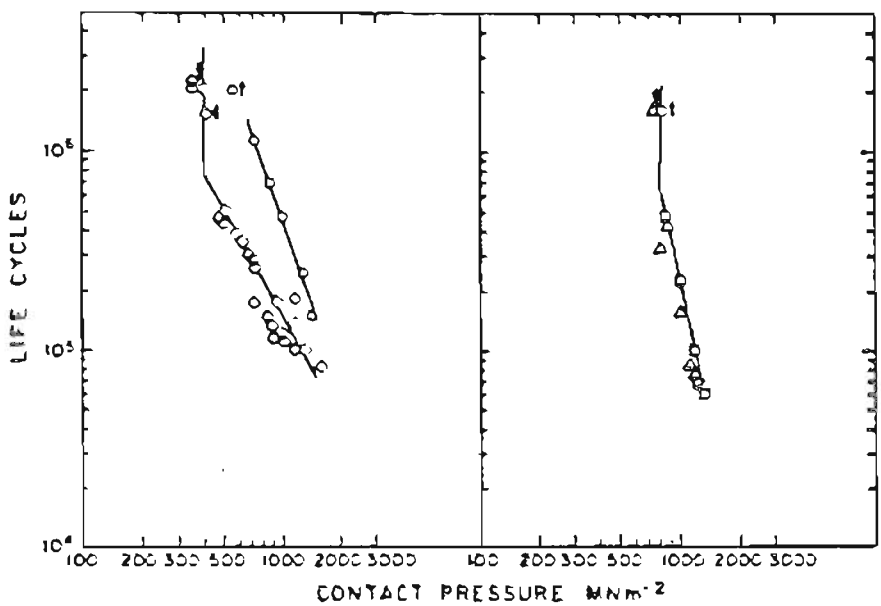

FIGURE 3. RCF LIFE AS A FUNCTION OF CONTACT PRESSURE AT DIFFERENT CREEPAGES [2]

□ 5%, △ 10% [15]

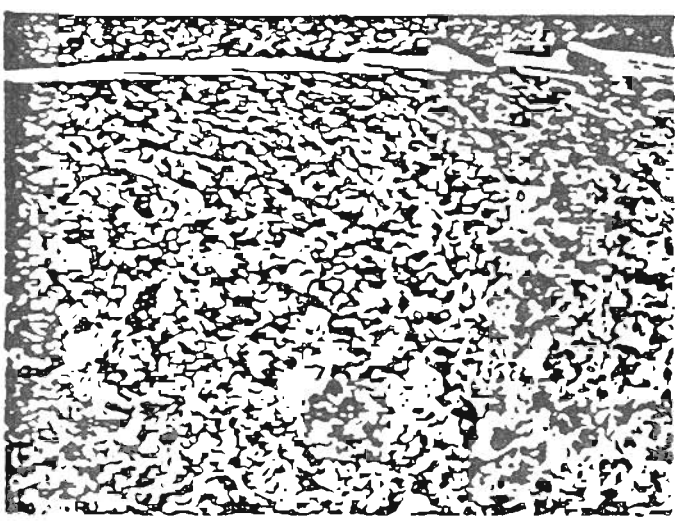

FIGURE 4. RCF CRACKS AND PLASTIC FLOW IN 0.5 WT.%C RAIL STEEL [2]

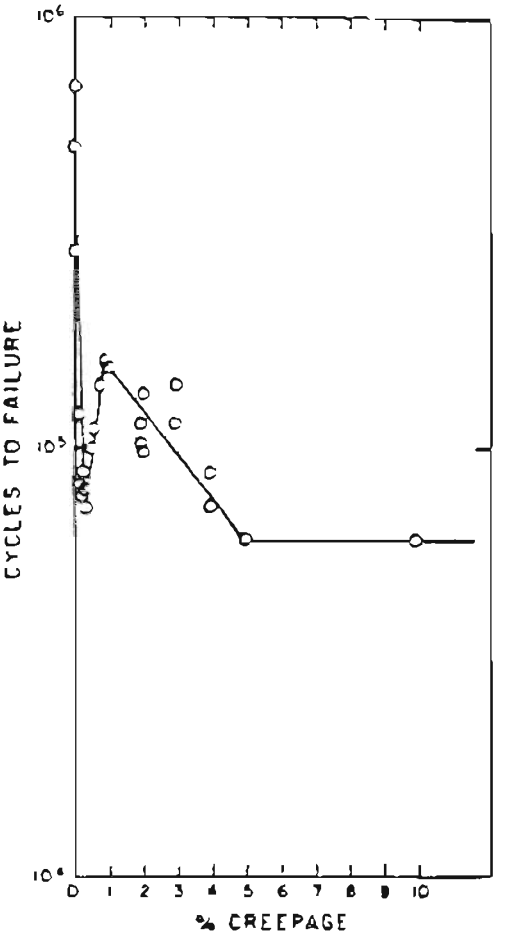

FIGURE 5. EFFECT OF CREEPAGE ON RCF LIFE UNDER WATER LUBRICATED CONDITIONS [2]

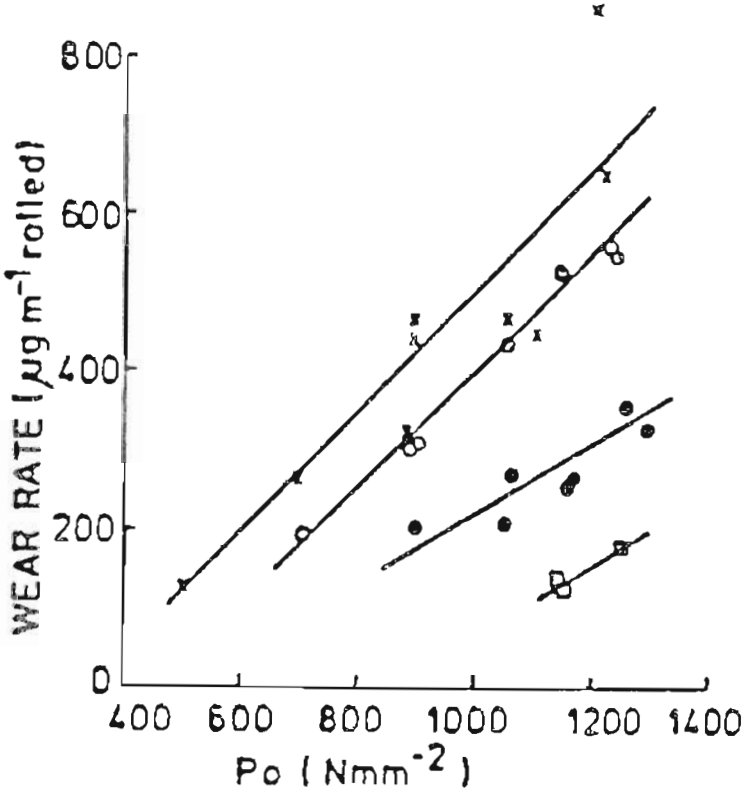

FIGURE 6. WEAR RATE OF UICA RAIL STEEL AS A FUNCTION OF CONTACT PRESSURE AT VARIOUS CREEPAGES [39]

×, 10%; ⊙, 7%; ⊛, 5%; ⊡, 3%;

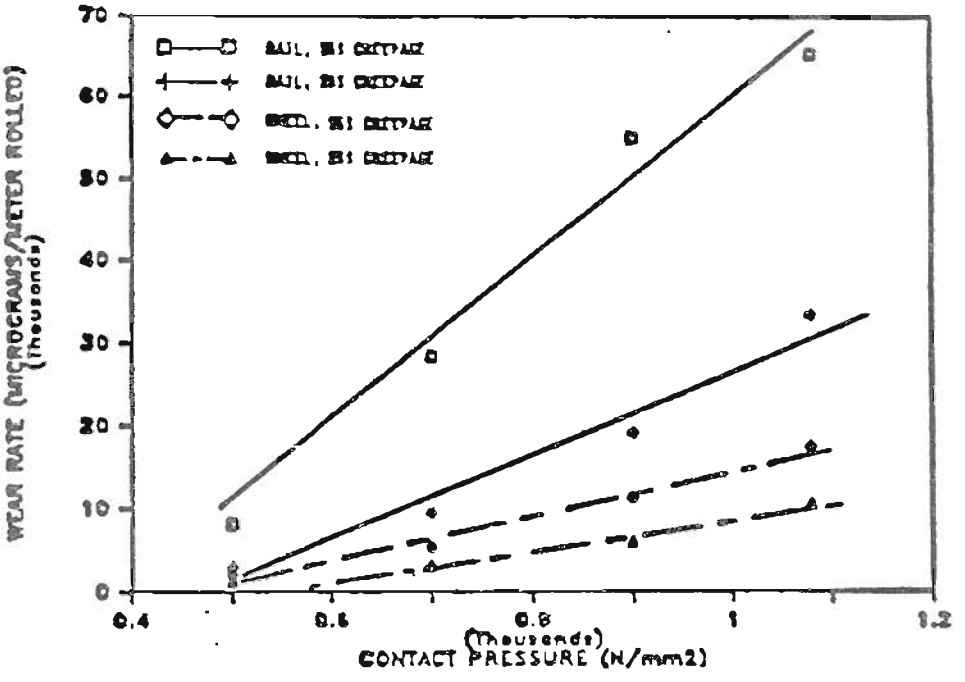

FIGURE 7. WEAR RATE OF RAIL AND WHEEL STEELS AS A FUNCTION OF CONTACT PRESSURE AT 25% AND 35% CREEPAGES [39]

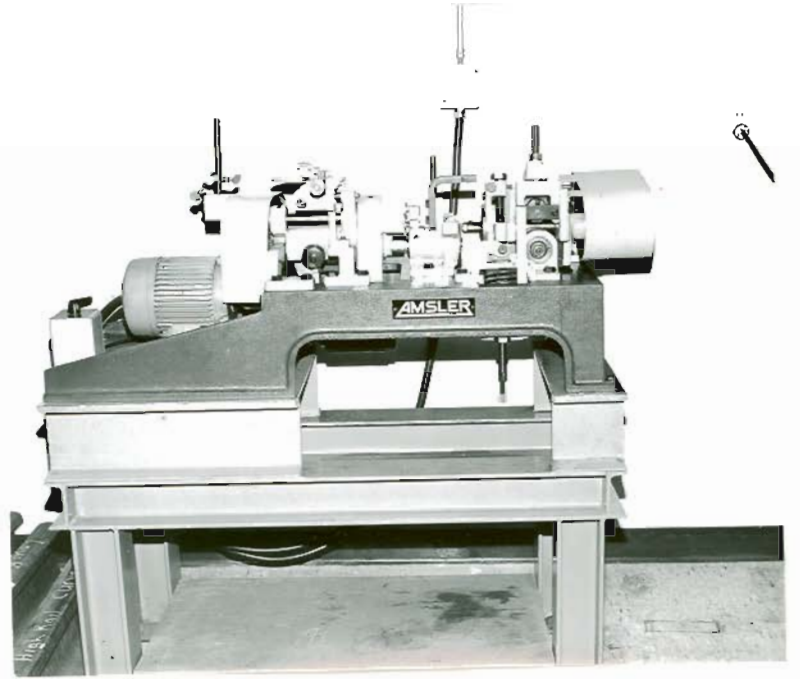

FIGURE 8. AMSLER TESTING MACHINE (MODEL A135)

OREGON GRADUATE INSTITUTE

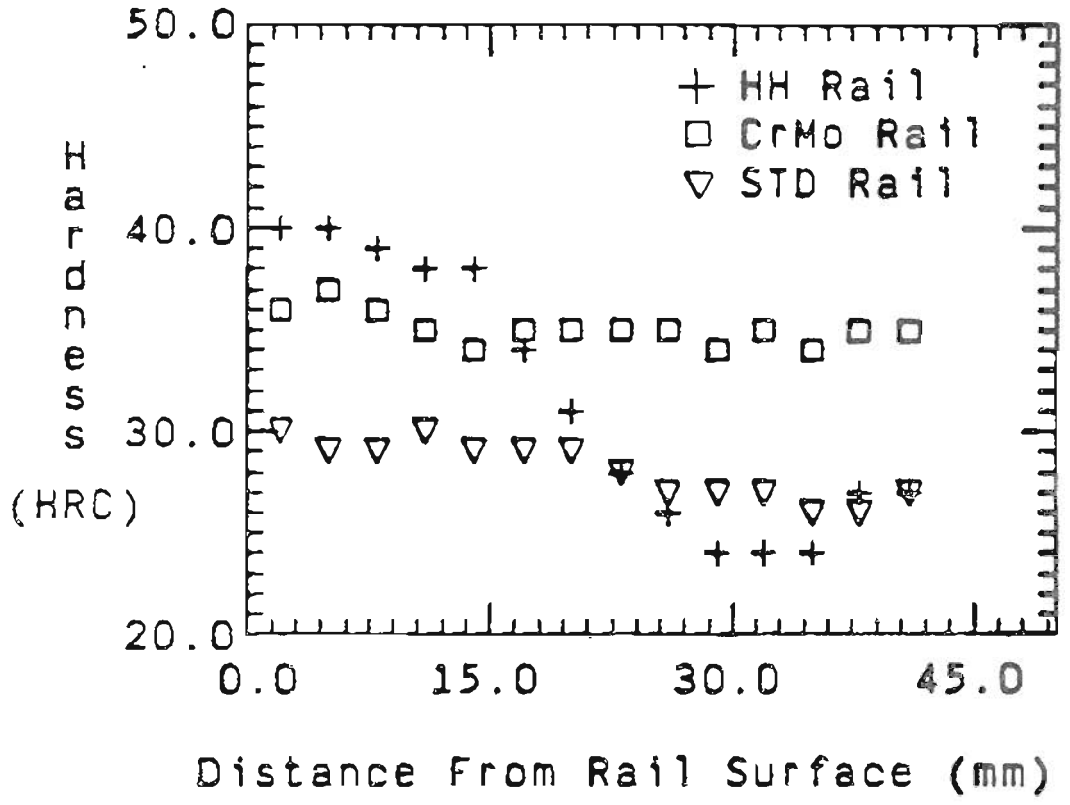

FIGURE 9. HARDNESS PROFILE IN A TRANSVERSE RAIL HEAD SECTION FOR THREE RAILS

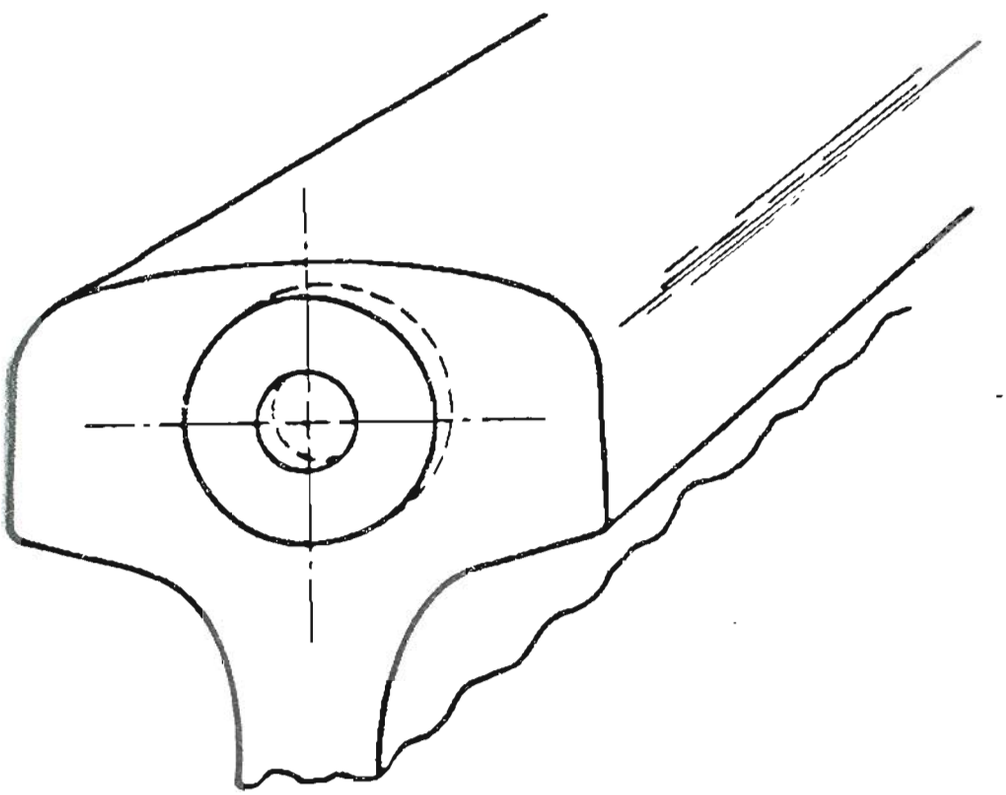

FIGURE 10. SCHEMATIC REPRESENTATION OF ROLLERS TAKEN FROM RAIL

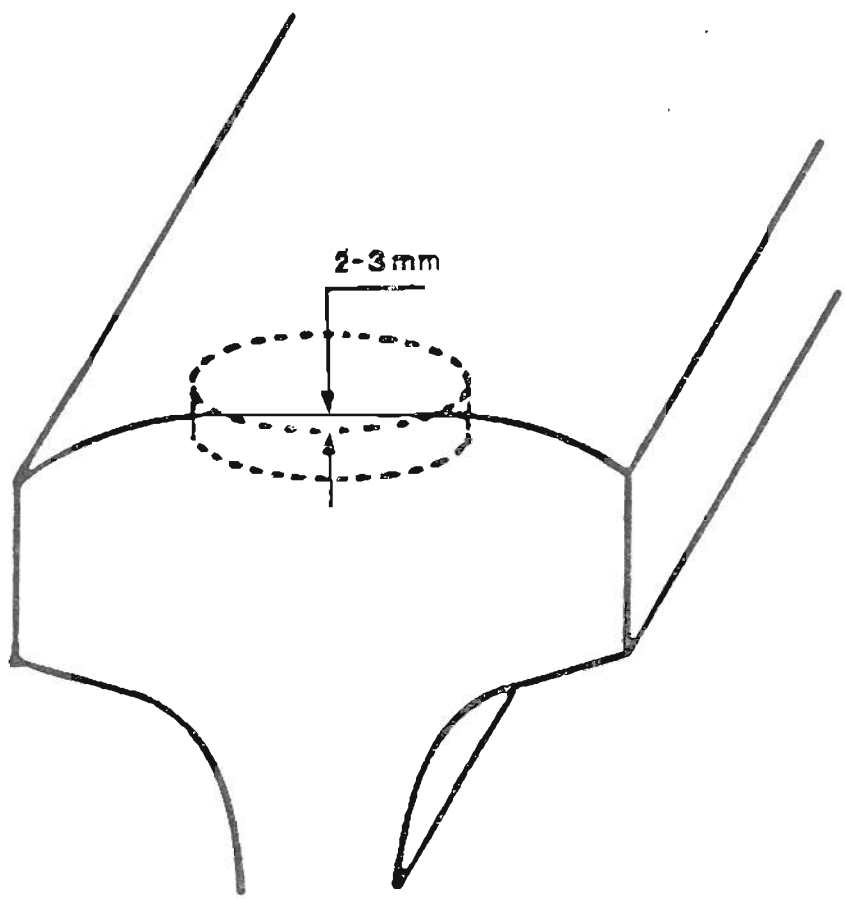

FIGURE 11. SCHEMATIC REPRESENTATION OF ROLLERS TAKEN FROM HH RAIL

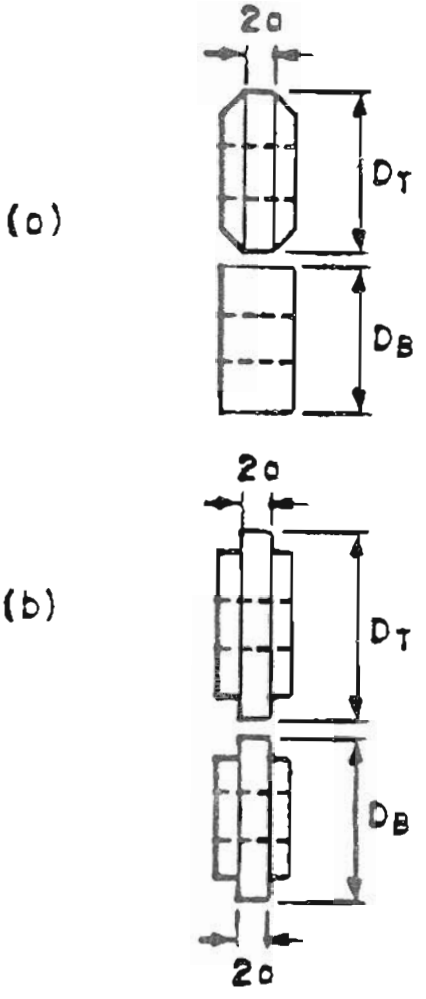

2a = CONTACT WIDTH
D_T - 35.00 mm
D_B - TO SUIT CREEPAGE

FIGURE 12. SPECIMEN GEOMETRY (a) 2a = 4mm
(b) 2a = 5mm

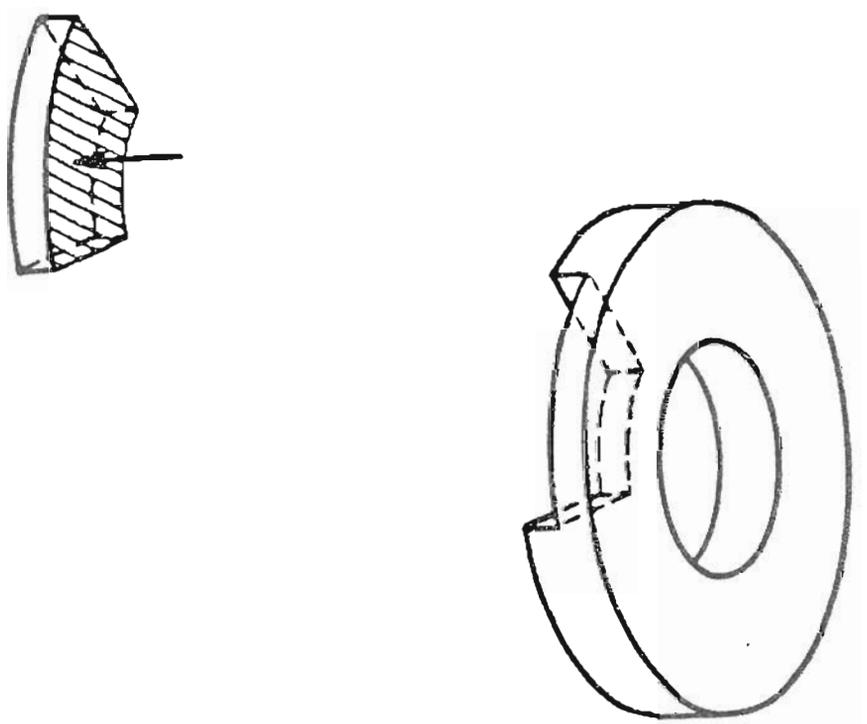

FIGURE 13. SCHEMATIC REPRESENTATION OF SPECIMEN FOR CRACK EXAMINATION TAKEN FROM A LONGITUDINAL SECTION OF FAILED ROLLER

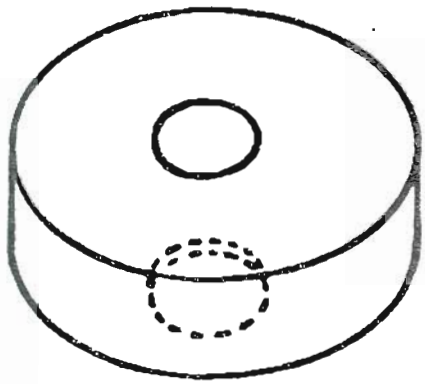

FIGURE 14. SCHEMATIC REPRESENTATION OF BOTTOM ROLLER TAKEN FROM A WHEEL FOR WEAR TESTS.

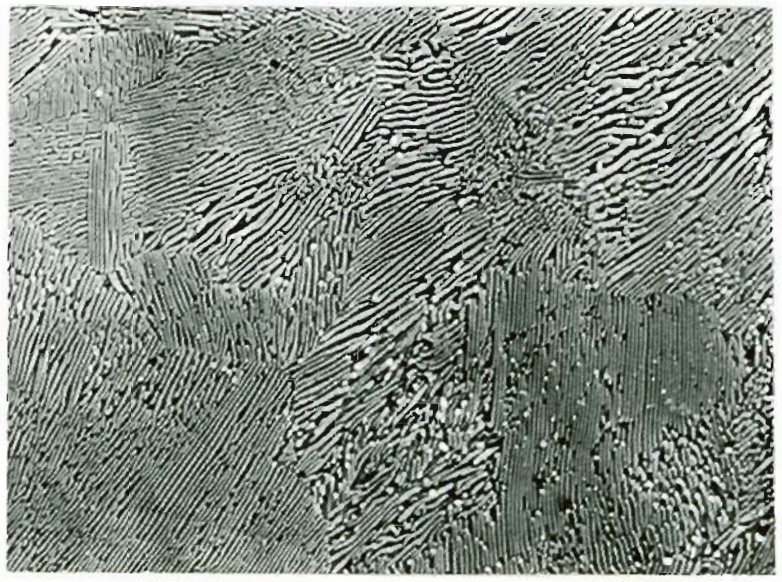

(a)

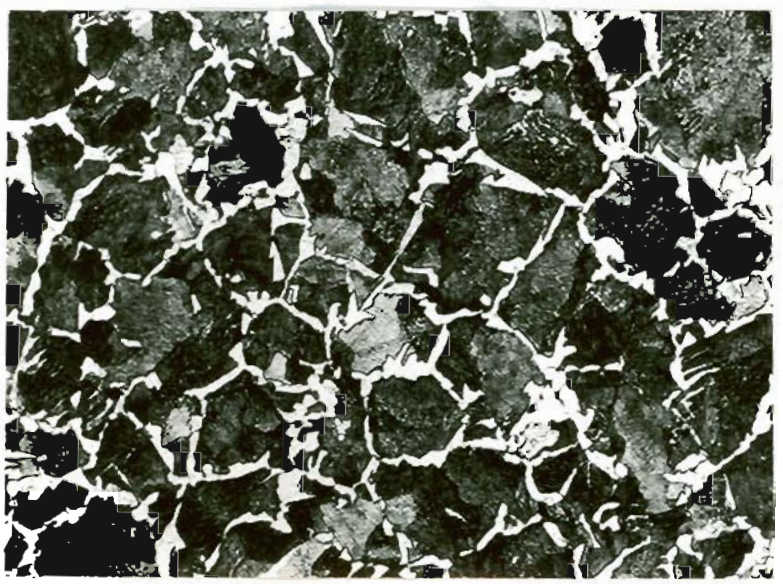

(b)

FIGURE 15. (a) SCANNING ELECTRON MICROGRAPH OF PEARLITIC MICROSTRUCTURE FOR STD RAIL, (b) OPTICAL MICROGRAPH OF PRIOR AUSTENITE GRAINS FOR STD RAIL MAG 200X

OREGON GRADUATE INSTITUTE

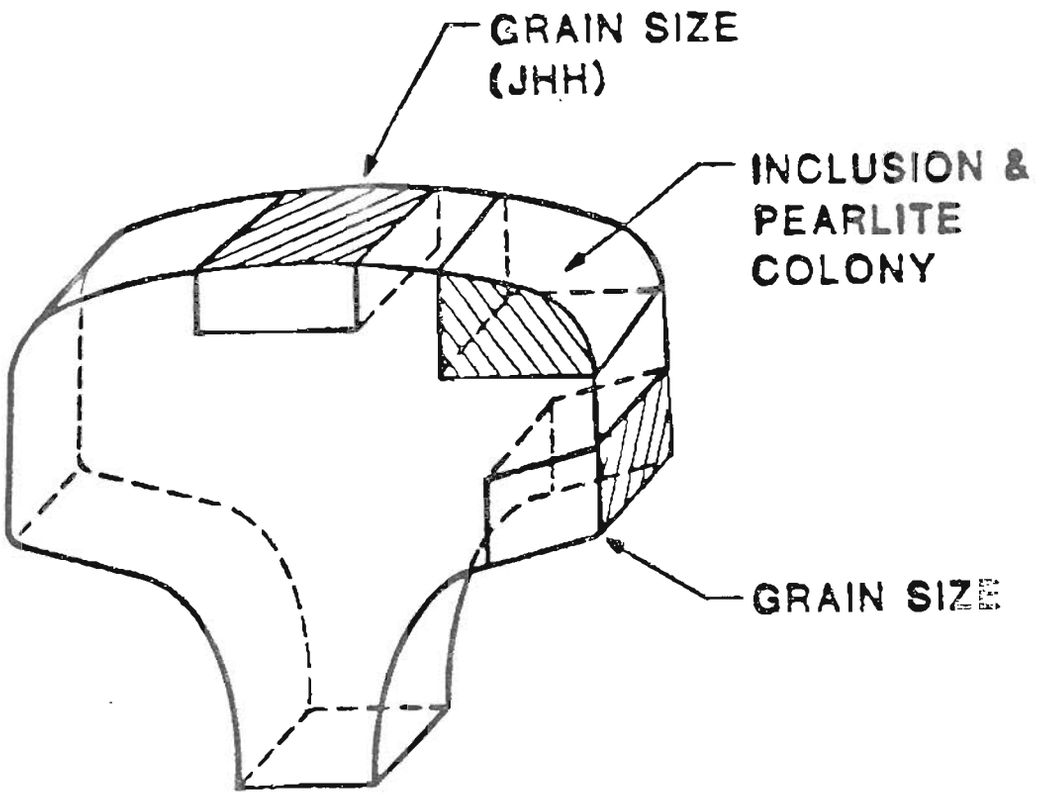

FIGURE 16. SCHEMATIC REPRESENTATION OF SPECIMENS TAKEN FROM RAIL FOR MICROSTRUCTURAL EXAMINATION

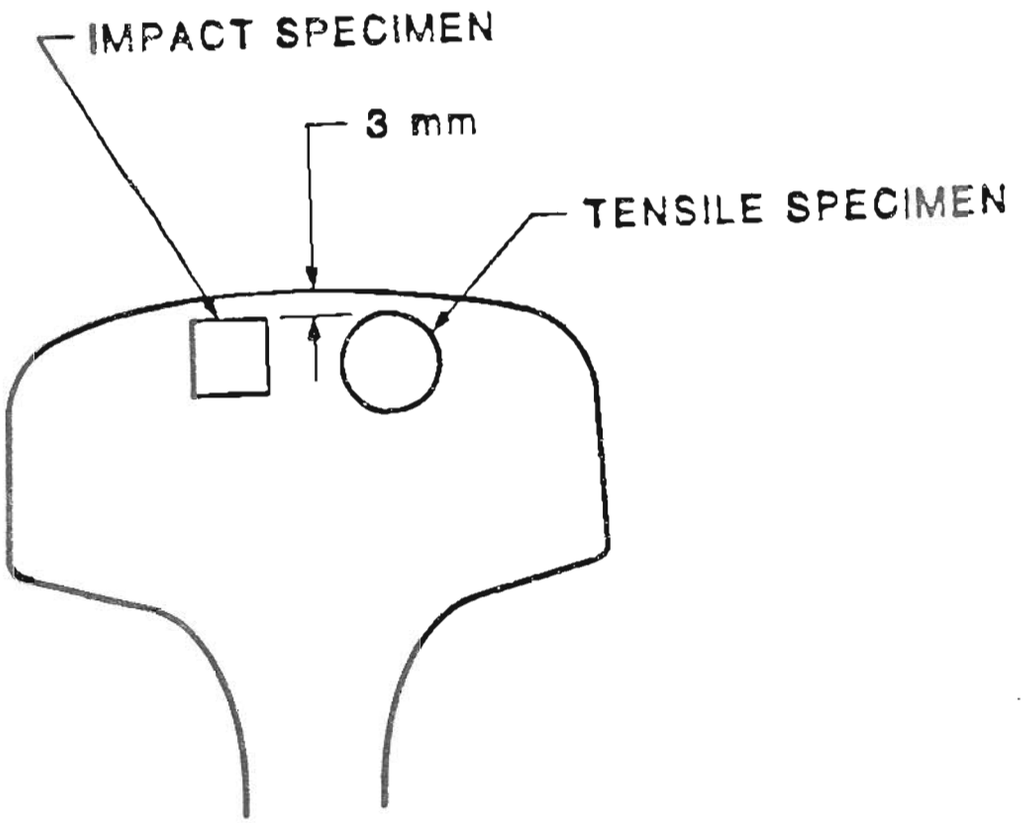

FIGURE 17. SCHEMATIC REPRESENTATION OF TENSILE AND CHARPY V-NOTCH IMPACT TEST SPECIMENS TAKEN FROM HH RAIL

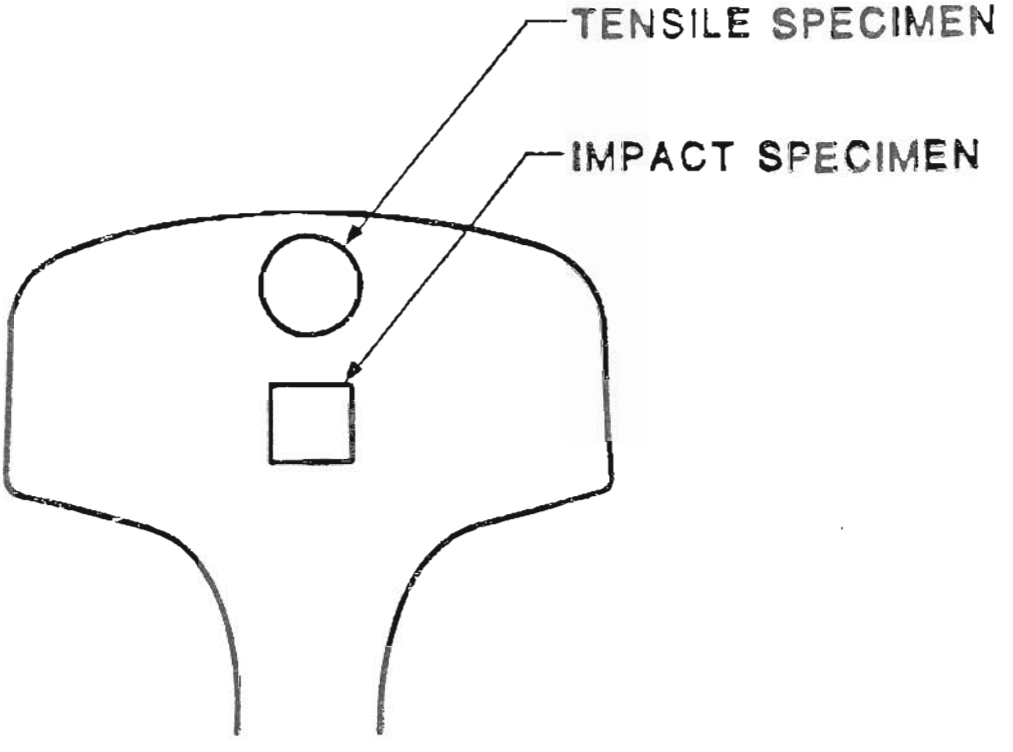

FIGURE 18. SCHEMATIC REPRESENTATION OF TENSILE AND CHARPY V-NOTCH IMPACT TEST SPECIMENS TAKEN FROM CrMo AND STD RAIL

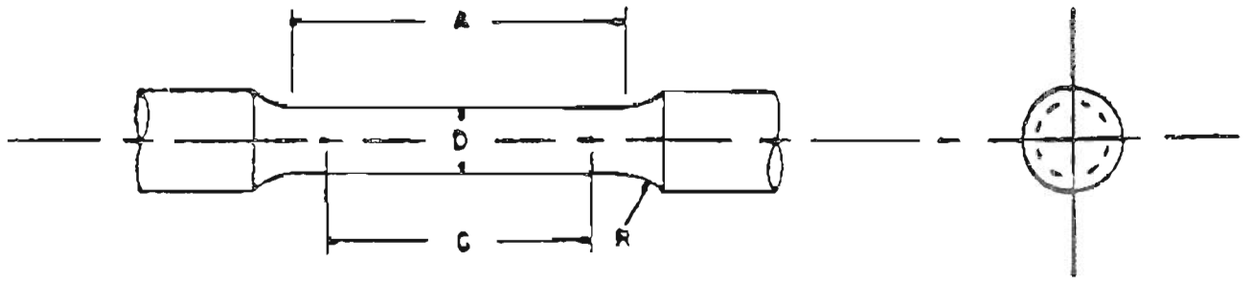

Dimensions

Small-Size Specimens

	in
Nominal Diameter	0.250
G—Gage length	1.000 ± 0.005
D—Diameter	0.250 ± 0.005
R—Radius of fillet, min	3/16
A—Length of reduced section, min	1¼

FIGURE 19. GEOMETRY OF TENSILE SPECIMEN

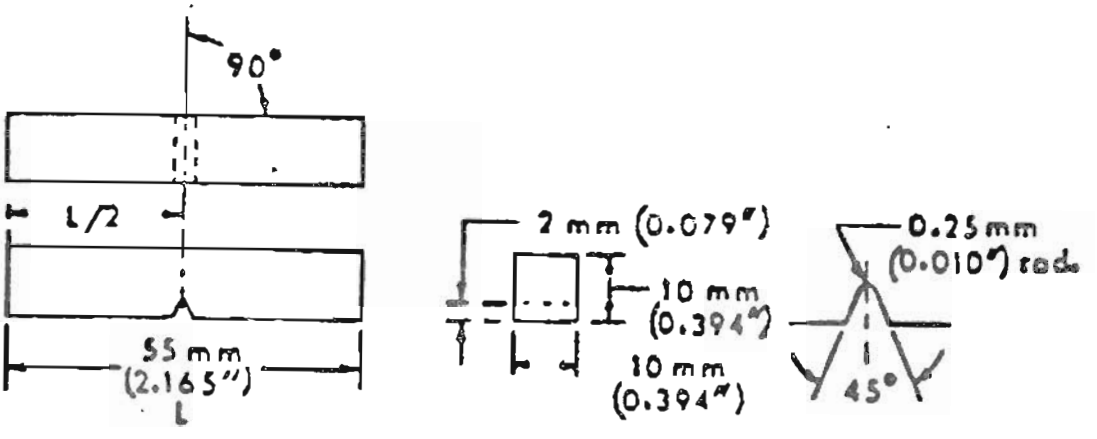

FIGURE 20. GEOMETRY OF CHARPY V-NOTCH IMPACT SPECIMEN

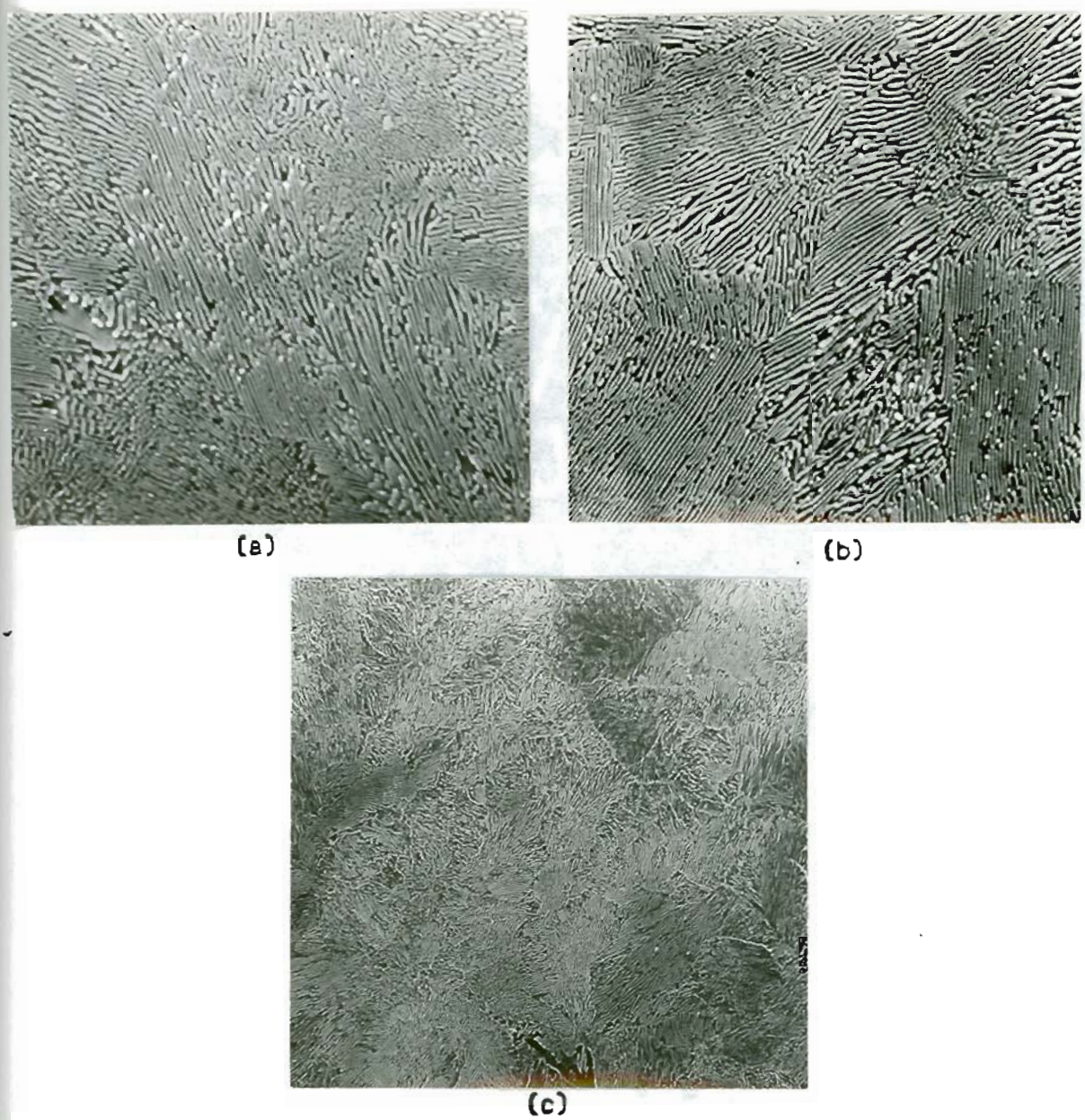

FIGURE 21. SCANNING ELECTRON MICROGRAPHS SHOWING THE PEARLITIC MICROSTRUCTURE FOR DIFFERENT RAIL STEELS
(a) CrMo (b) STD (c) HH
MAGNIFICATION 3000X

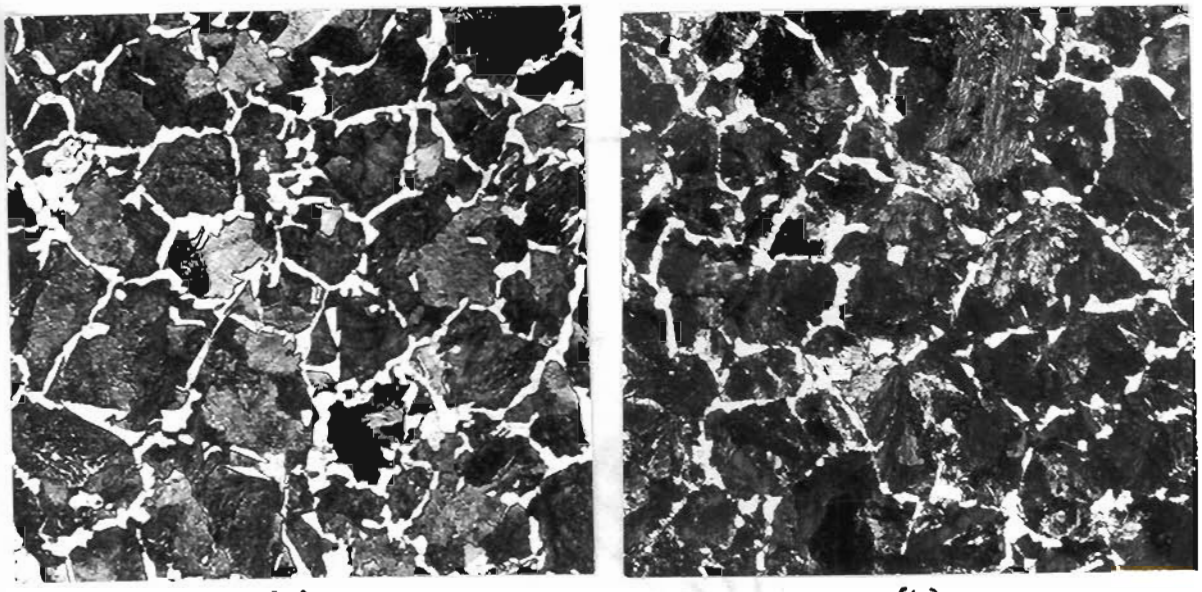

(a) (b)

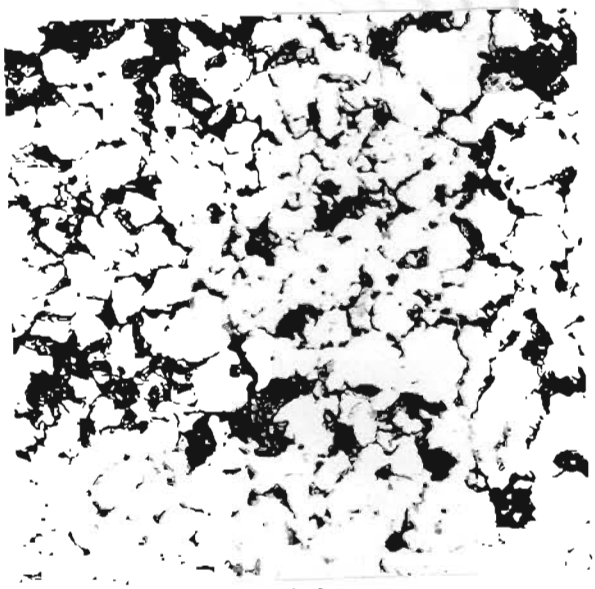

(c)

FIGURE 22. OPTICAL MICROGRAGHS SHOWING THE PRIOR AUSTENITE GRAIN SIZE FOR DIFFERENT RAIL STEELS
(a) STD (b) CrMo (c) HH
MAGNIFICATION 200X

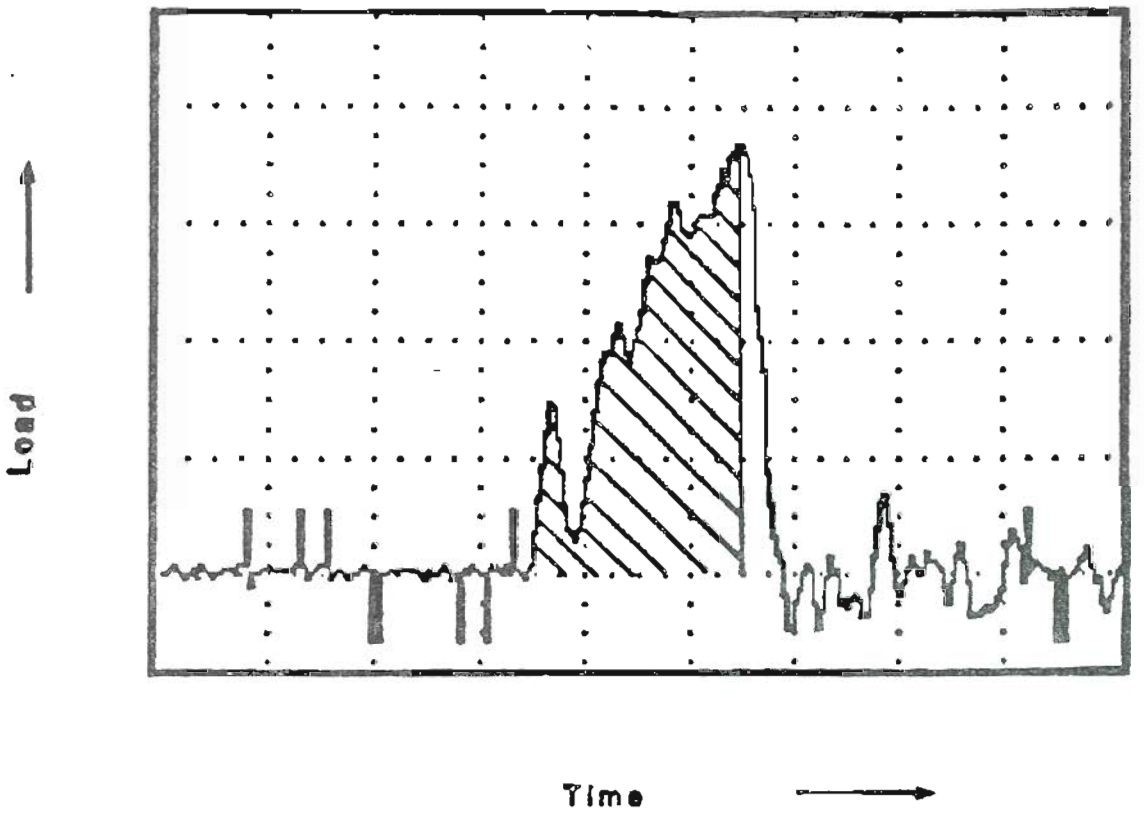

FIGURE 23. LOAD-TIME CURVE OF THE INSTRUMENTED IMPACT TESTS FOR HH RAIL STEEL AT ROOM TEMPERATURE (SHADED AREA REPRESENTS PREMAXIMUM LOAD ENERGY)

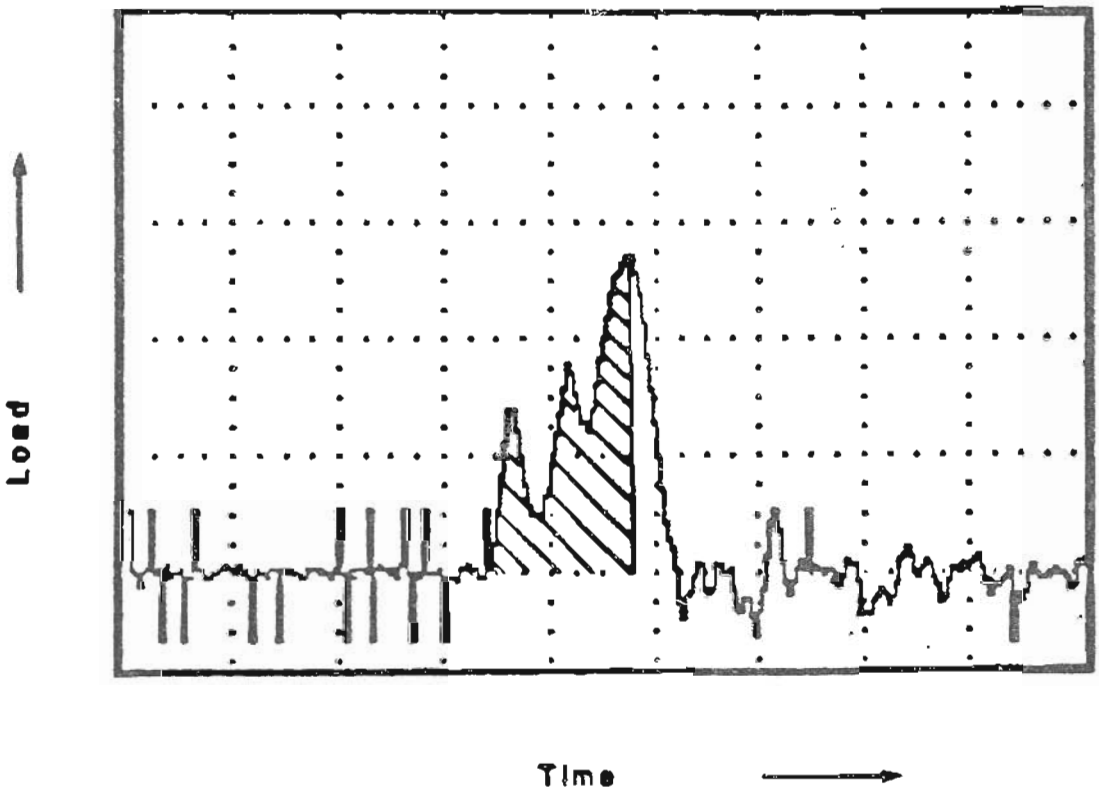

FIGURE 24. LOAD-TIME CURVE OF THE INSTRUMENTED IMPACT TESTS FOR HH RAIL STEEL AT $-20^{\circ}C$ TEMPERATURE (SHADED AREA REPRESENTS PREMAXIMUM LOAD ENERGY)

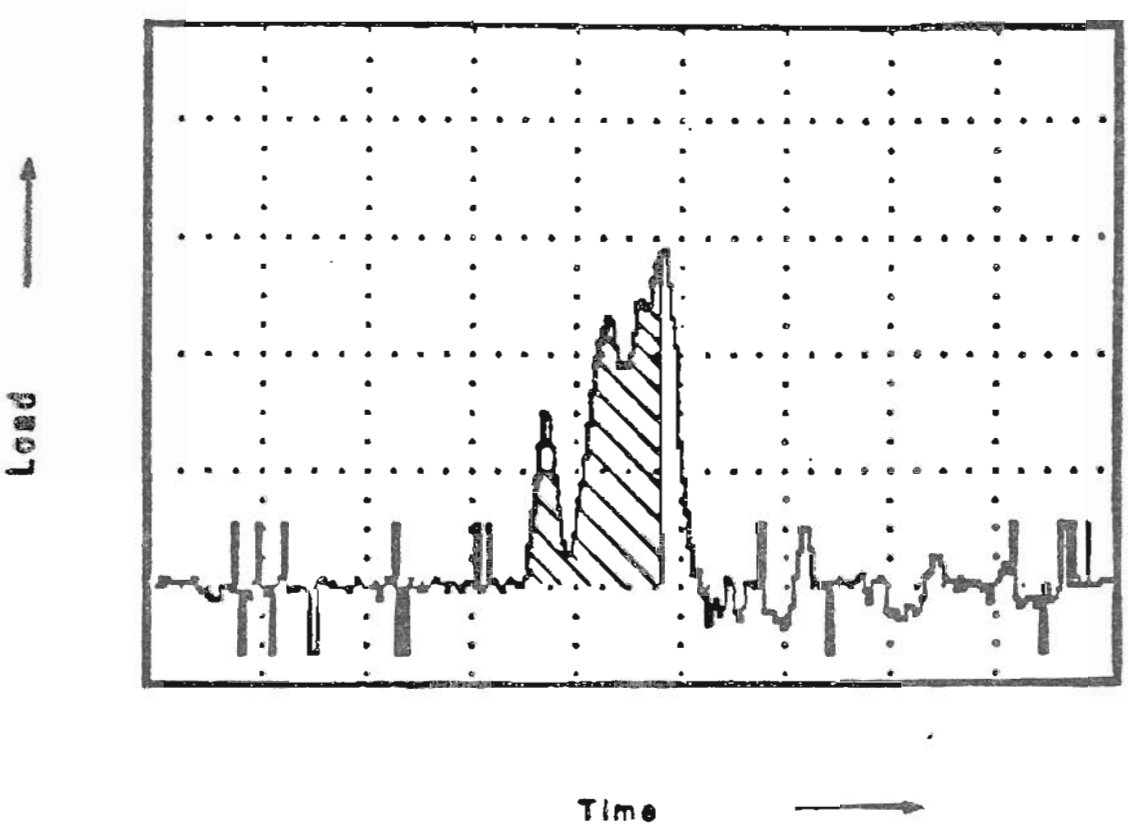

FIGURE 25. LOAD-TIME CURVE OF THE INSTRUMENTED IMPACT TESTS FOR CrMo RAIL STEEL AT ROOM TEMPERATURE (SHADED AREA REPRESENTS PREMAXIMUM LOAD ENERGY)

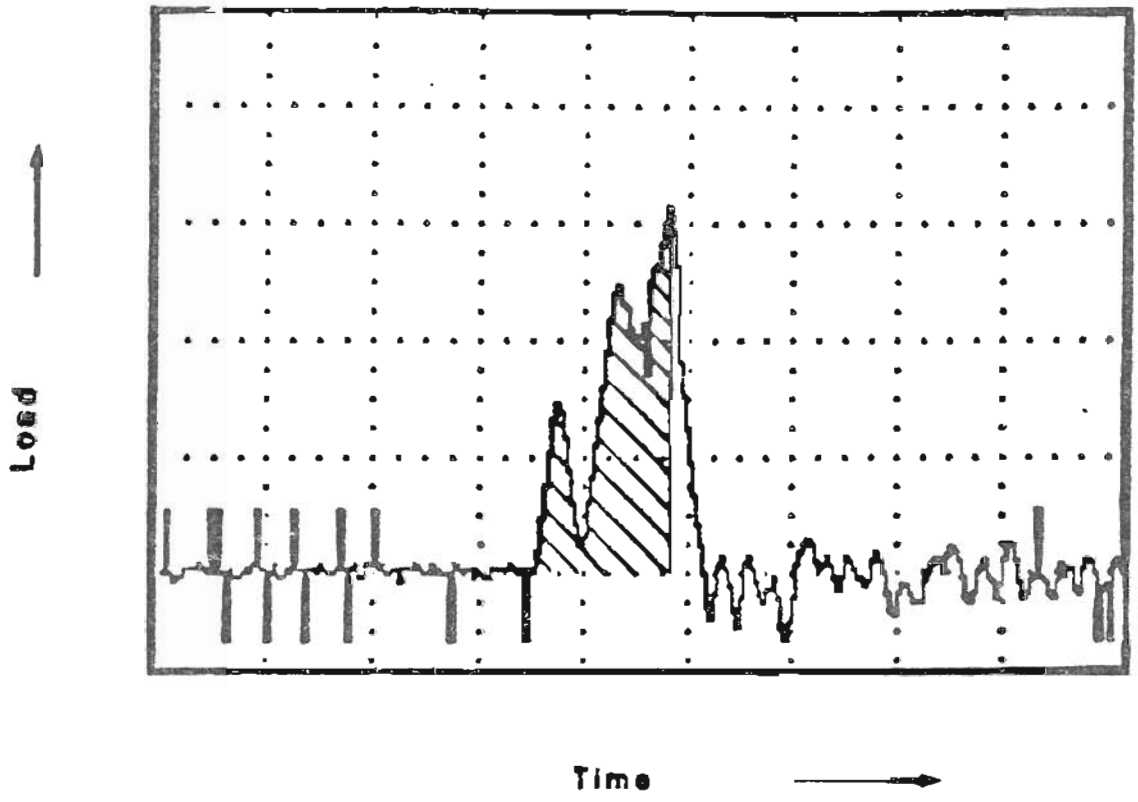

FIGURE 26. LOAD-TIME CURVE OF THE INSTRUMENTED IMPACT TESTS FOR CrMo RAIL STEEL AT $-20^{o}C$ TEMPERATURE (SHADED AREA REPRESENTS PREMAXIMUM LOAD ENERGY)

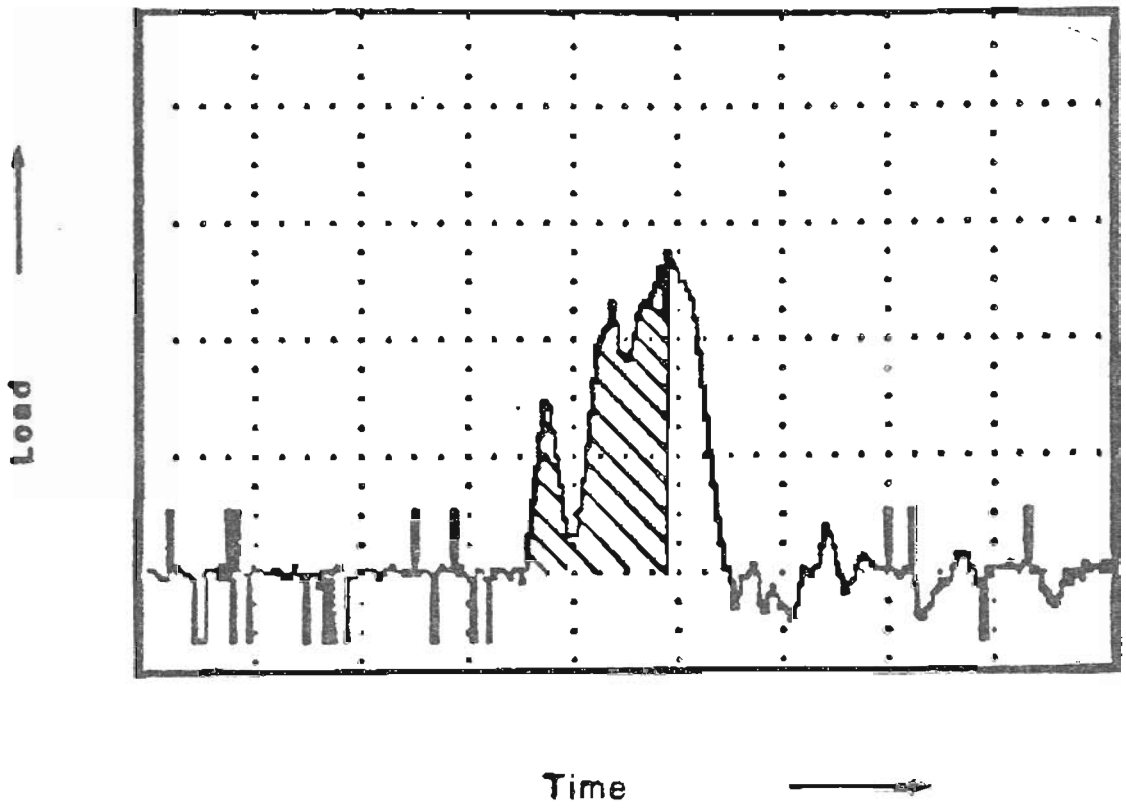

FIGURE 27. LOAD-TIME CURVE OF THE INSTRUMENTED IMPACT TESTS FOR STD RAIL STEEL AT ROOM TEMPERATURE (SHADED AREA REPRESENTS PREMAXIMUM LOAD ENERGY)

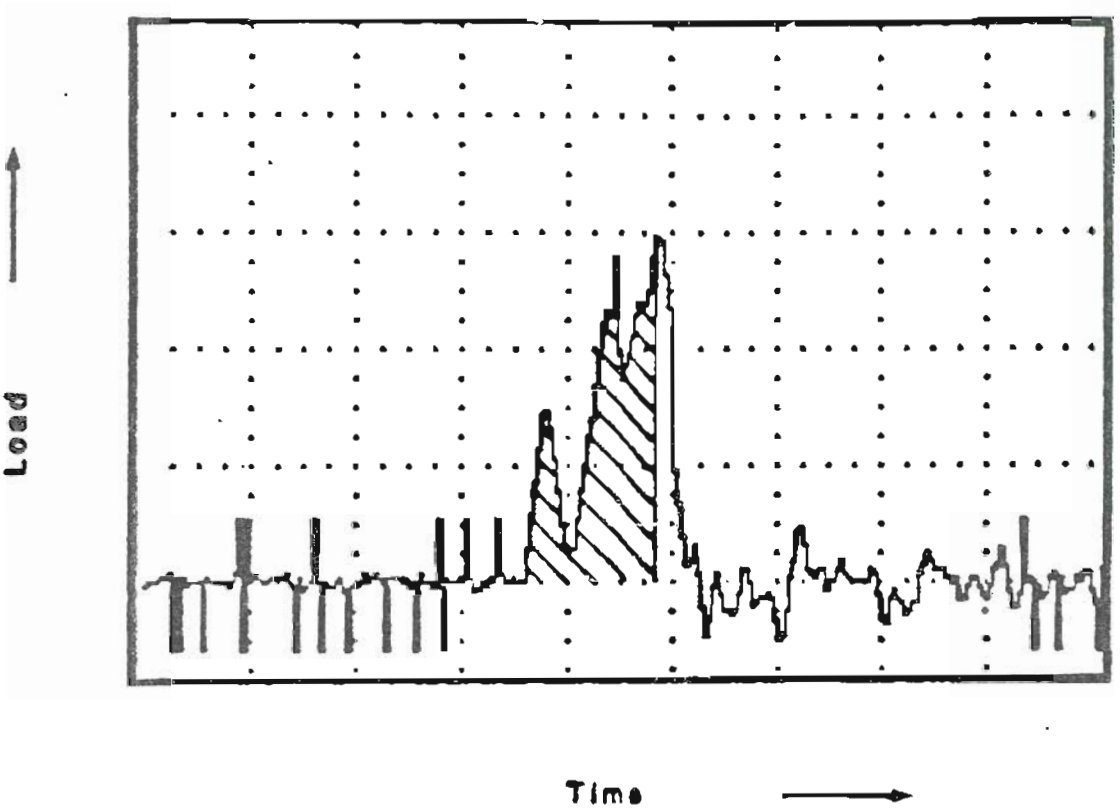

FIGURE 28. LOAD-TIME CURVE OF THE INSTRUMENTED IMPACT TESTS FOR STD RAIL STEEL AT $-20^{\circ}C$ TEMPERATURE (SHADED AREA REPRESENTS PREMAXIMUM LOAD ENERGY)

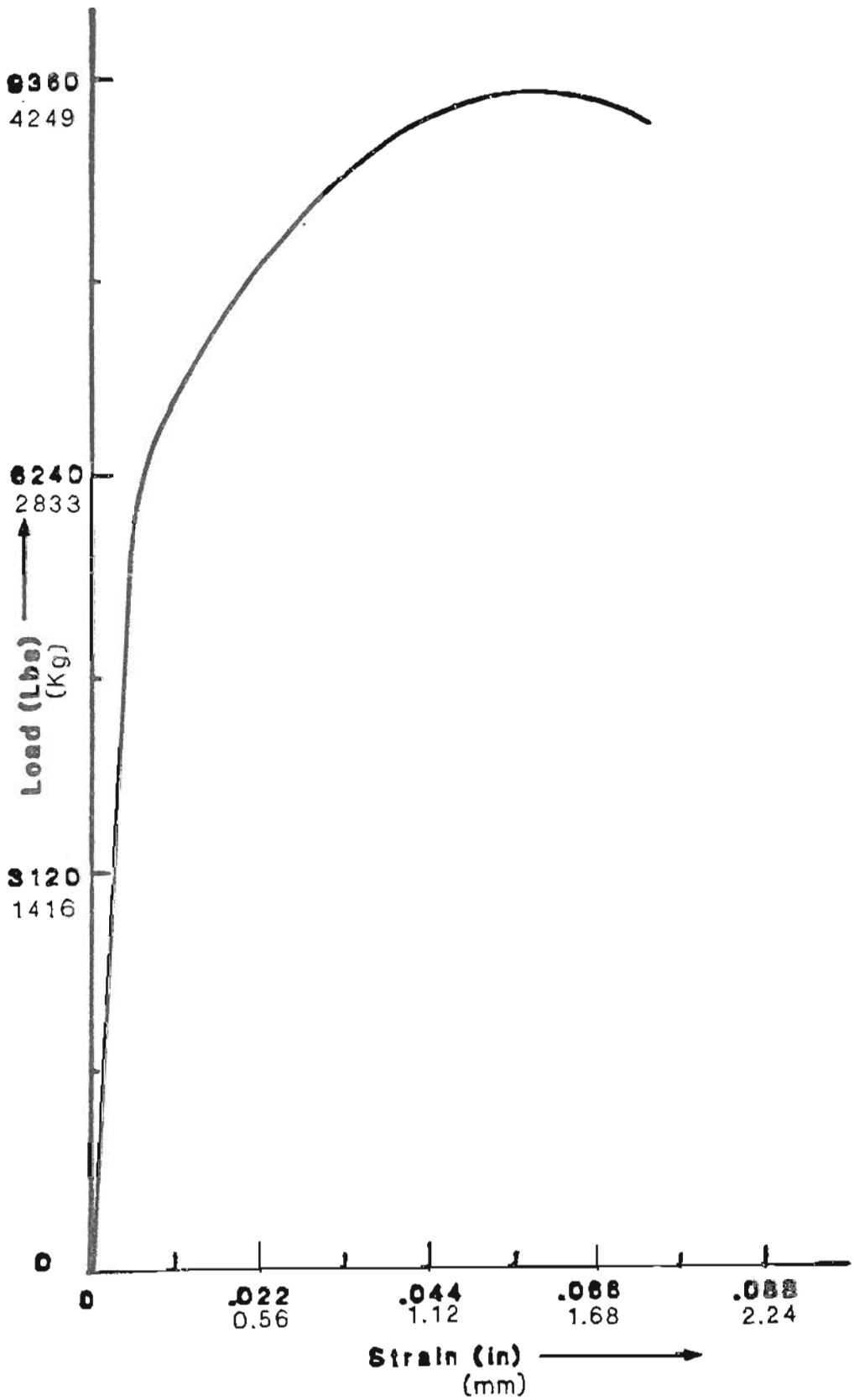

FIGURE 29. LOAD-STRAIN CURVE FOR HH RAIL STEEL

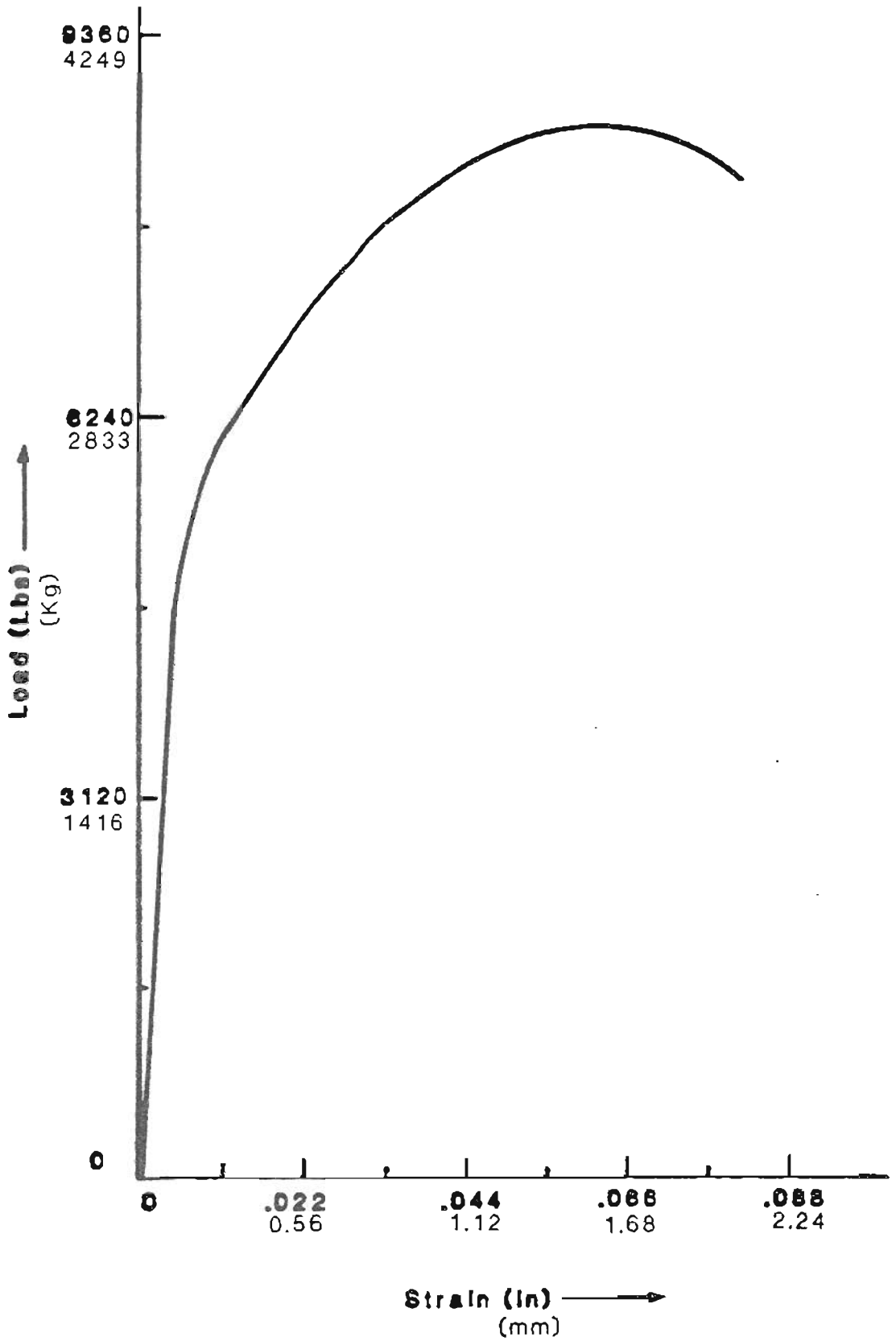

FIGURE 30. LOAD-STRAIN CURVE FOR CrMo RAIL STEEL

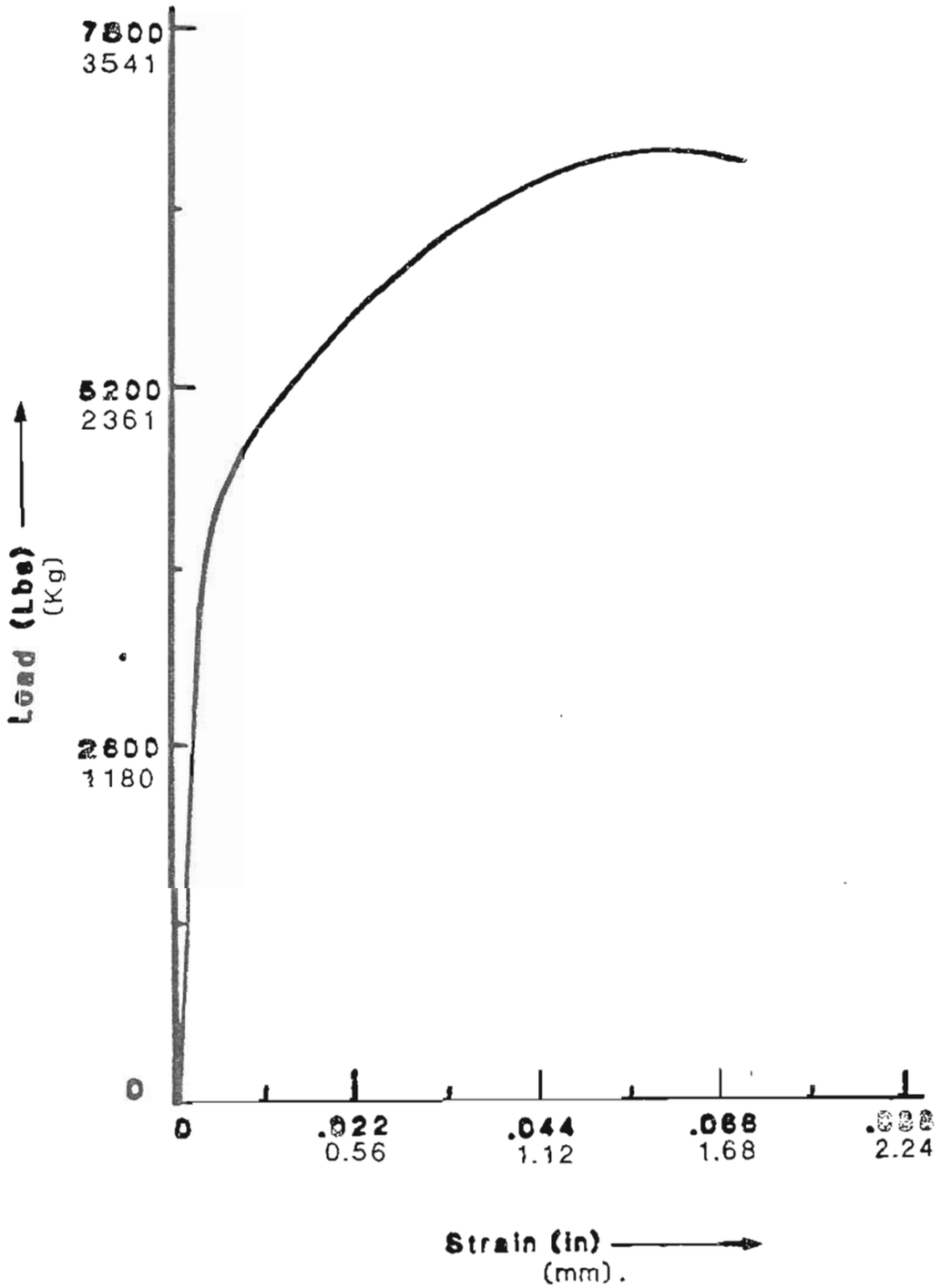

FIGURE 31. LOAD-STRAIN CURVE FOR STD RAIL STEEL

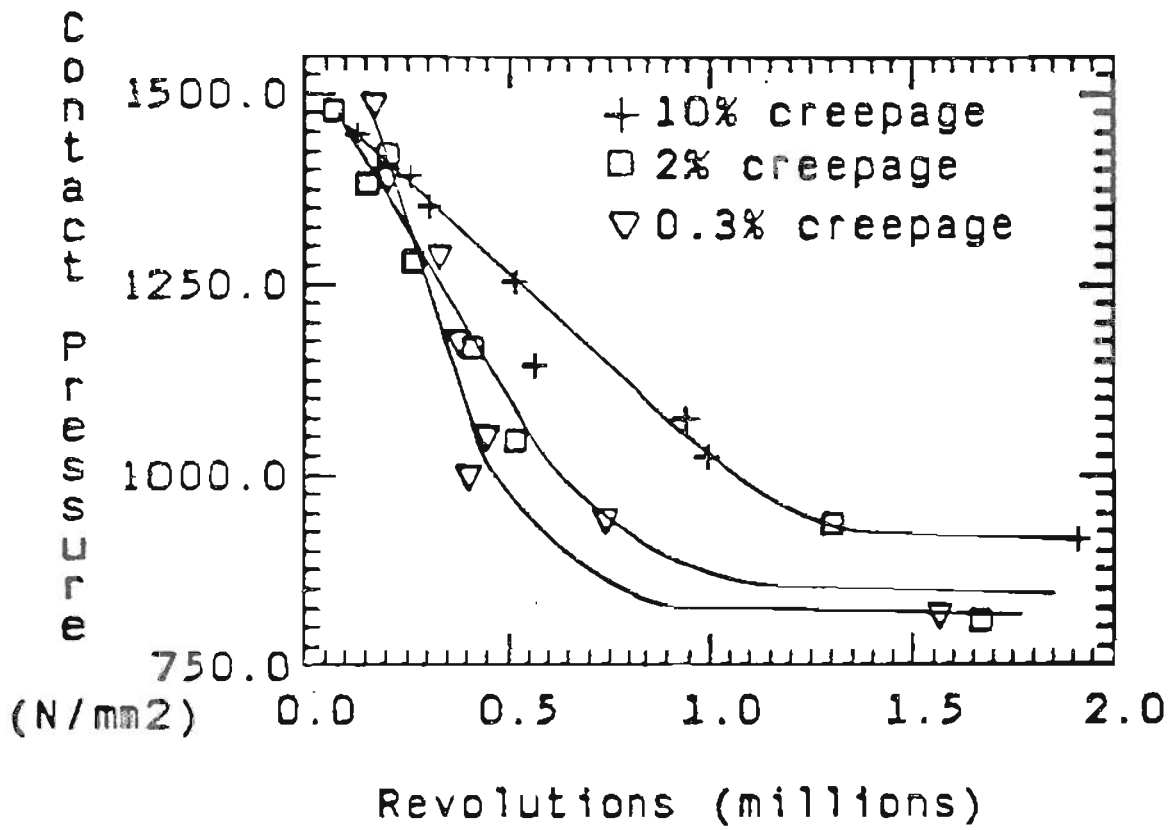

FIGURE 32. EFFECT OF CREEPAGE AND CONTACT PRESSURE ON RCF FOR STD RAIL STEEL

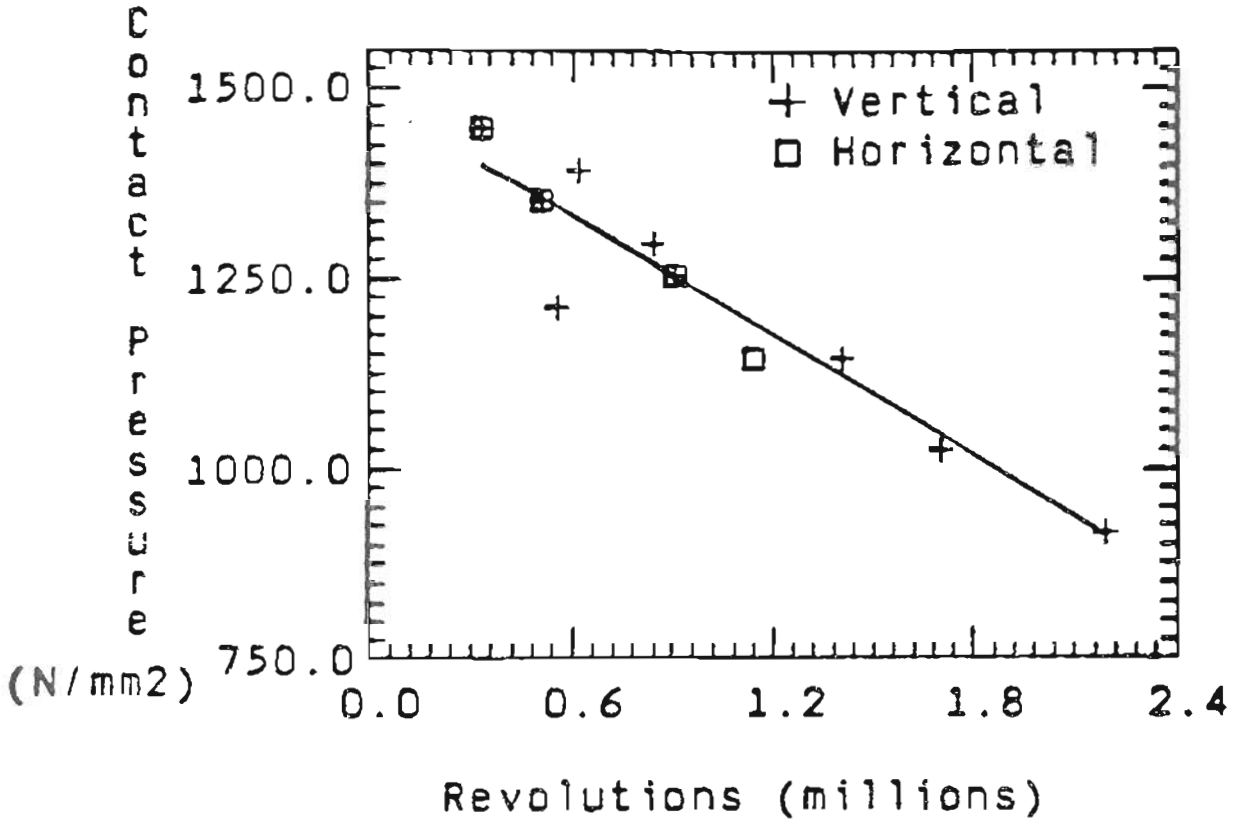

FIGURE 33. EFFECT OF ORIENTATION ON RCF FOR CrMo RAIL STEEL

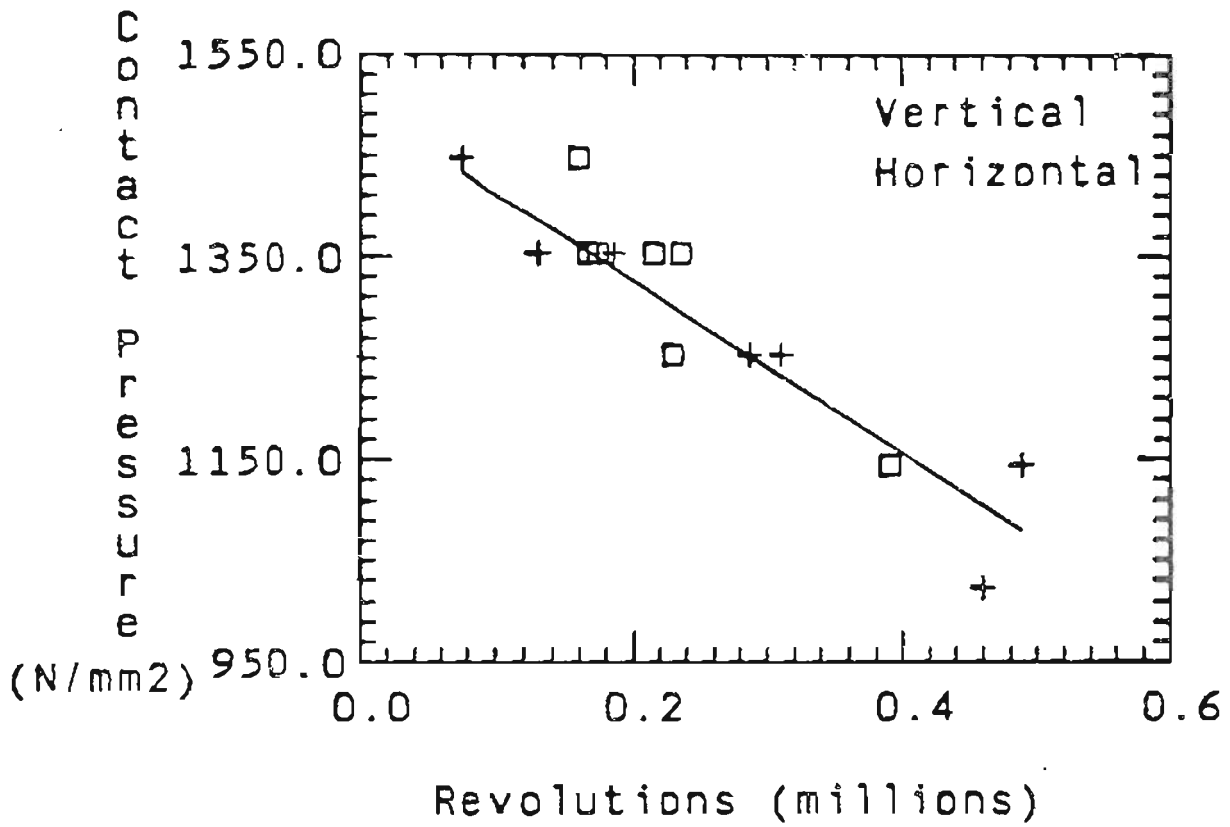

FIGURE 34. EFFECT OF SPECIMEN ORIENTATION ON RCF

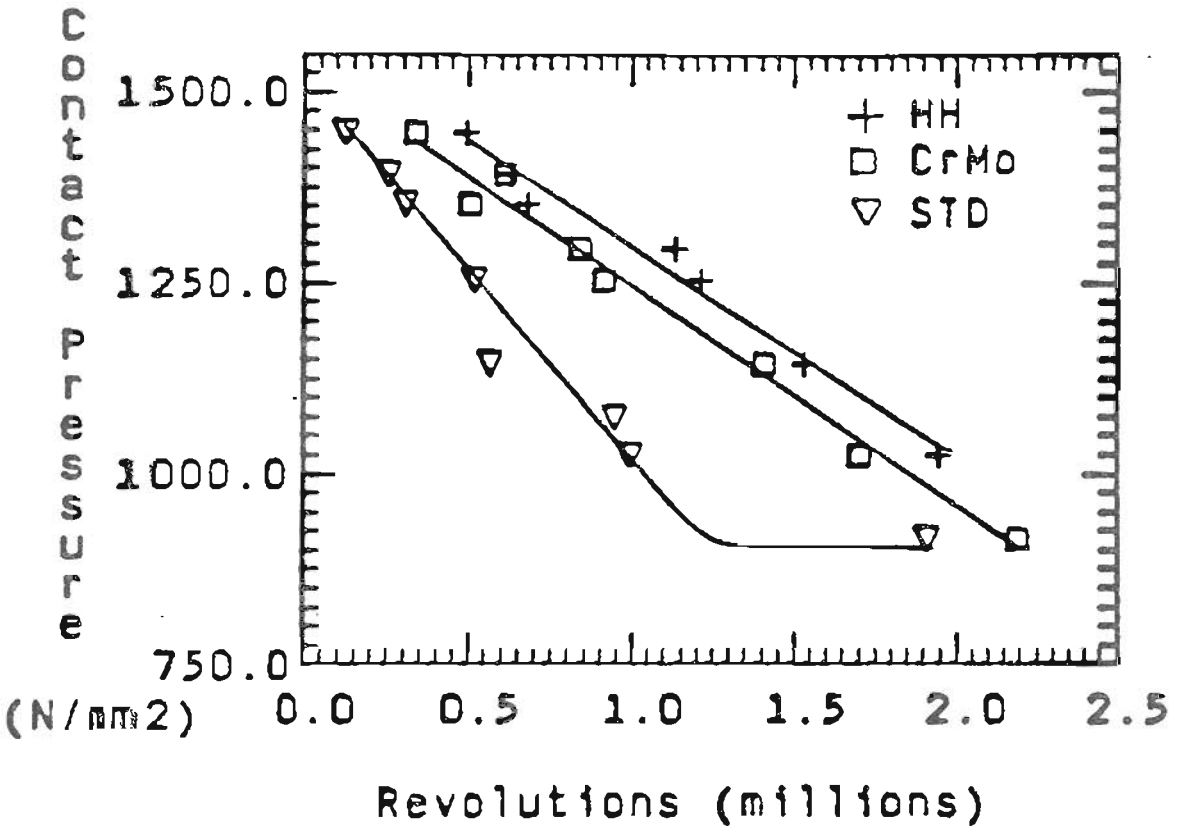

FIGURE 35. EFFECT OF DIFFERENT RAIL STEEL AND CONTACT PRESSURE ON RCF

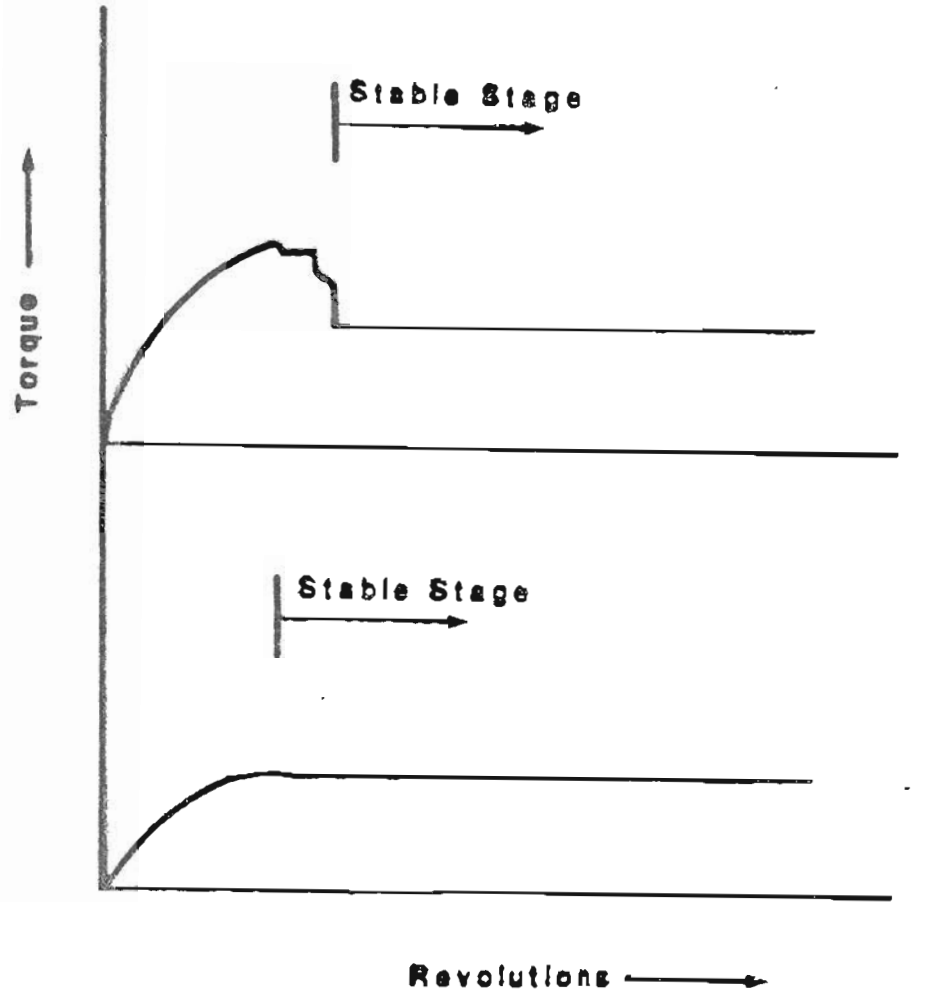

FIGURE 36. SCHEMATIC ILLUSTRATION OF TORQUE-REVOLUTION CURVE IN THE RCF TESTS

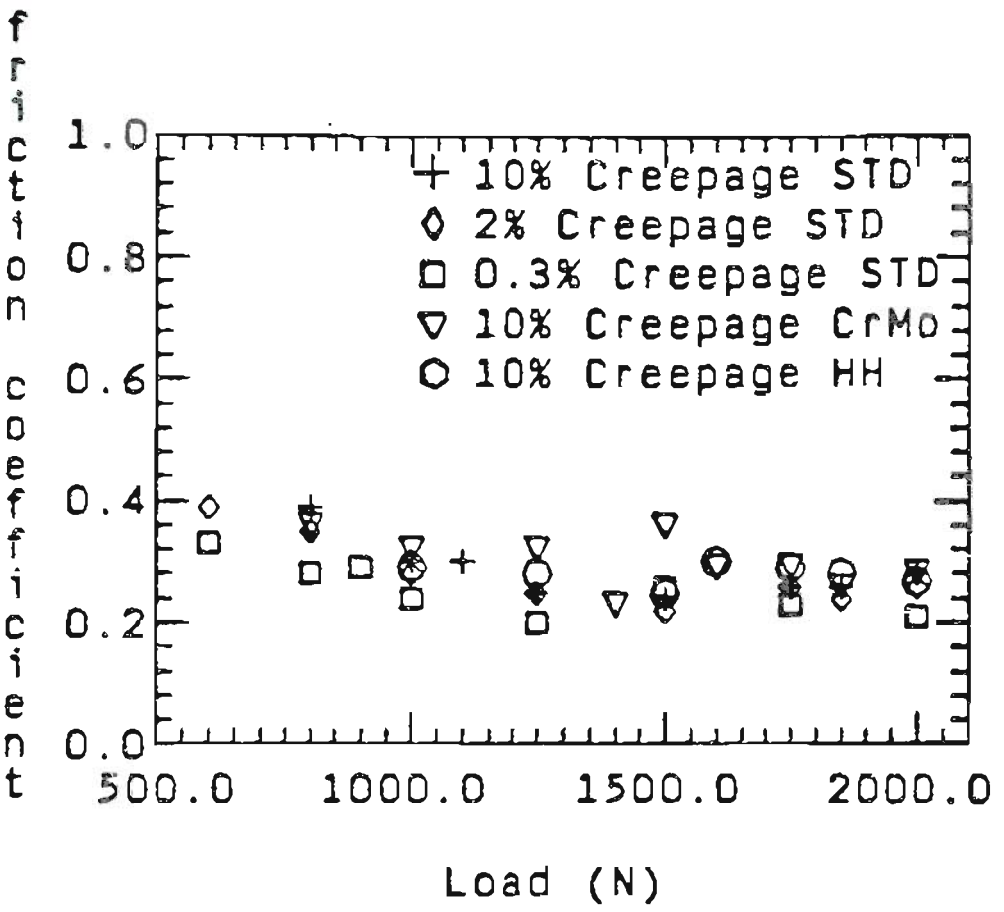

FIGURE 37. EFFECT OF LOAD AND CREEPAGE ON FRICTION COEFFICIENT UNDER WATER LUBRICATED CONDITIONS

(a)

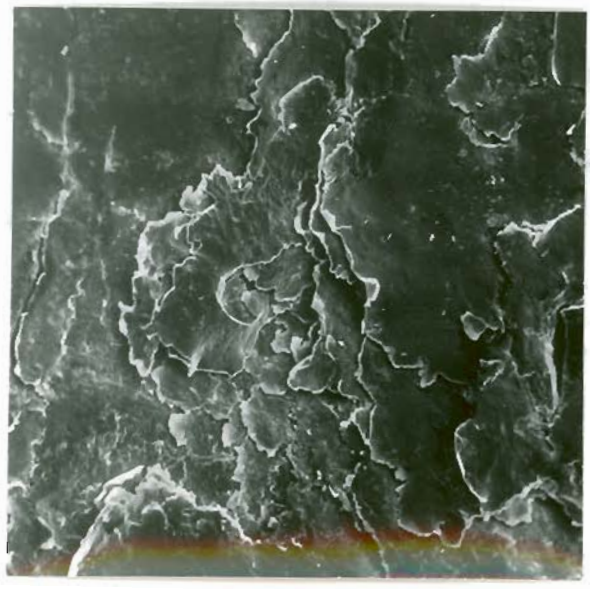

(b)

FIGURE 38. SCANNING ELECTRON MICROGRAPHS SHOWING THE SURFACE APPEARANCE OF THE FAILED ROLLER FOR HH RAIL STEEL
(a) MAG 15x (b) MAG 150x

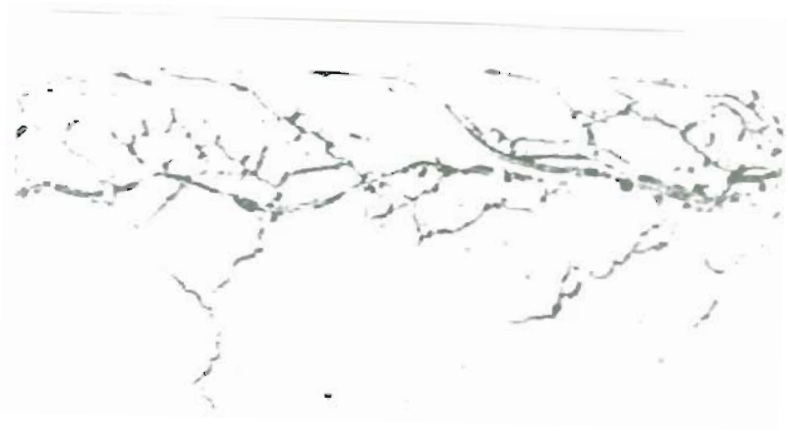

(a)

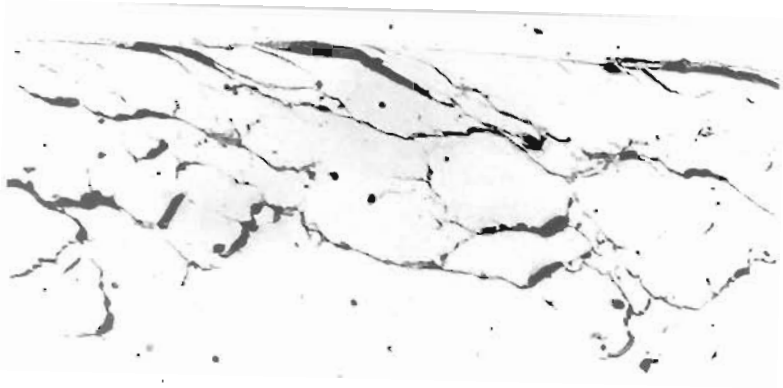

(b)

FIGURE 39. OPTICAL MICROGRAPHS SHOWING THE CRACK APPEARANCE OF FAILED ROLLERS AT CONTACT PRESSURE 1354 (N/mm2) FOR DIFFERENT RAIL STEELS, TRACTION FORCE FROM RIGHT TO LEFT
(a) HH (b) CrMo
MAGNIGICATION 100X

(c)

(d)

FIGURE 39. OPTICAL MICROGRAPHS SHOWING CRACK APPEARANCE OF THE FAILED ROLLER (c) AND SUBSURFACE PLASTIC FLOW (d) FOR STD RAIL STEEL AT CONTACT PRESSURE 1354 N/mm2, TRACTION FORCE FROM RIGHT TO LEFT
MAGNIFICATION 100X

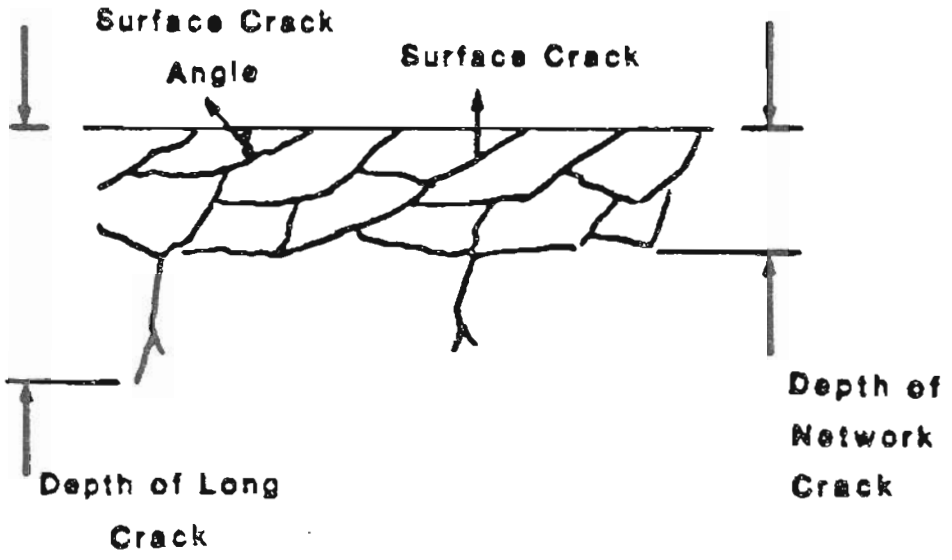

FIGURE 40. SCHEMATIC ILLUSTRATION OF CHARACTERIZATION OF THE CRACK APPEARANCE IN THE LONGITUDINAL SECTION OF FAILED ROLLER

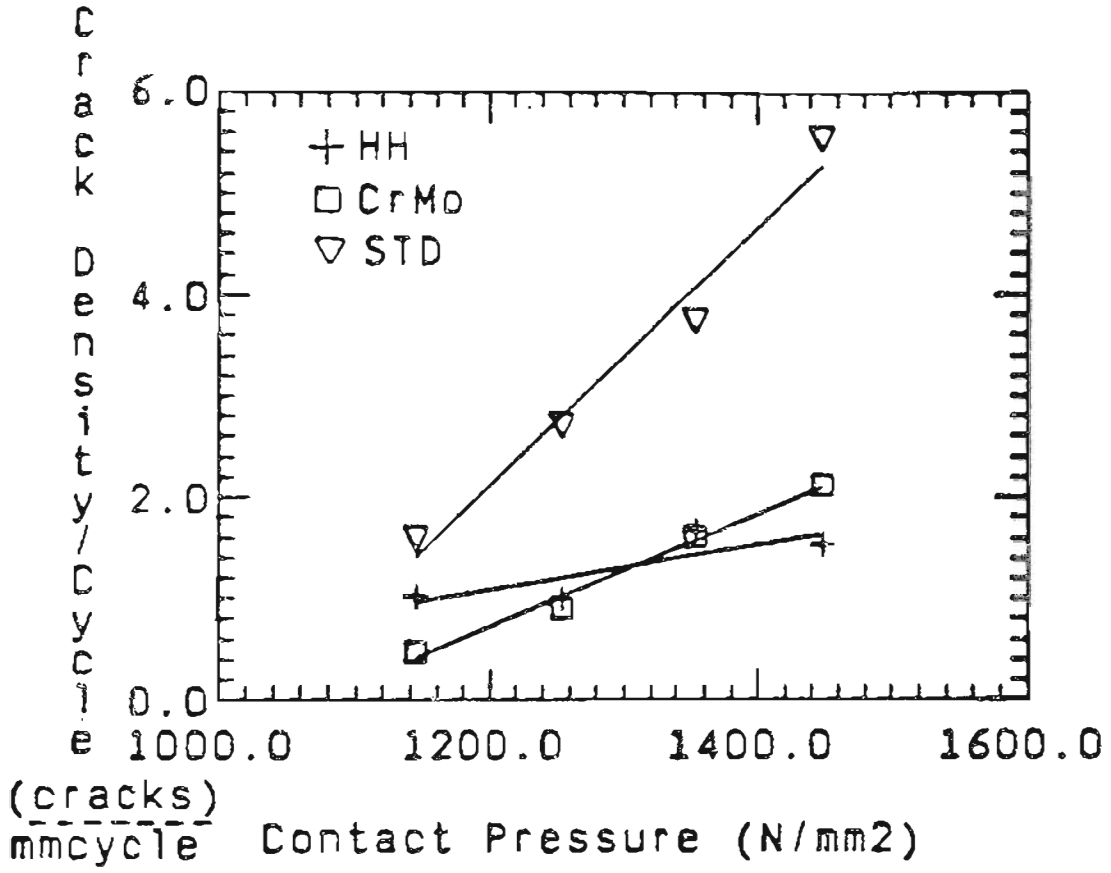

FIGURE 41. EFFECT OF DIFFERENT RAIL STEELS AND CONTACT PRESSURE ON SURFACE CRACK DENSITY PER CYCLE

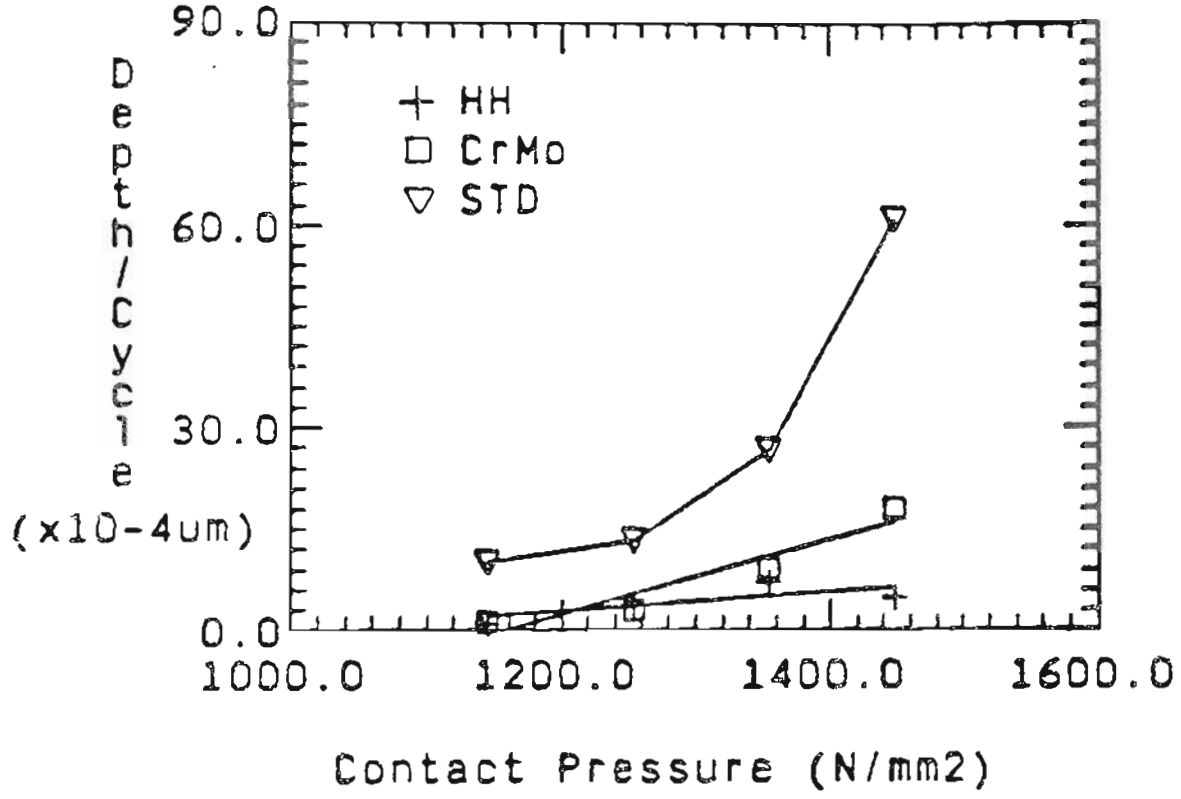

FIGURE 42. EFFECT OF DIFFERENT RAIL STEELS AND CONTACT PRESSURE ON DEPTH OF LONG CRACK PER CYCLE

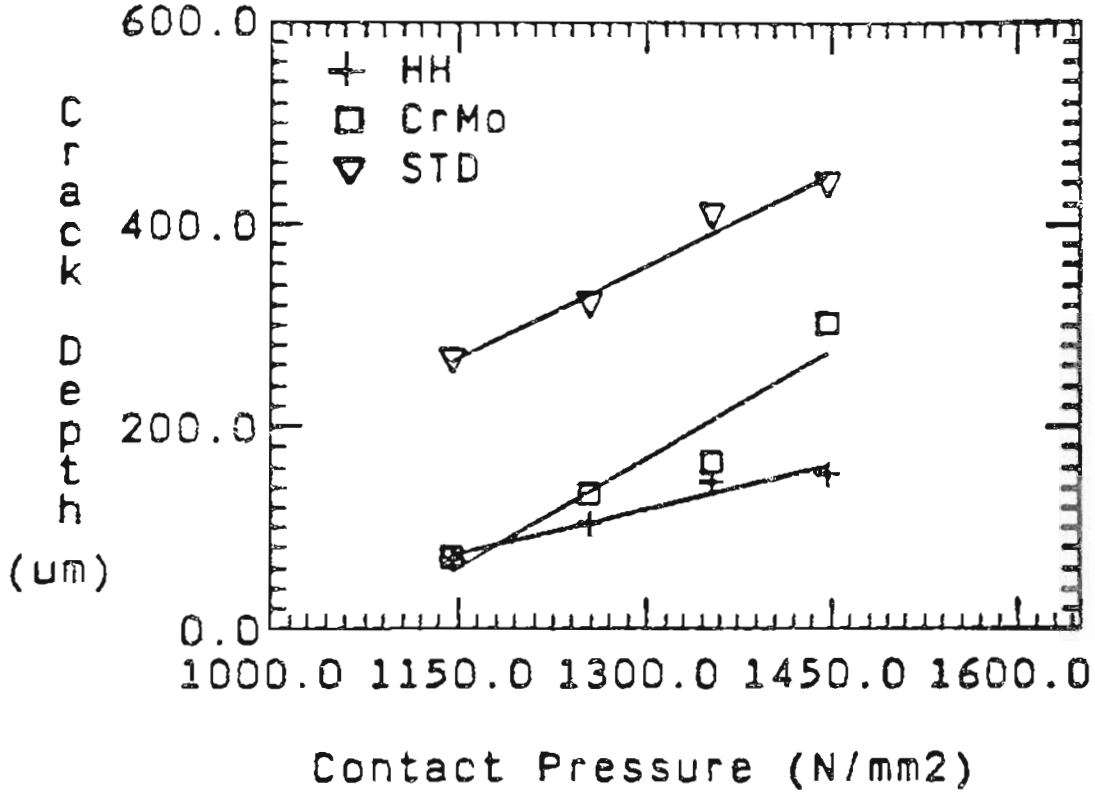

FIGURE 43. EFFECT OF DIFFERENT RAIL STEEL AND CONTACT PRESSURE ON DEPTH OF NETWORK CRACKS

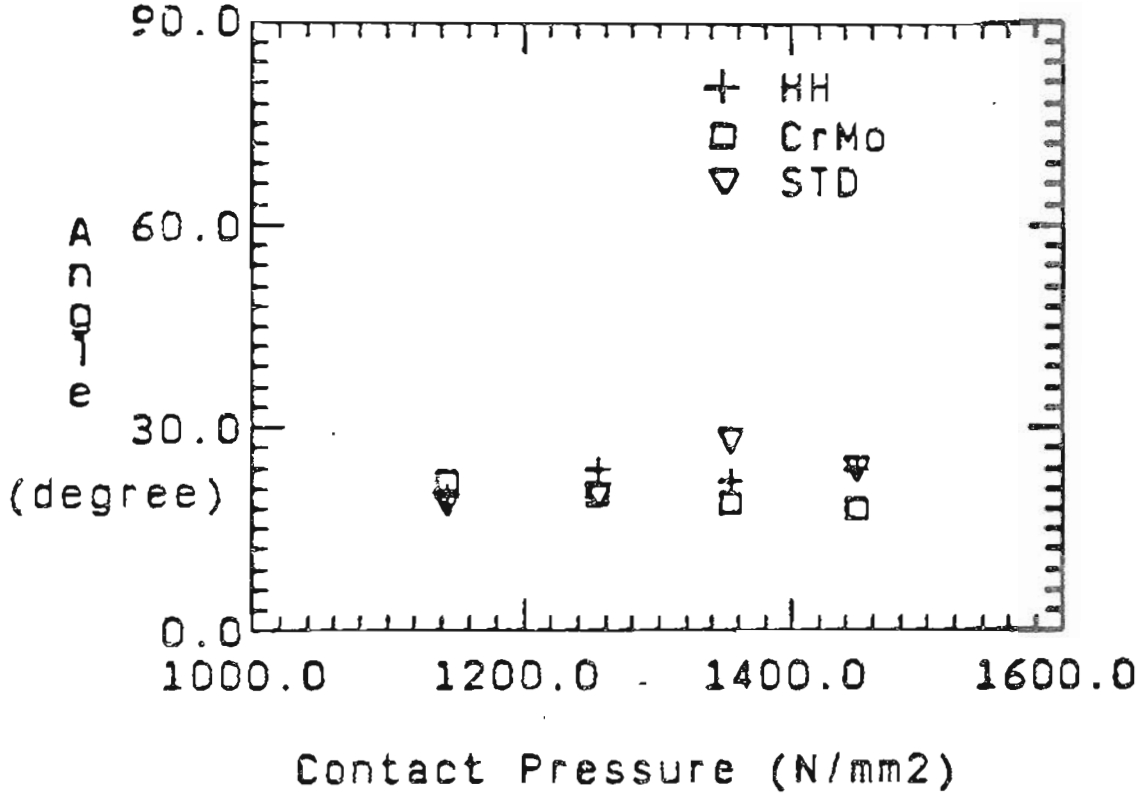

FIGURE 44. EFFECT OF DIFFERENT RAIL STEELS AND CONTACT PRESSURE ON SURFACE CRACK ANGLE WITH RESPECT TO SURFACE

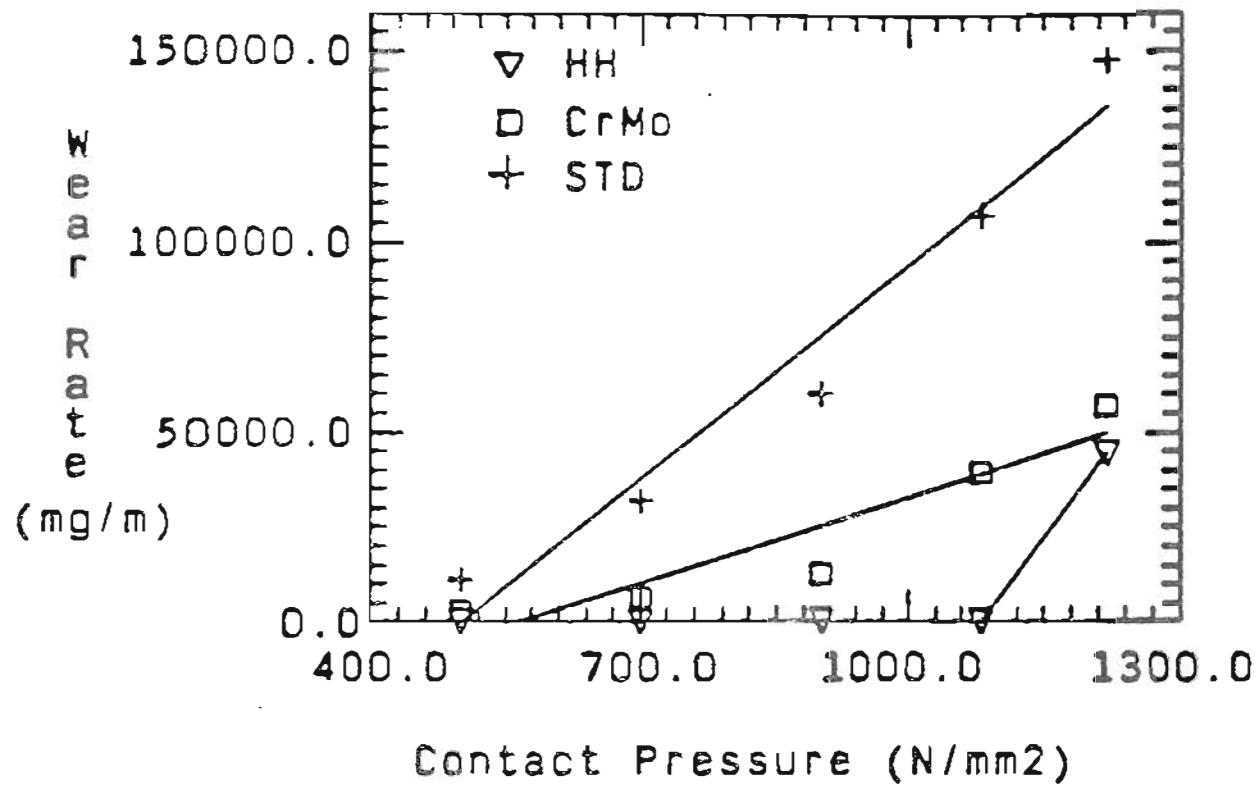

FIGURE 45. EFFECT OF DIFFERENT RAIL STEELS AND CONTACT PRESSURE ON WEAR RATE

(c)

(d)

FIGURE 46. SCANNING ELECTRON MICROGRAPHS SHOWING WEAR SURFACE APPEARANCE OF ROLLER FOR HH RAIL STEEL, MAGNIFICATION X100
(a) WITH A BLACK FILM, Po=900N/mm^2
(b) WITHOUT A BLACK FILM, Po=1220N/mm^2

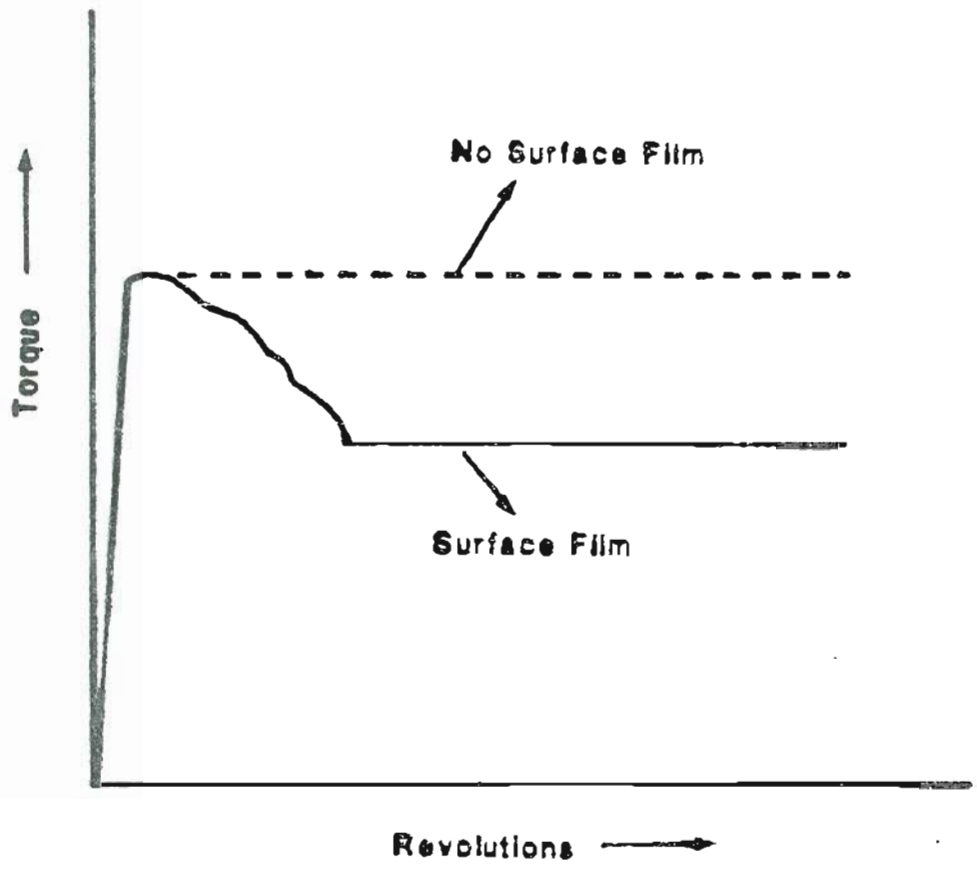

FIGURE 47. SCHEMATIC ILLUSTRATION OF TORQUE-REVOLUTION CURVE IN THE WEAR TESTS

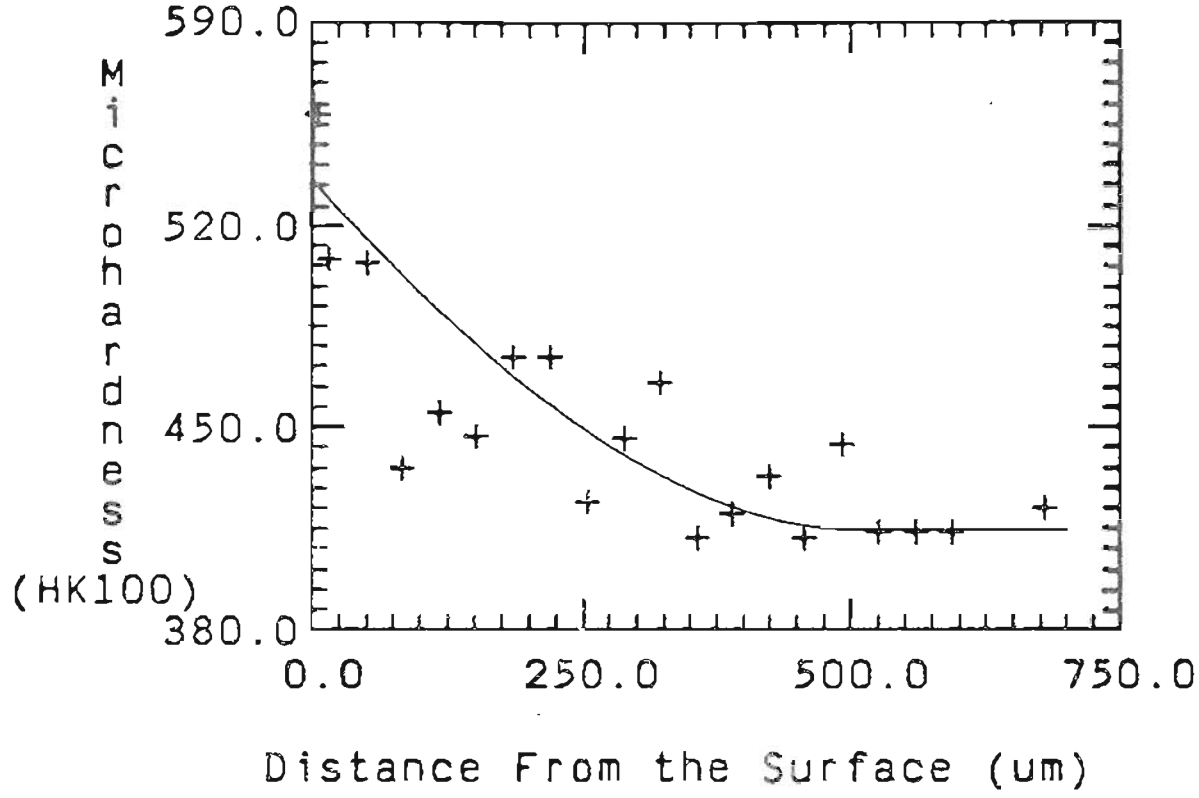

FIGURE 48. HARDNESS PROFILE IN FAILED ROLLER OF HH RAIL STEEL

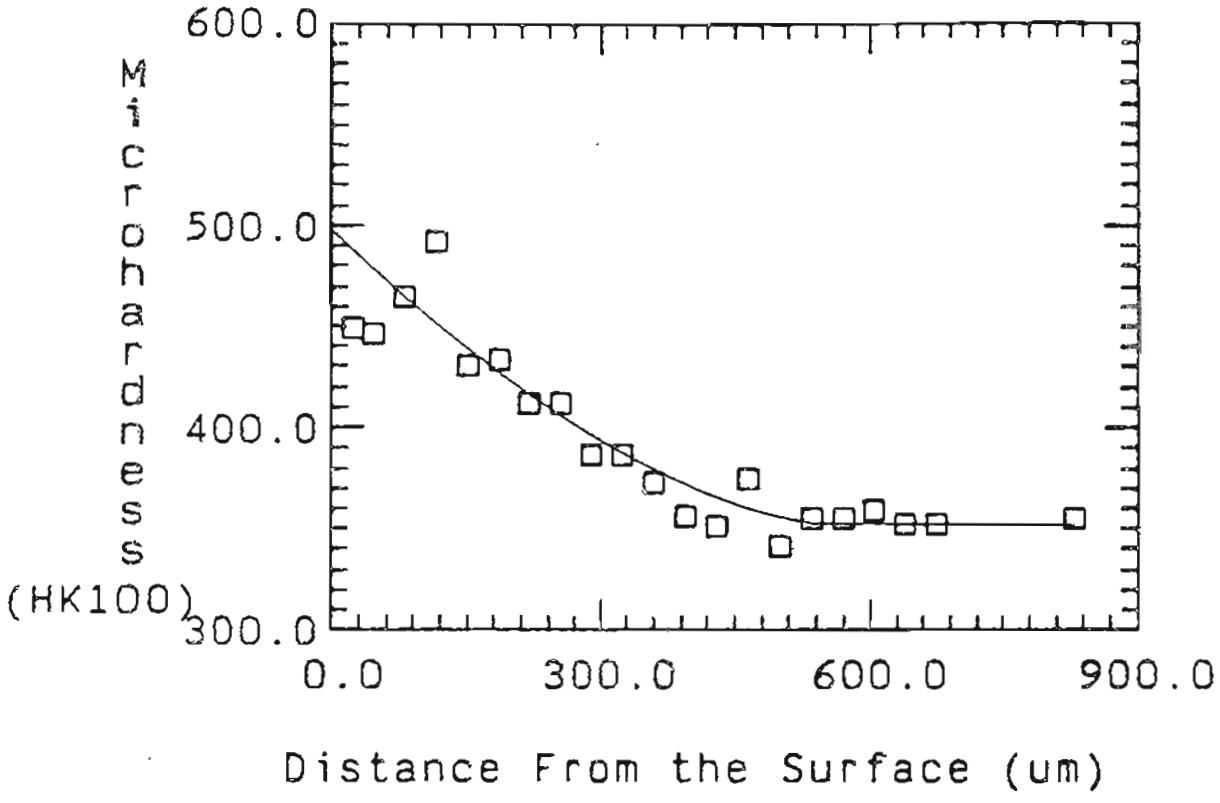

FIGURE 49. HARDNESS PROFILE IN FAILED ROLLER OF CrMo RAIL STEEL

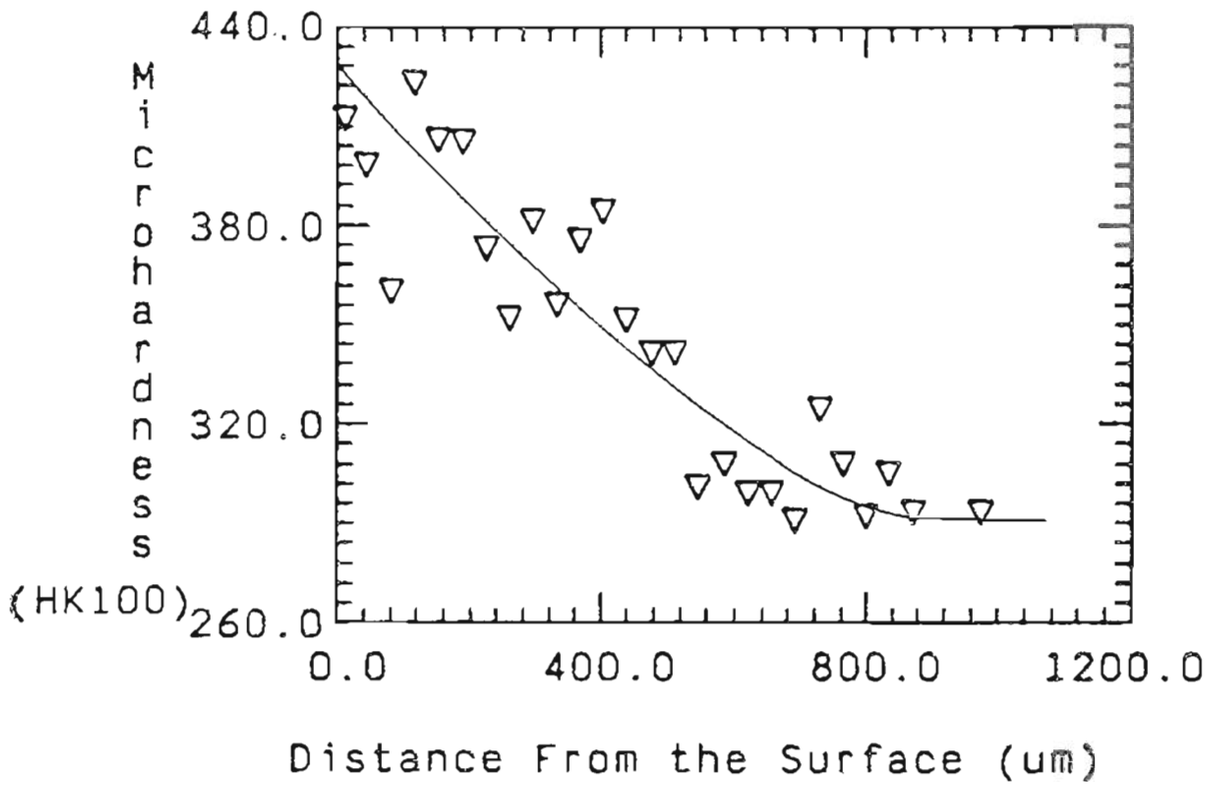

FIGURE 50. HARDNESS PROFILE IN FAILED ROLLER OF STD RAIL STEEL, P_o=1354N/mm^2

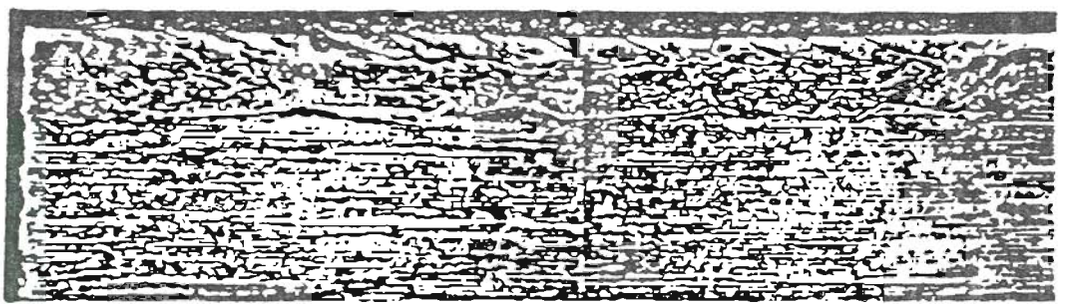

FIGURE 51. CRACK APPEARANCE OF RAIL STEEL (GERMAN) IN LONGITUDINAL SECTION [30], MAGNIFICATION X 2

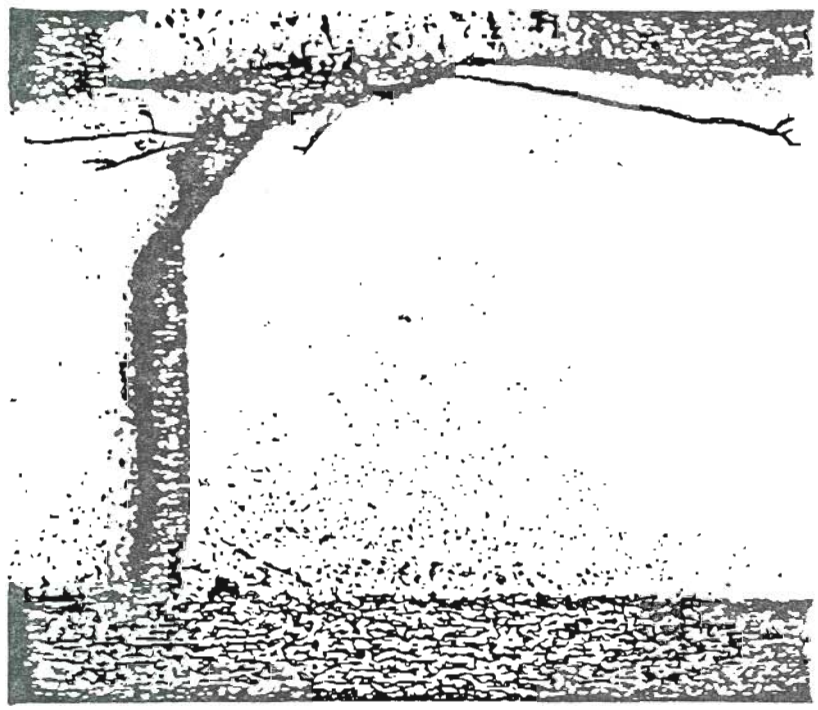

FIGURE 52. CRACK APPEARANCE OF RAIL STEEL (BRITISH) IN LONGITUDINAL SECTION [44], MAGNIFICATION X1.2

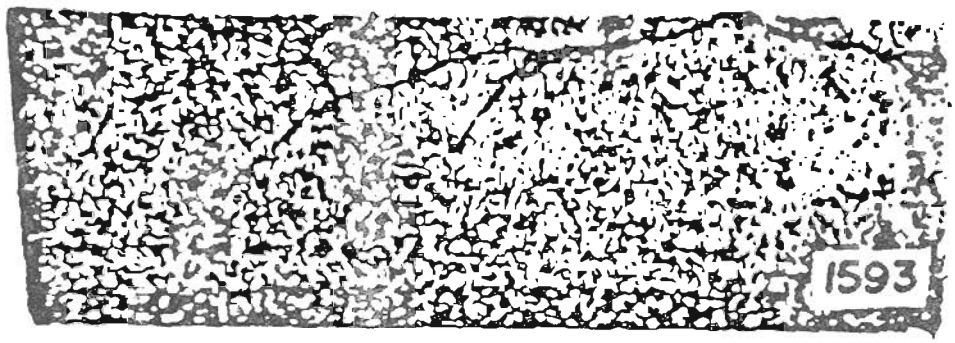

FIGURE 53. CRACK APPEARANCE OF RAIL STEEL (JAPANESE) IN LONGITUDINAL SECTION [1] X 1.3

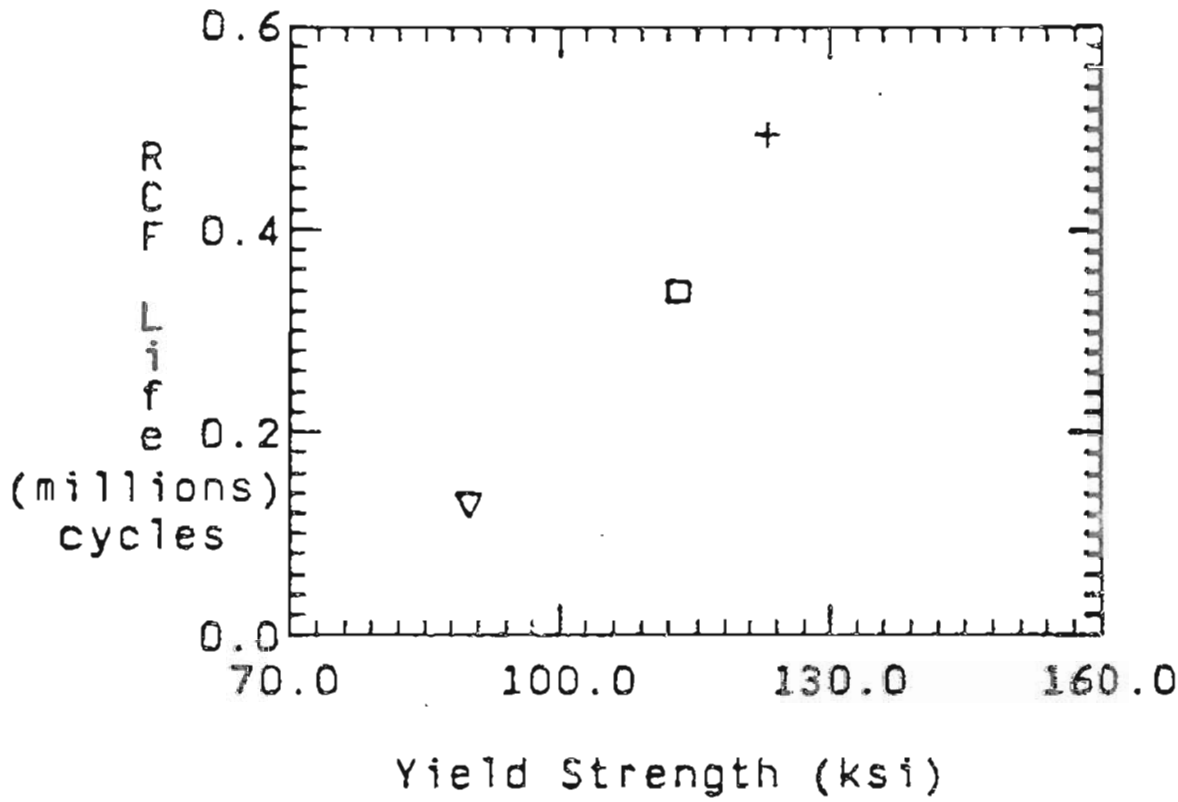

FIGURE 54. EFFECT OF YIELD STRENGTH ON RCF

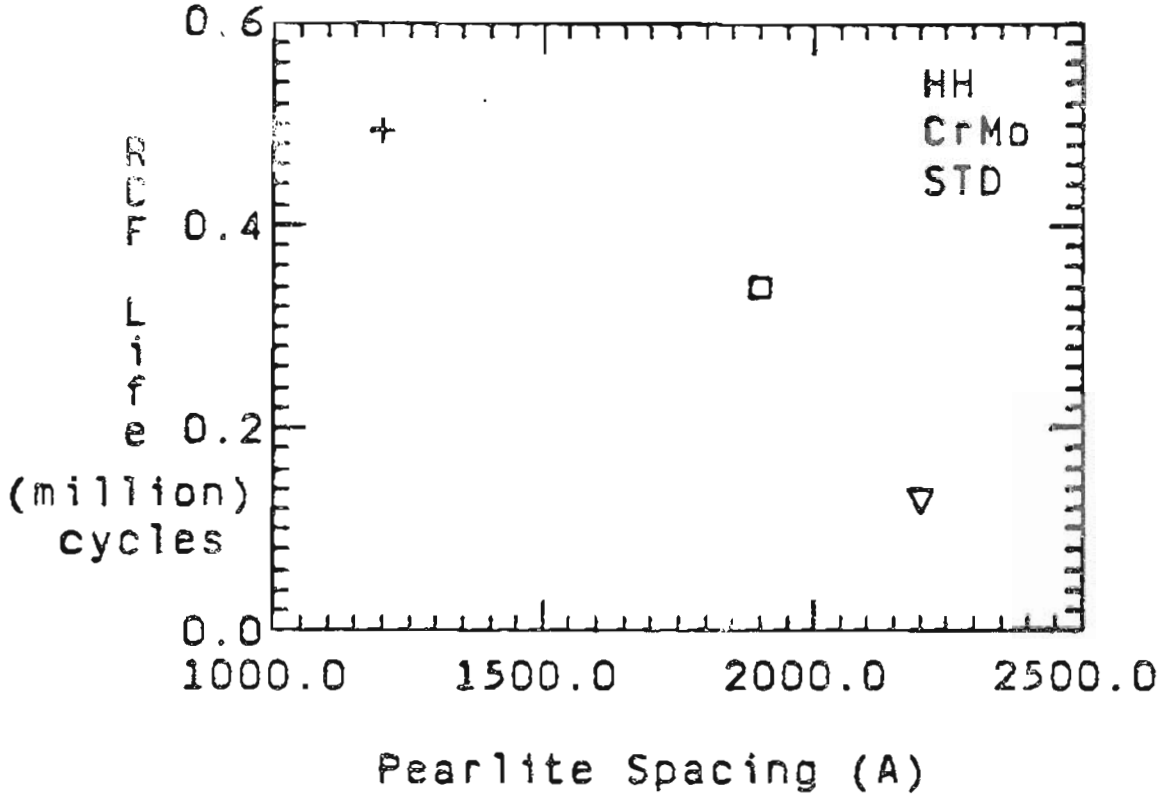

FIGURE 55. EFFECT OF PEARLITE INTERLAMELLER SPACING ON RCF

BIOGRAPHICAL NOTE

The author was born in Beijing, China on November 26, 1955. From 1970 until 1972, he attended Re Tan High School in Beijing. He worked in the Beijing Agricultural Tool Factory as a worker from 1972 to 1978. He was then educated and received B.S. degree in Metallurgical Engineering at Beijing University of Iron and Steel Technology in 1982. In 1983, he worked as engineer in Beijing High-Temperature Alloys Factory. Also, he served as a qualified patent examiner in the patent office of The people's Republic of China in Beijing in 1984. He left his job to pursue higher education in Materials Science and Engineering at the Oregon Graduate Center, Where the requirements for the Master of Science Degree were completed by October 1987.